

**An Integrated Array-based Microfluidic Device for Parallel  
Loop-Mediated Isothermal Amplification (LAMP)**

**An Integrated Array-based Microfluidic Device for Parallel  
Loop-Mediated Isothermal Amplification (LAMP)**

By

**SHAYAN LIAGHAT.**

B.Sc. (Sharif University of Technology, Tehran, Iran)

A Thesis Submitted to the School of Graduate Studies in Partial Fulfilment  
of the Requirements for the Degree Master of Applied Science.

McMaster University © Copyright by Shayan Liaghat, December 2017.

McMaster University

MASTER OF APPLIED SCIENCE (2017)

Hamilton, Ontario

Mechanical Engineering

TITLE:

An Integrated Array-based Microfluidic Device for Parallel Loop-Mediated Isothermal Amplification (LAMP)

AUTHOR:

SHAYAN LIAGHAT, B.Sc.

SUPERVISOR:

Professor P. R. Selvaganapathy  
Department of Mechanical Engineering

NUMBER OF PAGES

xxi, 173

## **Abstract**

Nucleic-based acid technology (NAT) is a reliable and well-established method in molecular diagnosis for the detection of bacterial infection. Specifically, PCR (polymerase chain reaction) is the most popular technique to amplify the number of DNA or RNA copies in the sample. However, due to the thermal cycles in the PCR method, advanced equipment and technologies are required to precisely control the temperature during the cycles. To overcome this limitation, isothermal amplification methods have been developed which function at constant temperatures and help reduce the need for state-of-the-art machines to perform the amplification. Among isothermal amplification methods, LAMP (loop mediated isothermal amplification) has demonstrated robustness and sensitivity compared to PCR. Additionally, microfluidic lab-on-a-chip (LOC) technology can facilitate the intensive processes which have been used traditionally in laboratories by automating the required procedures, reducing the volume of the reagents and minimizing the cost and the time of experiments. Although many microfluidic LOC devices have been developed in order to be used in resource poor settings, there is still a need for a simple setup which is inexpensive, accurate and can be performed without the need for a trained technician.

In this thesis, a disposable microfluidic device was developed which is capable of performing high-throughput DNA amplification by using a simple segmentation method in order to digitize the sample into multiple micro-wells. Moreover, design and fabrication of a disposable, inexpensive flexible heater which is an inevitable part of the setup using a direct write process was introduced in order to provide the required energy for the LAMP reaction. Parallel real-time DNA amplification with limit of detection down to few copies per micro-well in less than an hour was illustrated. Using *E. coli* 0157, it was demonstrated that the detection time of *E.coli* can be as quick as 11 to 55 minutes with sample

concentrations varying from 700,000 copies/micro-well (11 minutes), 70,000 copies/micro-well (18 minutes), 700 copies/micro-well (31 minutes), 7 copies/micro-well (40 minutes) and 0.07 copies/micro-well (55 minutes). Finally, the capability of the device for on chip reagent storage up to 3 days without using any coating methods was illustrated.

## **Acknowledgements**

I would like to start off by thanking my supervisor, Professor Ponnambalam Ravi Selvaganapathy, for providing me with his unconditional support and guidance throughout my studies. It was an honor to work under the direct supervision of such a leading character in the field of biomicrofluidics. I am grateful for all you have taught me, particularly, the importance of critical thinking at every stage of the project. I truly admire you for your hard work, commitment and broad knowledge and extensive level of expertise. Also, I would like to express my gratitude and appreciation to Dr. James Mahony from the department of pathology and molecular medicine for his insights and support of my project.

During my time in the Center for Advanced Micro-Electro-Fluidics lab, I have been fortunate to work with many amazing and talented people. I would like to thank Reza Ghaemi, Mohammad Hosein Dabbaghi, Neda Saraei, Ali Shahid, Michael Zlatin, Harpreet Matharoo, Shubham Banik, Pankaj Saini, Juncong Liu, Nidhi Jain, AliAkbar Mohammedzadeh, Celine Ling, Melizeth Bolanos, Rana Attala, Kamrul Russel, Leo Hsu, Aditya Aryasomayajula, Yujie Zhu, Sreekant Damodara, Monika Śliwiak and Parker Bondi. Also, my sincere thanks go to Mechanical workshop technicians, Ron Lodewyks, Mark Mackenzie, John Colebrander, Michael Lee and Dan Wright, who helped me greatly and gave me precious advices.

Undoubtedly, this journey would not have been possible without the continuous support of my family. Mom and Dad, thank you for being the source of encouragement. I feel so indebted to you for your love and grace. Special thanks go to my grandma, Tooba, and my aunt, Kathy, for inspiring me to be the best version of myself. Also, my little brother, Andisheh, thank you for being there for me whenever I needed you. Love you!

Lastly, I would like to thank my dear friends for all the love, comfort and guidance.  
Pedram, Amin, Kaveh, Arash, Lili, Myrto and Ivan.

# Table of Contents

<b>Abstract</b> .....	iv
<b>Acknowledgements</b> .....	vi
<b>Table of Contents</b> .....	viii
<b>List of Figures</b> .....	xiv
<b>List of Tables</b> .....	xx
<b>Chapter 1: Introduction</b> .....	1
1.1 Motivation .....	1
1.2 Organization of the chapters .....	2
<b>Chapter 2: Literature Review</b> .....	4
2.1 Introduction .....	4
2.2 Nucleic-acid amplification methods.....	5
2.3 Implementing microfluidic technologies in NAT .....	10
2.3.1. PCR microfluidic devices .....	11
2.3.2. Isothermal amplification microfluidic devices .....	13
2.4 High-throughput amplification microfluidic devices .....	16
2.4.1. Pipette-based sample distribution .....	16
2.4.2. Capillary-based sample distribution.....	23
2.4.3. Centrifugal-based sample distribution .....	31
2.4.4. Droplet-based sample distribution .....	34

2.5	Summary .....	36
<b>Chapter 3: Device Design, Materials and Methods.....</b>		<b>38</b>
3.1	Device design .....	39
3.1.1.	Design criteria .....	39
3.1.2.	Schematic of the device .....	40
3.1.3.	Challenges to be tackled .....	43
3.1.3.1	Trapped bubbles.....	43
3.1.3.2	Difference between positive and negative samples .....	45
3.1.4.	Flexible heater design .....	46
3.2	Materials & Experimental Setup .....	48
3.2.1.	Silicon wafer .....	48
3.2.2.	Photoresist.....	48
3.2.3.	Polydimethylsiloxane (PDMS) .....	49
3.2.4.	Sealing film.....	49
3.2.5.	Micro-wire .....	50
3.2.6.	Pressure sensitive adhesive (PSA) .....	50
3.2.7.	Electrical interconnects .....	50
3.2.8.	Bacterial DNA .....	51
3.2.9.	DNA staining dye .....	52
3.2.10.	Fluorescein dye (free acid).....	53
3.2.11.	Methylene Blue .....	53

3.2.12.	Master Mix without dye .....	54
3.2.13.	Primer Mix .....	54
3.2.14.	Film sealing roller for PCR plates.....	54
3.2.15.	Power supply .....	55
3.2.16.	Kapton heaters.....	55
3.2.17.	Thermocouple.....	55
3.2.18.	Thermometer .....	56
3.2.19.	FLIR ONE thermal imaging camera .....	56
3.2.20.	ESEQuant tube scanner.....	56
3.3	Device fabrication .....	57
3.3.1.	Fabrication of the micro-well array .....	59
3.3.2.	Plotting micro-wire integration technique for making flexible heater.....	60
3.3.3.	Final assembly of the device.....	62
3.4	Experimental setup.....	64
3.4.1.	The schematic of the experimental setup.....	64
3.4.2.	Sample holder .....	65
3.4.3.	Large field of view fluorescence detection system.....	66
3.4.3.1	Electrical control unit .....	68
3.5	Sample preparation.....	68
3.6	Sample loading.....	69
3.6.1.	Autoclaving of the pipettes and the tips.....	69

3.6.2.	Surface modification of PDMS.....	70
3.6.3.	Device sealing.....	71
3.7	Image processing method.....	73
3.8	Summary .....	74
<b>Chapter 4:</b>	<b>Results and Discussions .....</b>	<b>75</b>
4.1	Introduction .....	75
4.2	Micro-wells .....	75
4.2.1.	Shape of the micro-wells .....	76
4.2.2.	Width of the micro-wells .....	79
4.2.3.	Effect of the height of the micro-wells on the intensity.....	81
4.2.4.	Effect of the waste channel on the filling process .....	83
4.2.5.	The final design of the micro-wells part .....	85
4.3.1.	Effect of the temperature on the performance of the LAMP reaction .....	86
4.3	Flexible heater .....	89
4.3.1.	Commercially available heaters .....	89
4.3.2.	Heaters made with plotting method .....	92
4.3.3.	Cost analysis .....	99
4.3.4.	Electrical power consumption.....	102
4.4	DNA amplification.....	104
4.4.1.	Demonstration of amplification in the integrated microfluidic device .....	104
4.4.2.	Real-time amplification measurement from the device .....	112

4.4.3.	Repeatability .....	116
4.4.4.	Amplification characterization.....	118
4.4.4.1	Effect of the initial DNA concentration on the amplification .....	118
4.4.5.	Parallel DNA amplification .....	126
4.4.6.	On Chip reagent storage.....	129
4.5	Summary .....	132
<b>Chapter 5:</b>	<b>Conclusion and Future Work .....</b>	<b>134</b>
5.1	Conclusion.....	134
5.2	Future work .....	137
Appendix A:	SU-8 master mold fabrication with the height of 700 $\mu\text{m}$ .....	142
Appendix B:	COMSOL simulation setup.....	144
Appendix C:	Detailed information for various micro-wires.....	149
Appendix D:	Decrease of the fluorescence intensity phenomenon .....	151
Appendix E:	Temperature calibration .....	153

## List of Figures

<b>Figure 2.1</b> The principle of PCR. Each cycle has three steps including denaturation, annealing and extension [9].....	6
<b>Figure 2.2</b> The principle of loop mediated isothermal amplification (LAMP)[23].....	9
<b>Figure 2.3</b> A flow-through PCR device example. Three heating regions are shown in the figure [43].....	12
<b>Figure 2.4</b> The SlipChip mechanism. (c) Lyophilized micro-wells located in the bottom plate. (e) Loading the sample in the micro-channel was made by ducts in the bottom plate and wells in the top plate. (g) Sample compartmentalization after the slipped move [87].....	30
<b>Figure 3.1</b> The schematic of the device. (a) The micro-well array. (b) The flexible heater. (c) The integrated device.....	41
<b>Figure 3.2</b> The micro-wells design for bacteria detection application where the dimension of each nano-well was $100*100*100\ \mu\text{m}$ [2].....	42
<b>Figure 3.3</b> A micro-well component composed of micro-wells with dimensions of $320*320*100\ \mu\text{m}$ was filled (a) once with the methylene blue solution (0.05 M) in DI water and (b) once with positive amplification solution. The high reflective edges are evident in the micro-wells with trapped bubble inside.....	44
<b>Figure 3.4</b> The excitation (left) and emission (right) spectra of EvaGreen dye [7].....	52
<b>Figure 3.5</b> The ESE-Quant TS95.....	57

**Figure 3.6** Fabrication process flow. (a) Photoresist spinning. (b) UV exposure. (c) After developing. (d) PDMS casting on master mold. (e) Peeling off the PDMS. (f) Writing the designed pattern on the PSA. (g) Attaching the connectors. (h) The final assembly.....58

**Figure 3.7** An example of a designed pattern in AutoCAD.....60

**Figure 3.8** Flexible Heaters. (a) Covered with a PDMS layer to protect the micro-wires. (b) Covered with a PSA film to protect the micro-wires.....62

**Figure 3.9** The integrated device including the micro-wells and the flexible heater made with plotting method.....63

**Figure 3.10** The schematic of the experimental setup.....65

**Figure 3.11** The sample holder composed of two parts, the frame and the glass slide holder.....66

**Figure 3.12** The large field of view fluorescence detection system.....67

**Figure 3.13** Sample loading on top of the hydrophilic PDMS surface.....71

**Figure 3.14** Device Sealing. (a) Before attaching the sealing tape. (b) After attaching the sealing tape.....72

**Figure 4.1** (a) Cuboid shaped wells with width of 500  $\mu\text{m}$  and height of 700  $\mu\text{m}$ . (b) Cylinder shaped wells with diameter of 500  $\mu\text{m}$  and height of 700  $\mu\text{m}$ .....77

**Figure 4.2** Filling comparison. (a) Cuboid design (500  $\mu\text{m}$  width, 700  $\mu\text{m}$  height). (b) Cylinder design (500  $\mu\text{m}$  diameter, 700  $\mu\text{m}$  height).....78

**Figure 4.3** Filling efficiency of different widths of the cuboids. The widths from the biggest to the smallest size were 1.58, 1.41, 1.22, 1, 0.7, 0.55, 0.45, 0.32 and 0.1 mm. All the micro-wells above had the same height of 100  $\mu\text{m}$ .....80

**Figure 4.4** Effect of the height of the micro-wells on the fluorescence intensity for three different heights. (a) 100  $\mu\text{m}$  height and 500  $\mu\text{m}$  width. (b) 500  $\mu\text{m}$  height and 500  $\mu\text{m}$  width. (c) 700  $\mu\text{m}$  height and 500  $\mu\text{m}$  width.....82

**Figure 4.5** Two solutions were mixed when there was no waste channel between the regions.....84

**Figure 4.6** Effect of the waste channel which eliminated the samples from different regions to get mixed.....85

**Figure 4.7** The final design of the micro-wells part which was filled with four different colors.....86

**Figure 4.8** The normalized real-time fluorescence intensities of the positive sample with concentration of  $4 \times 10^5 \text{ Copies}/\mu\text{L}$  at different temperatures by using ESEQuant tube scanner.....87

**Figure 4.9** Amplification time of the positive sample with concentration of  $4 \times 10^5 \text{ Copies}/\mu\text{L}$  at different temperatures by using ESEQuant tube scanner.....88

**Figure 4.10** Temperature gradient of three commercial heaters made by Minco Company which were analysed with FLIR Tools software. (a) 120 ohm. (b) 160 ohm. (c) 275 ohm.....90

**Figure 4.11** The schematic of all the designs. (a) Design 1: Constant spacing, 0.5 mm, made out of 50  $\mu\text{m}$  silver wire. (b) Design 2: Gradually increased spacing from 1 mm at

the edges to 2 mm at the middle made out of 50  $\mu\text{m}$  silver wire. (c) Design 3: Gradually increased spacing from 1 mm at the edges to 2 mm at the middle made out of 25  $\mu\text{m}$  copper wire. (d) Design 4: Gradually increased spacing from 1.5 mm at the edges to 2 mm at the middle made out of 50  $\mu\text{m}$  silver wire.....93

**Figure 4.12** Simulation result of Design 1 with the constant spacing, 0.5 mm, made out of 50  $\mu\text{m}$  silver micro-wire.....94

**Figure 4.13** Simulation result of Design 2 with variable spacing from 1 mm to 2 mm made out of 50  $\mu\text{m}$  silver micro-wire.....96

**Figure 4.14** Simulation result of Design 3 with variable spacing from 1 mm to 2 mm made out of 25  $\mu\text{m}$  copper micro-wire.....96

**Figure 4.15** Simulation result of Design 4 with variable spacing from 1.5 mm to 2 mm made out of 50  $\mu\text{m}$  silver micro-wire.....97

**Figure 4.16** Real temperature gradients of the heaters made by plotting method. (a) Design 2: Gradually increased spacing from 1 mm at the edges to 2 mm at the middle made out of 50  $\mu\text{m}$  silver micro-wire. (b) Design 3: Gradually increased spacing from 1 mm at the edges to 2 mm at the middle made out of 25  $\mu\text{m}$  copper micro-wire. (c) Design 4: Gradually increased spacing from 1.5 mm at the edges to 2 mm at the middle made out of 50  $\mu\text{m}$  silver micro-wire.....98

**Figure 4.17** Demonstration of amplification in the integrated device. (a) Positive sample before amplification. (b) Positive sample after amplification. (c) Negative sample before amplification. (d) Negative sample after amplification. (e) The quantified comparison between positive and negative amplifications. The average fluorescence increase

percentages of the positive (red) and negative (blue) samples are shown. The initial DNA concentration of the positive sample was  $4 \times 10^6$  Copies per  $\mu\text{L}$ .....106

**Figure 4.18** The spatial variation of the micro-wells at multiple random locations spread throughout the array chip. (a) Fluorescence increase distribution. (b) Amplification time distribution.....108

**Figure 4.19** (a) The infrared thermal image of the device taken with FLIR ONE camera indicating the location of the randomly selected micro-wells. (b) The temperature distribution of the randomly selected micro-wells.....110

**Figure 4.20** (a) The relationship between the fluorescence increase percentages and the temperatures. (b) The relationship between the amplification times and the temperatures.....111

**Figure 4.21** The real-time amplification curves of the highly concentrated positive solution (red lines) and the negative control (blue lines).....114

**Figure 4.22** The normalized real-time amplification curves of the highly concentrated positive solution (red lines) in comparison with the negative control (blue lines).....115

**Figure 4.23** Repeatability analyses of two different DNA concentrations with 10 folds difference.....117

**Figure 4.24** Amplification times for serially diluted concentrations.....120

**Figure 4.25** Real-time amplification profile of serially diluted concentrations by using ESEQuant tube scanner.....122

**Figure 4.26** Amplification times of serially diluted concentrations by using ESEQuant tube scanner.....123

**Figure 4.27** False negative ratio for serially diluted concentrations.....124

**Figure 4.28** Fluorescence increase percentage for serially diluted concentrations.....125

**Figure 4.29** Schematic of the device for parallel DNA amplification of four different LAMP reactions including E. coli 70000 Copies / micro – well solution (red), E. coli 7 Copies / micro – well solution (blue), negative control solution (black) and positive control solution (green) which contained  $\lambda$  DNA with concentration of  $100 \mu\text{g}/\text{ml}$ .....127

**Figure 4.30** Parallel DNA amplification of four difference reactions including E. coli 70000 Copies / micro – well solution (red lines), E. coli 7 Copies / micro – well solution (blue lines), negative control solution (black lines) and positive control solution (green dotted lines) which contained  $\lambda$  DNA with concentration of  $100 \mu\text{g}/\text{ml}$ .....128

**Figure 4.31** Amplification time of the primer-less positive solution with respect to time after the primer dehydration on the chip in order to analyze the shelf life of the frozen dried primers. The added DNA template had the concentration of 70000 Copies/micro-well.....131

**Figure 5.1** The proposal for the next generation of the device which includes a sandwich of three layers of hydrophilic vinyl, hydrophobic vinyl and sealing tape.....138

**Figure 5.2** The proof of concept of the proposal for the next generation of the device..139

**Figure B.1** The geometry of the heater.....144

**Figure B.2** The temperature distribution of the top surface.....146

**Figure B.3** Mesh independency analysis. The temperature distribution of the vertical line located on the top surface parallel to the Y axis for four different mesh sizes, 1.5 mm (black), 1 mm (grey), 0.75 mm (blue) and 0.5 mm (red).....147

**Figure D.1** Decrease of fluorescence intensity phenomenon.....151

## List of Tables

<b>Table 3-1</b> Kapton Heaters specifications.....	55
<b>Table 4-1</b> Applied voltages and currents to Minco heaters in order to reach the temperature gradient of 60 to 68 Celsius across the heater.....	90
<b>Table 4-2</b> Results of the temperature gradient analyses for three commercially available heaters.....	91
<b>Table 4-3</b> Design specification of the 3 fabricated heaters. (*) Minimum spacing at the edge: Spacing increment: Maximum spacing at the middle.....	95
<b>Table 4-4</b> Design and performance parameters of three different heaters made by plotting method.....	99
<b>Table 4-5</b> Summarized price information of flexible heaters from two companies, Minco and Omega.....	100
<b>Table 4-6</b> The estimated final cost of four different patterns. (*) NiCR80/20 with the size of 50 $\mu\text{m}$ in diameter from the Vape Mesh Company (CAD 0.04 per meter). (**) Additional 35 cents for the PSA film and copper tape. (***) The area of all the heaters are 30.2 $\text{cm}^2$ .....	102
<b>Table 4-7</b> The electrical power consumptions of all the mentioned heaters.....	103
<b>Table 4-8</b> The amplification times and standard deviations of different concentrations.....	119
<b>Table C-1</b> Detailed information for various micro-wires.....	150

<b>Table E-1</b> The measured temperatures using the thermocouple and the thermal camera.....	153
---	-----

## **Chapter 1: Introduction**

### **1.1 Motivation**

According to the data from Center for Disease Control and Prevention, around 48 million people get sick in the USA from foodborne diseases annually which results in 128000 hospitalization case and 3000 death reports. Foodborne illness costs Americans billions of dollars each year. Some microorganisms that were reported as the biggest reasons of foodborne illness by the U.S. Public Health Service are campylobacter, clostridium botulinum, E. coli, listeria monocytogenes, norovirus and salmonella, either because of the severity of the sickness or the number of cases of illness they cause. Between them, E. coli was chosen as the representative model organism to study in this project since it causes about 73,000 cases of foodborne illness each year in the U.S. which could be found in beef, raw milk, unpasteurized juices and ciders and even drinking water.

Early diagnosis of these bacteria could be lifesaver and reduce the cost of treatment. Moreover, the majority of the deaths due to the aforementioned diseases happen in poor countries where cost is a vital concern. Therefore, developing an inexpensive and at the same time precise, accurate and fast device for diagnosis of infectious bacteria is the main focus of the point-of-care (POC) research.

In this regard, various diagnostic methods are available such as immunoassay, detecting by specific epitopes on the pathogen cell membrane or their produced toxin, and nucleic-acid-based technology (NAT). Among them, NAT plays an important role in molecular diagnosis. Moreover, microfluidics can be used to automate the point-of-care devices and reduce the cost of operation by decreasing the volume of the required reagents, as well as eliminating the need for skilled laboratory technicians. Another advantage of

using microfluidic devices in point-of-care applications is the capability of performing high-throughput experiments. For instance, several amplification reactions can be performed simultaneously on the same device to detect multiple targets which is known as parallel or multiplex amplification. In this thesis, a disposable and inexpensive microfluidic device to perform parallel DNA amplification is introduced that is capable of detecting multiple pathogens.

## **1.2 Organization of the chapters**

The Organization of the chapters is as follows:

Chapter 2 presents a broad background review on the nucleic-acid-based technology (NAT) and its importance in molecular diagnosis. Isothermal and non-isothermal amplification methods are introduced, followed by the role of microfluidic technology in order to make the detection faster, cheaper and easier. Finally, high-throughput amplification microfluidic devices are categorized into four groups based on the method which was implemented to distribute the sample into various micro-chambers or micro-channels.

Chapter 3 covers the design criteria and the challenges that are required to be tackled, followed by illustrating a schematic from the device composed of two main components, the micro-well and the flexible heater. Next, the material which were used in fabricating the device are presented, as well as the reagents existed in the amplification solution. The fabrication method of the micro-well component as well as the plotting method to fabricate flexible heaters are explained in detail. Also, the experimental setup including the large-field-of-view fluorescence detection setup and other equipment that

were used in performing the experiments are introduced. Finally, the sample preparation method, the sample loading technique and image processing procedures are discussed.

Chapter 4 describes the result of the experiments. First, the characterization results of designing the micro-well component is discussed, followed by analyzing the fabricated flexible heater in comparison with the commercially available heaters. Finally, the DNA amplification results of the integrated device are presented, as well as the ability of the device in order to perform parallel DNA amplification.

Chapter 5 concludes the thesis by highlighting the main contributions of this research. Finally, a number of suggestions are proposed for the future work and in order to increase the efficiency of the device.

## **Chapter 2: Literature Review**

### **2.1 Introduction**

Nucleic acid-based technology (NAT) plays a key role in molecular diagnosis where the main purpose is to detect a target by the means of manipulation of biomarkers such as nucleic acids. Nevertheless, most of the techniques and approaches that have been used in this field, need to be performed by a trained technician and are time and energy consuming which increases the cost. Early diagnosis of diseases helps quick treatment, increases the survival rate and reduces the overall cost [1][2].

It has been shown that detection techniques which are based on nucleic-acid manipulation are more accurate and sensitive compare to other available methods such as detecting by specific epitopes on the pathogen membrane or their produced toxin, since all living organisms have unique sequence of nucleic-acids which can be found either in single-stranded RNA or double-stranded DNA. Deoxyribonucleic acid or DNA is a molecule which contains the genetic information and is located inside of a cell. DNA plays the main role in all the functions of a cell, including the growth, development, functioning and reproduction. This information is stored as a code which consists of four chemical bases, adenine (A), guanine (G), cytosine (C), and thymine (T).

Cell lysis is the method to break the cell membrane [3] and release its contents in order to extract the DNA or RNA, and is one of the most important steps in sample preparation for DNA analysis. Without cell lysis, no DNA is available for analysis. There are many different methods to lyse the cell, some of which are chemical disruption [4], mechanical lysis [5], thermal lysis [6][7], or even by applying electric field [8]. It has been

demonstrated that all of the mentioned methods are reasonably efficient to lyse bacteria and also mammalian cells.

The next step after cell lysis is to analyse the extracted nucleic-acids. Since the amount of extracted nucleic-acids is relatively small, the DNA is copied several times over in a process known as nucleic-acid amplification in order to makes its detection easier. In the next sections, the amplification methods are described and categorized more in detail, followed by recent innovations in microfluidic devices for high-throughput screening.

## **2.2 Nucleic-acid amplification methods**

There are many techniques to perform DNA amplification. These methods can be broadly classified based on their conditions (mainly temperature) of operation as: isothermal and non-isothermal. In isothermal methods, the temperature is kept constant. On the other hand, in non-isothermal techniques, the temperature of the amplification mixture is changed precisely between specific temperatures and cycled multiple times.

The most popular and well-known amplification method is called polymerase chain reaction (PCR), developed by Kary Mullis in 1983, which fits into the category of non-isothermal methods. PCR process goes through many cycles and each cycle has three different temperatures to control three steps called denaturation, annealing and extension [9]. After each cycle, the number of DNAs double. So, even if there is just one DNA molecule in the sample, the number of DNAs after 20 cycles ( $2^{20}$ ) is over a million.

The three steps of the PCR is shown in Figure 2.1. The first step is called denaturation which happens at a high temperature between 90 and 95 Celsius. In this reaction, double-stranded DNA breaks into two single-stranded DNAs. The next reaction

is called annealing which happens at the temperature around 55 Celsius. In this reaction, the specific designed primers match with the corresponding sequence on the single-stranded DNA and bind at those locations. Finally, the third reaction is called extension where the Taq DNA polymerase, binds to one end of the primer sequence and copies the sequence of the single-stranded DNA between the two primers and turns it to a double-stranded DNA [9]. The primers provide specificity to the PCR process as it is the presence of these double stranded primers that provide the cue for the polymerase enzyme to bind and copy. Thus, with appropriate design of the primers, the right sequence of DNA can be selectively amplified from the sample.

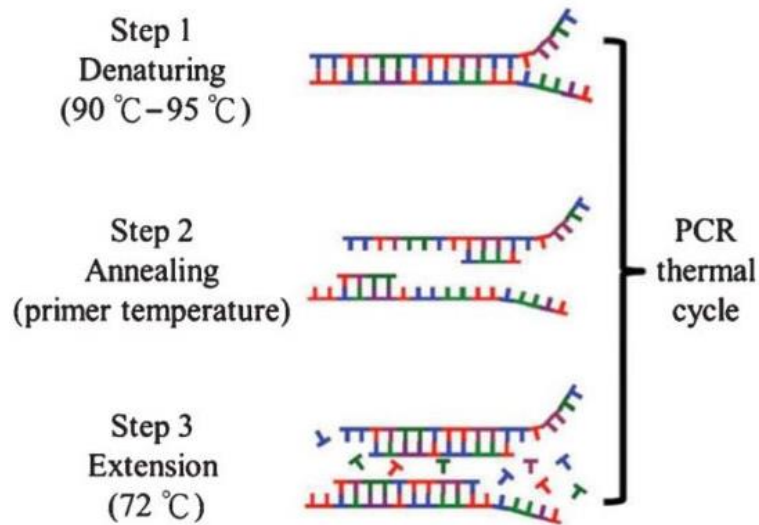


Figure 2.1 The principle of PCR. Each cycle has three steps including denaturation, annealing and extension [9].

PCR was the first amplification methods that was invented. Several variations based on the PCR method were developed later in order to increase its sensitivity and robustness. Some examples are as follows. Quantitative real-time PCR was used to quantify the number

of DNAs in the sample based on the intensity of fluorescence signal [10][11]. Reverse-transcription PCR (RT-PCR) was implemented for RNA quantification based on the intensity of fluorescence signal [12]. Also, nested PCR was developed to eliminate contamination because of false primer binding [13].

Although PCR is the most established method that is currently being used in laboratories and biology facilities, it needs relatively expensive and state-of-the-art technologies to precisely control the thermal cycling. Therefore, PCR may not be the best method to implement point-of-care diagnostics in resource-poor areas.

As a solution to this problem and in order to perform a fast diagnosis, isothermal nucleic acid amplification methods have been developed. These methods work at constant temperature and there is no need for expensive instrumentation in order to perform and control the amplification. Consequently, by advent of these technologies, a new door has been opened to the development of point-of-care devices. Some of the isothermal nucleic acid amplification methods include nucleic acid sequence- based amplification (NASBA) [14], transcription mediated amplification (TMA) [15], strand displacement amplification (SDA) [16], rolling circle amplification (RCA) [17], helicase dependent amplification (HDA) [18] and loop mediated isothermal amplification (LAMP) [19].

Each of the aforementioned techniques has some advantages and disadvantages compare to each other. For instance, NASBA has been used to amplify RNA sequences as an alternative to RT-PCR by using two specific primers to the target RNA and three enzymes. It can produce one billion RNAs in around 1.5 hours at constant temperature around 40 Celsius [14]. However, the low temperature reduces the specificity of the reaction in comparison with other methods. Another example is SDA to replicate DNA sequences by using a restriction endonuclease and a strand displacing DNA polymerase.

Although SDA is an isothermal amplification method, it requires an initial high temperature step in order to denaturize the dsDNA to start the reaction [16]. SDA takes almost 4 hours to be completed which makes it an inappropriate candidate to be used for the purpose of fast diagnosis. HDA is another isothermal amplification method which has been used frequently and needs single-stranded DNA-binding proteins in order to eliminate rewinding of the denatured double helix and it uses the DNA replication fork mechanism [18]. This additional protein increases the complexity and the cost of the reaction [1][20].

Among all the isothermal nucleic acid amplification methods, LAMP has been the most widely used method by scientists due to its high efficiency and specificity [21]. The latter is because of the use of four unique primers which are designed based on six regions on the sequence of the target. Moreover, LAMP is capable of amplifying the number of DNAs in the sample to billions in less than an hour which makes it an ideal candidate to implement on Lab-on-a-Chip devices for the purpose of fast diagnosis. Additionally, LAMP is capable of amplifying RNA as well just by adding reverse transcriptase to the reaction [22].

As it was mentioned earlier, there are four specific primers involved in the LAMP reaction, two inner and two outer primers, called F3, B3, FIP and BIP. In the initial steps all four primers are used. However, later in the cycling stage just inner primers, FIP and BIP, participate.

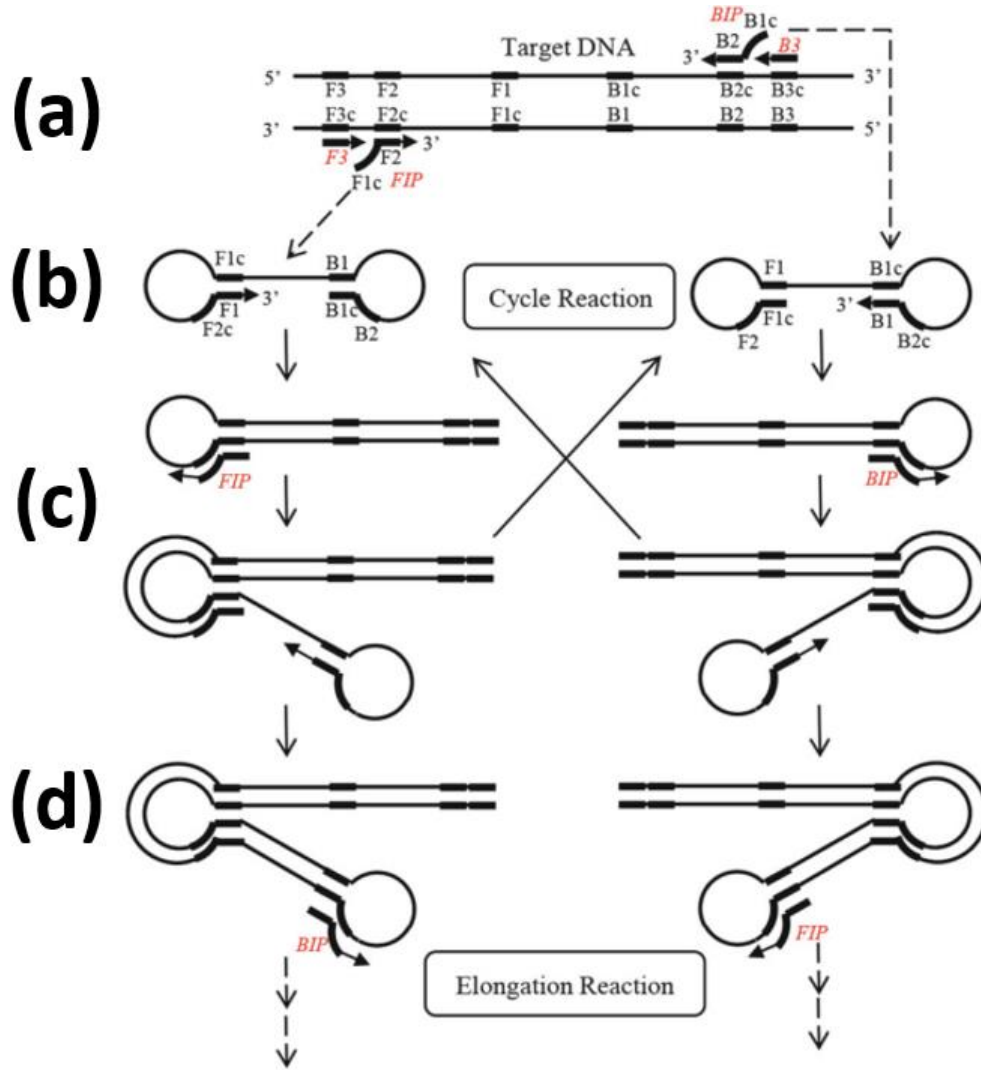


Figure 2.2 The principle of loop mediated isothermal amplification (LAMP) [23].

First the inner primer FIP hybridizes to F2c in the target DNA and starts strand synthesis (Figure 2.2a). Then, the outer primer F3 which is shorter in length and lower in concentration compare to FIP, slowly hybridizes to F3c that results in making a dumb-bell form DNA which is rapidly converted to a stem-loop DNA (Figure 2.2b) which is the basis of the second part of the LAMP reaction, cycling. In the cycling stage, FIP helps to make

two loops at the opposite sides of the sequence (Figure 2.2c). Next, BIP helps to finish the cycling stage (Figure 2.2d). It is interesting to mention that the target sequence is amplified 3-fold every half cycle in the LAMP reaction [19].

### **2.3 Implementing microfluidic technologies in NAT**

Microfluidic lab-on-a-chip (LOC) technology is attractive to implement with conventional laboratory scale NAT as it could be used to automate the assay, reduce the time for analysis and most importantly use less reagents and require less sample [24]. All the laboratory steps can be integrated in a single chip by the means of microfluidic devices [25] which can lead to higher throughput as well. Automated systems can perform not only DNA amplification but also sample processing prior to it, are desirable due to the minimum contamination issues which are one of the key challenges for NAT. Microfluidic has entered into many different applications where NAT assays have been used such as pathogen detection [26], cancer cell analysis [27], microinjection [28], drug discovery [29], and so on.

Before the introduction of microfluidic technology, the typical time for performing conventional PCR reactions was between two to three hours because of the high heat capacity of the solution which resulted in 20 to 30 seconds for each denaturation and annealing steps [30]. However, recent research showed that these times can be reduced significantly [31]. Therefore, modern PCR machines are able to perform PCR amplification in around 30 minutes. Moreover, the typical time of performing LAMP reaction is around 60 minutes which has the ability to amplify the number of DNAs from a few to  $10^9$  copies with high specificity for the target sequence [19].

The biggest advantage of microfluidic technology is the high surface to volume ratio which drastically increases the heat transfer rates, either to increase or to reduce the temperature. Also, the sample volume is significantly lower compared to the conventional methods which makes it easier to have more PCR cycles in the same amount of time which eventually leads to faster amplification and diagnosis.

### **2.3.1. PCR microfluidic devices**

In general, microfluidic PCR devices can be categorized into two main groups, stationary PCR devices and flow-through PCR devices. In the case of the former, the amplification solution is kept stationary in a chamber or a micro-channel and it does not flow through the device [32][33][34][35][36][37]. Designing a stationary PCR device is easier compared to the flow-through format since there is no need for any extra instrumentation to control the flow rate. However, the heat transfer rate of this design is normally slower compare to the other group since in addition to the sample, the whole device should be heated up which results in a larger thermal mass and consequently slower cycling time. The reaction volume of a typical microfluidic stationary PCR devices have been reported to be between the range of 0.45 nL [38] to 50  $\mu$ L [39]. Additionally, the heating rate of the microfluidic stationary PCR devices were reported between the range of 3 Celsius/second [40] to 175 Celsius/second [41].

On the other hand, the flow-through PCR devices have smaller thermal mass [42][43][44][45][46][47]. In this design, sample flows through micro-channels and passes through the areas on the device with different temperatures. The advantage of this design

over the previous format is the smaller thermal mass. Therefore, there is no need to cool down the device as in the case of the stationary devices. Therefore, the experiment time can be reduced to the minimum time possible which is the time required for the chemical reaction to happen. However, it is crucial to control the flow rate to give the solution enough time in each region to reach to the equilibrium state at the expected temperature. For instance, G. Munchow et al [48] reported a microfluidic flow-through PCR device which was able to perform 40 cycles in 300 seconds. Additionally, the reaction volume of the microfluidic flow-through PCR devices were reported between the range of 500 nL [49] to 8  $\mu$ L [48].

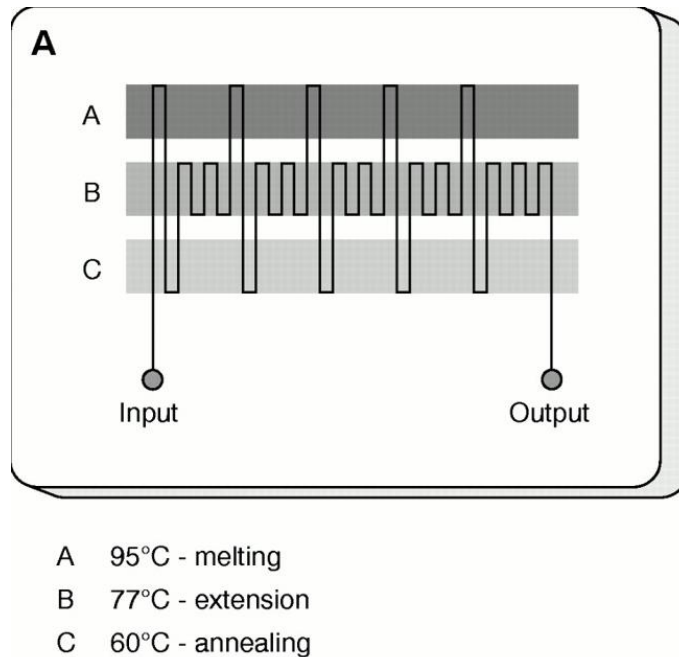


Figure 2.3 A flow-through PCR device example. Three heating regions are shown in the figure [43].

Flow-through PCR devices normally require a pumping setup to control the flow rate. Several pumping methods have been introduced, including syringe pumps [45][50][51], electro kinetic micro-pumps [52][53], peristaltic micro-pumps [54], piezoelectric micro-pumps [55] and so on. However, there have been some attempts to perform flow-through PCR without the need for the pumps to eliminate the use of bulky equipment. For instance, thermal gradient drive convective flow was used to move the sample between different temperature zones and performed PCR successfully [56][57]. In this method, the driving force for the fluid to flow is the temperature difference between denaturation, annealing and extension regions which results in buoyancy driven instability when the sample is heated up from below that can cause the fluid to move vertically from higher temperature zone (lower density) to the lower temperature zone (higher density). This type of convective flow is known as Rayleigh Bernard convection and can be characterized through Rayleigh number (buoyancy forces over diffusion forces). When Rayleigh number passes a threshold number according to the dimensions, a circulatory motion can occur. This circulatory motion was exploited to move the fluid between the temperature zones for thermocycling.

### **2.3.2. Isothermal amplification microfluidic devices**

As it was explained earlier, isothermal amplification methods, specifically LAMP, is more suitable for implementing on the point-of-care LOC devices as compared to PCR primarily because of the simpler instrumentation that is required. Several attempts have been made to miniaturize the LAMP amplification devices using microfluidic technology.

One of the first attempts was introduced by Y. Baba et al [58] in 2004 where they showed the amplification and detection of prostate-specific antigen gene with the

concentration of  $23 \text{ fg}/\mu\text{L}$  and the well volume of  $10 \mu\text{L}$  in around 15 minutes using LAMP by using microchip-based electrophoresis. However, in order to perform the electrophoresis, a power source which was capable of providing 750 volts was required.

After that, many other research groups have demonstrated significant improvements for implementing LAMP to LOC devices. For instance, C. Lin et al [59] successfully illustrated a device for amplification of Hepatitis B virus (HBV) with the low concentration of 50 Copies/tube in 60 minutes in a micro-reactor with volume of  $25 \mu\text{L}$  by electrophoretic analysis. Moreover, an optical detection unit was used in order to quantitatively detect the by-product of the LAMP reaction (magnesium pyrophosphate). Although they decreased the detection limit significantly, a miniature spectrometer was required for the suggested detection method.

Later, H. Noji et al [60] displayed LAMP in a PAA gel-based micro-chamber at a single molecule level using fluorescent imaging by drastically reducing the volume of required reagents including template and primers down to 75% lower which resulted in  $10 \mu\text{L}$  sample solution. Also, the limit of detection was lowered down to 2  $\lambda\text{DNA}$  molecule in 50 minutes of incubation at 65 Celsius. Titanium deposition with the thickness of 200 nm on glass was used to fabricate the micro-heater and the sensor. Although the detection limit was lowered significantly, the efficiency and the repeatability of the method was as low as 50%.

In another study, a disposable, plastic cassette with thermo-responsive PDMS valve [61] in order to seal the reaction chamber was presented, made out of a composite of PDMS and expandable microspheres. The device had the potential to be used in point-of-care applications. The limit of detection was as low as 10 E. coli DNAs per well with the volume

of 20  $\mu\text{L}$  in an hour. However, a commercially available flexible heater was used to heat up the device to the required temperature which resulted in high cost of operation.

In order to make the device cheaper and easier to perform, H. Bau et al [62] introduced a self-heating cartridge without the need for any temperature control systems by using paraffin as a phase change material with high latent heat capacity for keeping the temperature constant. The required energy for the reaction to happen was provided from an exothermic chemical reaction which its rate was controlled by the rate of added water to the reaction chamber. A paper filter was responsible for controlling the flow rate of the added water based on the capillary action. The device was capable of detecting as few as 10 E. coli DNAs per well with the volume of 15.6  $\mu\text{L}$  in 60 minutes. However, just end-point detection method was introduced. Therefore, their device lacked the real-time detection technology.

G. Lee et al [63] introduced an integrated microfluidic device which was capable of doing extraction and amplification on one run which significantly reduced the chance of contamination. Extraction was done by hybridizing the target DNA by using specific probe-conjugated magnetic beads which were purified by applying a magnetic field. The limit of detection (LOD) was  $10^7 \text{fg}/\mu\text{L}$  of MRSA bacterium and the amplification was performed in under 60 minutes with the chamber volume of 20  $\mu\text{L}$ .

In another study, LAMP amplification and detection of E. coli was demonstrated without the need for the DNA extraction and purification steps in a single chamber with the volume of 35  $\mu\text{L}$  [64]. The electrochemical detection method was chosen to achieve the limit of detection of 48  $\text{CFU}/\text{ml}$  in 35 minutes.

## **2.4 High-throughput amplification microfluidic devices**

One of the promising aspects of implementing microfluidic technology in the medical diagnostics is the capability of performing high-throughput experiments. For instance, several amplification reactions can be performed simultaneously on the same device to detect multiple targets which is known as parallel or multiplex amplification. Parallelization can potentially reduce the cost and the time of the operation as well as increase the reliability of the results by decreasing the chance of false negative and positive results. Many efforts have been made towards multiplexing pathogen detection which are discussed in detail in the following sections.

There are various methods available to classify high-throughput lab-on-a-chip devices. In this thesis, high-throughput devices are categorized based on the mechanism which was used to distribute the sample into various micro-chambers or micro-channels. Therefore, four main groups are introduced including pipette-based sample distribution, capillary-based sample distribution, centrifugal-based sample distribution and droplet-based sample distribution.

### **2.4.1. Pipette-based sample distribution**

In this section, high-throughput devices which their sample distribution method into various micro-chambers or micro-channels was based on pipetting are introduced in order to perform isothermal or non-isothermal amplification techniques.

In 1998, M. Chaudhari et al [65] introduced a micro machined PCR silicon device composed of 18 well array with volume of 2  $\mu\text{L}$  each which could perform PCR amplification by controlling the temperature precisely, with precision of 0.1 Celsius.

Thermochromic liquid crystals (TLC's) were implemented in the vessels with a layer of polymer around them to measure the temperature gradient accurately. Also, the samples were loaded into the chambers manually. It was shown that the device is capable of amplify a PCR solution with human DNA concentration of 1200 copies/ $\mu\text{L}$  in 40 cycles. However, additional instrumentation required to perform the PCR amplification with this method including PID temperature controller, fiber optic lights and digital video effects generator.

Q. Xiang et al [66] introduced a simple, cheap and disposable device including a miniature thermal cyler and a PDMS micro-array part. Three micro-chambers were implemented in their design for the means of parallel PCR amplification. A puncher was used to fabricate the micro-chambers with different sizes, 3, 2 and 1 mm in diameter which resulted in 7, 3 and 0.9  $\mu\text{L}$  in volume, respectively. Therefore, there was no need for any micromachining or photolithography techniques. Also, the micro-chambers were covered by mineral oil to seal the device in order to eliminate sample evaporation during the PCR thermal cycling. E. coli bacterium was used as the DNA template in order to perform 35 PCR cycles in 85 minutes. The lowest DNA concentration tested was 0.019 ng/  $\mu\text{L}$  which was amplified in 45 minutes. However, the manual punching method is not suitable for scaling up to 100s of micro-wells.

J. Luo et al [67] illustrated an octopus-like microfluidic device for simultaneous amplification of eight LAMP reactions with the volume of 20  $\mu\text{L}$  each. The detection method was based on electrochemical detection of methylene blue (MB) since it is an active indicator for dsDNA through intercalation which can be monitored by measuring the change in the redox current with respect to the voltage [68]. The device composed of two parts, the etched ITO glass and the PDMS. The former was patterned by using a laser to make conductive electrodes on ITO. The latter was fabricated by using a master mold made

with lithography and was attached to the ITO glass by applying air plasma. Afterwards, the wires were connected to the electrodes by applying silver paste. Moreover, the chambers were pre-treated with specific set of primers before loading the sample. A ZNJR-B smart thermostat electric heating plate was used to provide constant temperature of 63 Celsius during the amplification time. The parallel amplification and detection of three respiratory bacteria including Mycobacterium tuberculosis (MTB), Haemophilus influenza (HIN), and Klebsiella pneumonia (KPN) was shown successfully as a proof that this device could be used in clinical detection. The limits of detection were 28, 17 and 16 copies/ $\mu\text{L}$  for MTB, HIN and KPN, respectively, in 45 minutes. However, the sample loading process involved a lot of pipetting steps which could potentially increase the chance of cross contamination. In addition, the sample volume of each chamber was relatively high compare to other devices which directly affected the overall cost.

In another study, multi-chamber PCR device was presented composed of a plastic chip fabricated by thermal forming and a multi-layer thermal cycler made of high thermally conductive silicon [69]. The design consisted of 16 chambers with volume of 20  $\mu\text{L}$  each in order to perform multiple PCR amplification. Also, a custom designed software could control the temperature of each micro-chamber individually. 30 PCR cycles could be performed in 15 minutes. No detail information about the PCR solution, DNA concentration and limit of detection of the device was reported. However, this study lacked two important factors, the low fabrication cost and the simplicity of the design.

C. S. Liao et al [70] demonstrated a micro-PCR device which was fabricated on soda-lime glass substrates by using photolithography and lift-off techniques in order to minimize the temperature non-uniformity. Moreover, the heaters and temperature sensors were located inside the micro-chambers with the volume of 10  $\mu\text{L}$  in order to monitor the

temperature in real-time. Parallel amplification of five common upper respiratory tract infection microorganisms including *Streptococcus pneumoniae*, *Haemophilus influenzae*, *Staphylococcus aureus*, *Streptococcus* and *Neisseria meningitidis* with concentration of 10 ng/  $\mu\text{L}$  were illustrated. 30 PCR cycles were performed before the amplification products were analyzed by using gel electrophoresis method. It was shown that the efficiency was comparable to the results of commercially available PCR machines. However, myriad of pipetting steps were required in order to fill the chambers and also to perform gel electrophoresis. Also, real-time detection of the amplification was not shown.

X. Fang et al [71] presented a multichannel microfluidic device which was capable of performing eight LAMP reactions in micro-channels simultaneously with the volume of 5  $\mu\text{L}$  each. Conically shaped inlets and outlets were implemented manually which helped to fill the channels without trapped bubbles. The novel part of the paper was the detection method, which was based on turbidity as a result of appearance of a white by-product, magnesium pyrophosphate, as the LAMP reaction happened. The turbidity could be either detected qualitatively by naked eye or quantitatively by a digital fiber optic sensor with sensitivity comparable to the benchtop fluorescent microscopes. Pseudorabies virus (PRV) was used as the DNA template. Also, the limit of detection was reported 10 fg/  $\mu\text{L}$  where the LAMP reaction was performed in water bath for an hour at the constant temperature of 63 Celsius. The disadvantages of using this device were dealing with a lot of pipetting steps which could increase the chance of cross contamination, non-reproducibility of the device because of manually implemented conically shaped inlets and outlets, as well as the need of specific optic equipment for quantitative detection.

In 2005, Z. Q. Zou et al [72] introduced a multi-chamber array device which was located on top of a printed circuit board (PCB) to accurately control the temperature for

performing PCR. Platinum sensors at the bottom of each reaction chamber were responsible for measuring the temperature individually. This device composed of 4 micro-wells with the volume of 2.5  $\mu\text{L}$  each. The amplification of 10 ng DNA in 25  $\mu\text{L}$  solution (the specification was not reported) was illustrated. Although their device showed a good potential to control the required temperature to perform 30 PCR cycles in 30 minutes due to the precise control over every micro-chamber, it was not an ideal candidate for disposable applications in terms of cost since it needed so many steps for fabrication including micromachining, photolithography as well as surface treatments which resulted in high cost of fabrication. Also, this method needed many pipetting steps in order to load the sample into micro-chambers and to extract the samples after the amplification in order to be analyzed by using electrophoresis methods. Additionally, real-time detection of the amplification was not shown.

W. Oh et al [73] designed a dual mode plastic cartridge with built-in valves including sample loading mode and sample sealing mode. A plastic fitting composed of the pipette tip guides and the rubber sheet facilitated the sample loading by using pipette, and sealed the device properly in order to eliminate evaporation and cross contamination. It was claimed that this sealing method had no dead volume with no leakage even when the temperature was increased to 100 Celsius for 30 minutes or the pressure raised to 8.1 Psi. Four micro-chambers with the volume of 0.95  $\mu\text{L}$  each were designed in order to perform parallel PCR amplification by using an external silicon-based heater plate. A HBV plasmid DNA was used as the DNA template to perform 50 PCR cycles in 25 minutes. Moreover, the lowest DNA concentration tested was  $10^5$  copies/ $\mu\text{L}$  which was amplified in about 12 minutes. However, performing high-throughput amplification by using this device was not feasible in resource-poor areas due to the need for many required pipetting steps which

could increase the chance of cross contamination as well as the need for a well-trained technician.

P. Neuzil et al [41] developed an ultra-fast microfluidic device for performing high throughput PCR including 10 PCR reactions simultaneously, which was able to go through 40 cycles in less than 6 minutes. After a few steps of deposition and lithography, the prepared silicon wafer was soldered to a printed circuit board (PCB) to enhance the mechanical support and for better electrical connections. Each reaction contained 100-nL of PCR solution covered by 1.1  $\mu\text{L}$  of M5904 mineral oil to eliminate sample evaporation and cross contamination. The PCR solution and the mineral oil were dispensed manually by using an adjustable pipetter onto the glass cover slip. The template used in the experiments was cDNA converted from total RNA of brain tissue from transgenic GFAP-GFP mice. A successful PCR amplification was illustrated in 14 minutes (the concentration was not reported). However, the detection setup introduced in the paper could only support one fluorescent sample per analysis. Although this device was capable of performing 40 cycles of PCR in a short time, it lacks the simplicity in terms of design and fabrication. Also, many pipetting steps were required in the sample loading process which is an important issue for devices to be used in resource-limited areas.

Y. Matsubara et al [74] presented a silicon micro-array chip which used a new method for DNA concentration quantification by counting the number of micro-wells which showed high fluorescence signal. The common method which had been used previously for quantification was based on real-time fluorescence intensity curve. The PCR solution was dispensed into the micro-chambers with volume of 40-nL each by using a nanoliter dispensing system. Also, the micro-chambers were covered by mineral oil to eliminate evaporation and cross-contamination. In order to fill the micro-chambers easily, an oxidized layer was left inside the micro-wells by photolithographic techniques to make

the surface hydrophilic. A conventional thermal cycling system was used to perform 40 cycles of PCR in 100 minutes. Moreover, parallel amplification and detection of five different genes related to *E. coli* was illustrated. The limit of detection was 0.4 copies/micro-well. Although this device showed a highly parallel amplification efficiency with low limit of detection, it needed sophisticated facilities and machines for device fabrication, sample loading, amplification and detection including a nanoliter dispensing system and a thermocycler. Moreover, the cost of operation and the disposability of the device could not satisfy the required criteria in order to be used in point-of-care settings.

C. Duarte et al [75] presented a silicon-based microfluidic device for detection of foodborne pathogens using LAMP. Four arrays of 6\*6 micro-wells with the volume of 30-nL each were fabricated on a silicon wafer by micromachining. Also, silane was coated on the surface of the micro-wells in order to prevent the adsorption of biomolecules. Prior to amplification, the primer sets were injected precisely in the micro-wells by using a micro-injector IM-300, followed by covering the micro-wells with mineral oil after dehydration of the primer solutions. The same micro-injector was used to insert primer-less solutions in the micro-wells. Next, the chip was put on an mK1000 heated stage in order to provide constant temperature of 65 Celsius. The lowest tested concentration of *E. coli* was 3 copies/micro-chamber which was amplified in 65 minutes. It was shown that primers re-suspended in the primer-less solution and the amplifications were done successfully. However, it was shown that the efficiency of the re-suspension of the primers decreased by time. For instance, after 10 days, the false negative ratio which was an indicator of the shelf life of the primers, increased drastically compare to day one. Although parallel detection of three foodborne pathogens were shown successfully without cross contamination (*E. coli*, *Salmonella* and *Listeria*), this device was not an ideal candidate to be used in resource-poor areas due to the required equipment like the micro-injector, the heated stage and the

fluorescence microscope for the real-time detection. Moreover, fabrication cost and disposability of the device were two other factors which make it not suitable for point-of-care devices.

T. Morison et al [76] demonstrated a microarray consisting of 3072 micro-chambers with volume of 33-nL each. It was claimed that the accuracy and precision of the real-time PCR was close to 384-well microplate but with less volume and higher throughput. Stainless steel was used as the substrate and the microarray pattern was implemented on its surface using photolithography and etching. Also, after a few deposition steps, the inner surface of the micro-chambers were became hydrophilic and compatible with PCR reagents and the outer surface of the micro-chambers were became hydrophobic to ensure a precise sample loading. Moreover, a 4-axis robot (XYZ $\theta$ ) was used to store the primer mix in the chambers. The RT-PCR was performed on a CycA amplicon titration and it showed that the device was capable of amplifying even 1 copy of the template (human heart and human liver RNA) per micro-well. Also, 66  $\mu$ L of PCR solution was required to fill the whole device. On the other hand, the fabrication cost was not mentioned in the paper and it was estimated to be relatively high compare to other techniques. Additionally, some advanced machines were needed to fabricate the device and perform the amplification such as 4-axis robot (XYZ $\theta$ ). Moreover, this device cannot satisfy the disposability criterion in order to be used in resource-poor settings.

#### **2.4.2. Capillary-based sample distribution**

In this section, the second group of high-throughput lab-on-a-chip devices, capillary-based sample distribution, is presented. In this group, the sample is separated into

different micro-channels or micro-wells through capillary action in order to perform either isothermal or non-isothermal amplifications.

N. Ramalingam et al [77] introduced a microfluidic device containing 5 unsealed micro-arrays with the volume of 5  $\mu\text{L}$  each, which were connected fluidically through a loading channel. However, the micro-reactor inside each micro-array had the volume of 192-nL. The sample was spread through the chambers based on capillary flow without a need for micro-valves and micro-pumps in order to reduce the complexity of the operation. Moreover, an absorbent pad was implemented in the waste chamber in order to remove the extra solution after sample loading. Also, the chambers were preloaded with HDA primers to perform HDA isothermal amplification. In terms of parallel amplification, 5 real-time HDA reactions were performed on this device at constant temperature of 62 Celsius for 30 minutes. A circular plasmid of SARS cDNA was used as a DNA template with the concentration of 0.01 ng/  $\mu\text{L}$ . Additionally, the evaporation problem which is the biggest issue in open chambers designs, was studied carefully. The disadvantage of this device was the large waste solution volume, 96% of the initial sample, including expensive reagents such as primers and enzymes which resulted in high cost of operation.

X. Fang et al [78] presented an octopus-like microfluidic device contained 10 micro-channels pre-coated with specific LAMP primers to perform parallel LAMP amplification. All channels had a same inlet but different outlets. Also, in order to prevent the cross-talk of probes among different micro-chambers, the inlet was connected to thin micro-channels with low-mass-transfer coefficients, followed by dimension gradient bridges and micro-chambers with the volume of 3.4  $\mu\text{L}$  each at the end of the channels. Parallel amplification of three influenza A subtypes including flu A virus, seasonal H1N1, and pandemic H1N1 subtypes were illustrated with limit of detection of 9, 10 and 8

copies/ $\mu\text{L}$ , respectively, within 0.5 hour. The qualitative detection by naked eye and quantitative detection by fluorescent microscopy and gel electrophoresis were shown successfully. Moreover, real-time detection of the LAMP reaction based on the change in the turbidity of the solution was displayed by implementing optical fibers and a mirror underneath the chip. However, advanced facilities were required in order to perform turbidity-based quantitative detection. Also, due to the loading mechanism introduced, significant amount of solution including expensive reagents was wasted.

M. Tourlousse et al [79] introduced a microfluidic device for performing parallel LAMP reactions which contained 15 interconnected micro-chambers with the volume of 1  $\mu\text{L}$  each. This device composed of three layers which were fabricated by using a hot embosser machine and a digital knife plotter. The primers were lyophilized in the micro-chambers prior to the layers assembly by using a pipettor. To avoid surface treatment in order to make it hydrophilic for more efficient sample loading, the inlet was designed in a way to be fitted with a 200  $\mu\text{L}$  pipette tip. Therefore, the sample was injected into the micro-channel by the means of the pipettor pressure and the trapped air inside the micro-channels escaped through the hydrophobic air vents located at the end of the channels. Moreover, parallel amplification of salmonella, campylobacter jejuni, shigella, and Vibrio cholerae with template concentration of  $10^5$  copies/ $\mu\text{L}$  was illustrated. Although the lowest limit of detection was not reported, the sensitivity between 10-100 copies/ $\mu\text{L}$  was achieved in 20 minutes. Beside the fact that this design displayed a good potential to be used in resource-limited areas, the fabrication process needed cumbersome facilities and delicate aligning of layers by a trained technician and the process of filling may not be scalable to hundreds of nanoliter micro-wells due to the many pipetting steps. Also, the lyophilisation process needed a lot of pipetting steps which could possibly increase the risk of cross contamination.

R. D. Stedtfeld et al [80] presented a wireless device for genetic testing called Gene-Z composed of a disposable microfluidic array, fluorescence detector, and an iPod Touch or an iPhone for data analyses. The design of the microfluidic device consisted of 4 arrays with 15 interconnected, pre-treated micro-wells with the volume of 1  $\mu\text{L}$  each, which was fabricated by using hot embossing method. The device design and the sample loading method by using a pipettor were similar to the previous described device [79]. It was claimed that it took a few seconds in order to fill all the channels completely. There was one LED per micro-well in the detection setup as an excitation light. Also, the highest sensitivity that was reported using Gene-Z was 13 copies of *E. coli* per reaction well in less than 30 minutes. In conclusion, Gene-Z showed a high potential to be used and manufactured in commercial scale for point-of-care applications. It was claimed that the whole package would cost around \$600 and each disposable chip would cost \$1.24 which are reasonable prices to be used at resource-poor areas. However, the process of filling may not be scalable to hundreds of nanoliter micro-wells due to the many pipetting steps. Also, half of the sample including expensive reagents was wasted by using the loading method introduced which was quite considerable since it resulted in higher cost of operation.

R. D. Stedtfeld et al [81] fabricated a microfluidic card with a novel distribution mechanism called airlock and it was designed to be used in Gene-Z machine [80]. An acrylic sheet was used as the substrate for the card and was patterned by using a laser cutter. The design composed of 64 interconnected micro-wells with the volume of 1.8  $\mu\text{L}$  each. The loading mechanism was based on capillary action in a way that an air bubble which was called airlock, was trapped between two successive micro-wells. Therefore, the airlock eliminated the mixing of the sample between the micro-wells. Also, the micro-wells were pre-treated with specific primer sets before loading the sample. This design was just suitable for isothermal amplification since by performing PCR, the airlock would move

around due to the temperature cycling and disturb the proper position of the sample. The sensitivity of the device was reported 20 copies of *E. coli stx2* per reaction in 30 minutes. Although this card was fabricated on a cheap material and there was no need for sophisticated equipment for fabrication, it still needed the Gene-Z in order to amplify and detect the signals. In addition, 160 microliter of sample was needed to fill the device completely which was relatively high compare to other designs. Moreover, around 30 percent of the injected sample was wasted in the connected micro-channel which could be considered as a flaw in its design.

C. N. Liu et al [82] developed a PCR-capillary electrophoresis (PCR-CE) device with four parallel systems. Each system had a separate chamber with volume of 380-nL and a capillary electrophoresis channel with the length of 5 cm for the means of detection. This device illustrated a decent sensitivity, down to 10 copies of pUC19 DNA per reaction in 30 minutes. The fabrication method was complicated where four different layers should have fabricated separately. Additionally, this method was readjusted to perform RT-PCR for RNA amplification by the same group of people by adding an extra step at beginning of the amplification for reverse transcription followed by 30 cycles of PCR [83]. Moreover, after each perform, the glass and PDMS parts were removed. Also, the channels and chambers were needed to be cleaned by using piranha to avoid cross contamination. Consequently, this device was not the best of its own to use in resource-poor areas where limited facilities, cost and time are vital factors.

Yu et al [84] presented one of the first attempts for high-throughput PCR amplification back in 2003. A microarray consisted of 1064 micro-chambers with the volume of 25 nL each was tested by fabricating a 3D mold which was made by doing two layers lithography. The chambers were connected to each other by the means of main and sub-channels. End-point detection method was performed by using a cofocusing Raman

spectroscopy. The identification of point mutations in the anemic family was shown by performing 30 PCR cycles in 45 minutes by using a thermocycler. Also, the limit of detection and DNA concentration were not reported. The disadvantages of this method were lack of real-time amplification as well as the need for advanced machines such as Raman spectroscopy machine and thermocycler.

O. Frey et al [85] presented a multi-channel microfluidic device with integrated liquid handling with capability to perform 10 parallel PCR reactions. The sample with the volume of 100-nL was precisely controlled and moved through different temperature zones by using a pneumatic actuation setup. Therefore, the sample was shuttled back and forth through the channel over three constantly heated regions. It took 0.5 second in order to move the sample from one heating area to the next one (12 mm distance). Also, the fluorescent detection was performed by focusing an inverted microscope on the second chamber of the channel where the extension reaction occurred (72 Celsius chamber). The PCR amplification of a plasmid DNA (the bacterium strain was not reported) with a concentration of  $4.4 * 10^6$  copies/ $\mu$ L was shown in 3 minutes (12 PCR cycles). Although the actuation and heating were done externally which reduced the overall cost, this method still required extra equipment to adjust the samples in parallel channels and lots of pipetting to perform parallel amplifications, which made it hard to be used in poor-resources areas.

Q. Zhu et al [86] introduced a novel digital LAMP microfluidic device which was able to compartmentalize the sample without the need for any external equipment. The key point is the PDMS porosity and its ability to dissolve air molecules. This design consisted of 4 main micro-channels and each micro-channel was responsible to connect 1200 micro-chambers with the volume of 6-nL each. After the PDMS device was fabricated, it was put in a vacuum chamber for 40 minutes to get rid of the trapped-air in the PDMS. Therefore, after the device was brought out of the vacuum chamber, there was a pressure difference

between the PDMS and the ambient pressure which was the driving force for the sample to fill the micro-channels and micro-chambers. Next, the sample filled the chambers completely followed by injection of fluorinated oil through the inlet port. Due to the pressure difference, the fluorinated oil filled the micro-channel and pushed the sample out of the micro-channel and discretized the micro-chambers. It was shown that the micro-chambers were disconnected after the fluorinated oil completely filled the micro-channel. Also, the serial dilutions of the DNA template (the  $\beta$ -actin DNA) were tested in order to quantify the initial concentration of the sample. The higher the concentration, the more micro-chambers were amplified. It was shown that the device was capable of quantifying the template concentration of 0.005 copies per micro-well. Moreover, a bench-top PCR machine was used to provide the constant temperature of 63 Celsius for 40 minutes in order to perform the LAMP reaction amplification. However, a CCD camera was required for the detection process as well as a well-trained technician.

J.S. Marcus et al [38] proposed a high-throughput microfluidic device to perform parallel RT-PCR in 72 micro-chambers with volume of 450-pL each. The push-up valves in each device were controlled by using an individual pressure sources. Multilayer soft lithography was used to fabricate the negative master mold. The device composed of three layers of PDMS and a glass coverslip which resulted in eight flow channels composed of two channels as the controls. Human male total RNA was used as the template. A flat plate thermal cycler was used to perform 30 cycles of RT-PCR which took about 75 minutes. End-point fluorescent microscopy was used for detection. Also, the limit of detection was reported as low as 34 copies/chamber. On the other hand, no real-time detection was illustrated. Additionally, some advanced facilities were required in order to use this device for point-of-care applications such as an individual pressure sources, a thermal cycler and a fluorescence scanner.

R. F. Ismagilov et al [87] introduced a microfluidic device called SlipChip composed of two plates which could move or slip relative to each other. The SlipChip mechanism is illustrated in Figure 2.4. The bottom and top plates contained lyophilized reagents in the micro-wells and micro-channels for loading the sample, respectively (Figure 2.4c). After loading the sample using a simple pipettor into the micro-channel, which was made by ducts in the bottom plate and wells in the top plate (Figure 2.4e), the top plate is slipped relative to the bottom plate in order to compartmentalize or digitize the sample into 1280 micro-wells with volume of 2.6-nL each containing specific dehydrated primers (Figure 2.4g). A lubricating layer of fluorocarbon was implemented between two plates to make the slipped move smoother.

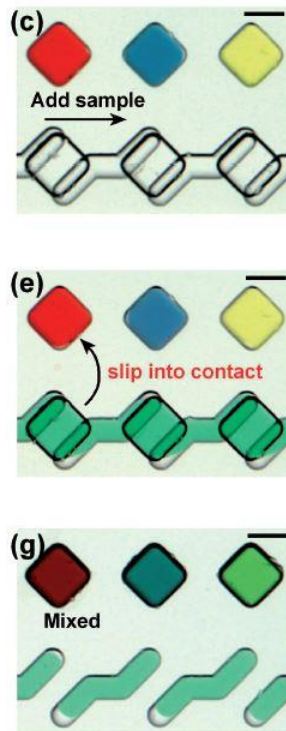


Figure 2.4 The SlipChip mechanism. (c) Lyophilized micro-wells located in the bottom plate. (e) Loading the sample in the micro-channel was made by ducts in the bottom plate and wells in the top plate. (g) Sample compartmentalization after the slipped move [87].

This device was used by the same group for various applications including but not limited to digital PCR for quantitative measurement of the DNA template concentration [88] and digital RPA as an isothermal amplification method [89]. In order to perform digital PCR, a thermocycling machine (Eppendorf) was used. The limit of detection of SlipChip device was reported 1 fg/ $\mu$ L of *S. aureus* which resulted in 0.008 copies per well after 35 PCR cycles in 77 minutes. Also, the end-point detection was illustrated by using a Leica stereomicroscope in order to quantify the initial concentration of the template. Moreover, the mechanical slipping mechanism may not be suitable for scaling up to 10,000 wells or more. Additionally, the heater was not integrated into the device.

#### **2.4.3. Centrifugal-based sample distribution**

The third category which is also known as lab-on-a-CD devices, is based on centrifugal forces due to the rotation of the device in order to distribute the sample. At a constant RPM, the applied force to the sample increases by moving from the center of the CD to its edges linearly.

M. Focke et al [90] presented a centrifugal microfluidic cartridge which was fabricated by a novel method called microthermoforming. The main master mould was made out of PMMA using a milling machine. Then, a PDMS replica was made out of the PMMA mould by casting. This PDMS replica could be used at least 140 times as the master mould in the hot embossing process to make a polymer foil which was the main substrate of the cartridge. This design consisted of four main segments and each segment had eight micro-chambers with the volume of 10  $\mu$ L each. The limit of detection of this device was reported 10 copies of exfoliatin toxin A (ExfA) per reaction well in 50 minutes. Although this novel cartridge decreased the fabrication cost and time, it still required a Rotor-Gene

2000 thermocycling instrument for two reasons, performing the PCR cycles and more importantly for the real-time detection.

Similar to the previous paper, a microfluidic lab-on-a-foil device was introduced by S. Lutz et al [91] for performing recombinase polymerase amplification (RPA). The fabrication method was pretty similar to the fabrication method of M. Focke et al [90] device. Also, the same thermocycler, a Rotor-Gene 2000, was used to perform RPA in order to keep the temperature constant at 37 Celsius as well as for real-time fluorescent detection. The design consisted of six main segments and each segment had five micro-chambers with the volume of 10  $\mu\text{L}$  each. A capillary siphon and a centrifugo-pneumatic valve in conjunction with the modified Rotor-Gene 2000 were in charge of distributing the fluid into 30 different micro-chambers which could potentially amplify 30 different samples with lyophilized reagents beforehand. The antibiotic resistance gene *mecA* of *Staphylococcus aureus* was used as the template. The sensitivity was reported 10 copies per reaction well in less than 20 minutes. Again similar to the previous mentioned paper, although this device decreased the fabrication cost and time, it needed expensive equipment such as the thermocycler beside to the lots of pipetting steps to perform parallel amplifications.

A rotary RT-PCR system to perform parallel amplification was introduced by J.H. Jung et al [92] which combined stationary and flow-through designs. The propeller-shaped device had three micro-chambers with the volume of 1  $\mu\text{L}$  each which were precisely rotated and controlled by a stepper motor using a LabVIEW program on top of three stationary heaters which provided the required temperatures for PCR. After performing the PCR, the samples were collected for electrophoresis. Therefore, no real-time detection were illustrated using this setup. Influenza A H3N2 viral RNA was used as the template. The limit of detection was as low as 2 copies per chamber in 25.5 minutes of performing PCR followed by 5 minutes electrophoresis. Although a high-throughput design was not tested

in this paper, this simple design had the potential for high-throughput amplification by implementing a lot of micro-chambers in the design of each segment. Also, the suggested device required pipetting steps after amplification in order to perform electrophoresis.

S. J. Oh et al [93] presented a high-throughput microfluidic device to perform LAMP by combining the centrifugal approach and colorimetric detection by using Eriochrome Black T (EBT) which is a metal indicator based on the change of the concentration of the metal which in LAMP reaction is magnesium pyrophosphate. The device composed of four layers including two polycarbonate (PC) layers which were patterned by using CNC machining, one double-sided adhesive layer which was shaped by a cutting plotter, and a pressure sensitive adhesive foil layer. Five main segments with 5 micro-chambers with the volume of 12.5  $\mu\text{L}$  each were implemented in the design. Each segment included two zigzag-shaped micro-channels for holding the LAMP master mix and primer mix. After loading all solutions in the device and putting it on the custom-made centrifugal system, the solutions were moved to the micro-chambers sequentially by increasing the RPM after it passed the burst RPMs which were 500, 1000 and 2000 for the LAMP master mix, the LAMP primer mix and DNA template, respectively. A lab oven which was set at 65 Celsius, was used for 60 minutes to provide the required temperature for the LAMP reaction. The detection could be done either qualitatively with naked eye due to the change of the color of the mixture from purple to sky blue or quantitatively by measuring the UV-vis absorbance of the EBT using a spectrophotometer. Also, detection sensitivity and specificity were analyzed thoroughly. The limit of detection of the device was reported 380 copies of *E. coli* O157:H7 per chamber in an hour using the colorimetric based detection introduced. However, for completely loading all the solutions and samples into the device, 35 pipetting steps were needed which could possibly increase the chance of cross contamination. Also, an oven was needed as a heat source which added an extra

equipment for performing the device, on top of the custom-made centrifugal system for sample distribution. In addition, real-time detection of the reactions were not possible with this configuration.

#### **2.4.4. Droplet-based sample distribution**

The last group of the categorization is droplet-based sample distribution which is based on two phase flows. In droplet-based microfluidic devices, myriad number of discrete volumes can be generated in short amount of time based on immiscible phases, normally water in oil. One of the methods to generate droplets is T-junction configuration where two channels intersect with each other perpendicularly, one containing the disperse phase and one the continuous phase. The uniformity of the droplets is an important issue which can be controlled by manipulating the geometry of the channels, viscosity of the solutions, flow rates and the surface wettability [94].

N.R. Beer et al [95] presented the first microfluidic device to generate picoliter size droplets in order to perform PCR amplification. T-junction method was implemented to generate 10-pL size droplets which were controlled by an off-chip valving system. This device was able to generate around 1000 droplets per second. According to the Poisson statistics, each droplet contained less than one copy of the DNA template. The PCR was performed by using a Melcor 3628 Peltier device with a PID controller which could finish 40 PCR cycles in 108 minutes. A Nikon TE2000-U microscope was used for real-time fluorescence detection. Moreover, Vaccinia Western Reserve genomic DNA was used as the template. The limit of detection was reported 0.06 copies per reaction which was amplified in 18.3 cycles (22 minutes). Therefore, this device showed a significant reduction in the volume of PCR reactions compare to commercial PCR machines and it was capable

of amplifying and detecting single copy of the DNA template. However, many state-of-the-art facilities were required in order to use the device such as two pumps to control the flow rates, an off-chip valving system, a PCR thermocycling machine, an expensive fluorescence microscope as well as cumbersome data analyses procedures which made it hard to use at resource-poor areas.

X. Leng et al [96] introduced a novel approach for high-throughput PCR amplification based on generating nanoliter-volume agarose droplets with PCR reagents in carrier oil. The device was able to generate 500 uniform agarose droplets per second. The size of the droplets were tunable based on the width of the channels and the flow rates. By diluting the PCR sample, it was shown that statistically, there were no more than one DNA template in each droplet with the volume of 3-nL which helped to quantify the initial concentration of the sample. Lambda DNA was used as the template to perform PCR. After the amplification, the temperature was reduced below the gelling point. Then, the agarose droplets turned into the solid gels to be able to keep them separate even after removing the carrier oil. Fluorescent detection was done after the amplification by staining the beads with SYBR Green. Therefore, no real-time detection was illustrated in this setup. The limit of detection was reported 0.15 copies per reaction after 25 PCR cycles. Also, having an accurate setup for controlling the flow rates was a vital factor to generate uniform size droplets which eventually, increased the operation cost. Additionally, the suggested detection method involved collecting and washing the beads after the amplification, staining the beads and taking the fluorescence picture followed by data analyses steps which was complicated and cumbersome for point-of-care applications.

Y. Zeng et al [97] developed a microfluidic emulsion generator with the capability of producing 3.4 million nanoliter-volume droplets per hour which was capable of analyzing a single cell. The size of the droplets was 2.5-nL. This device contained four

main layers including 3 layers of glass wafer and one layer of thin PDMS membrane. A homemade pneumatic setup was used to control the micro-pumps. *E. coli* O157:H7 cells was used as the template for PCR amplification. Also, a multicolor flow cytometer was used to analyze the droplets after performing the emulsion PCR. Detection of different pathogens was illustrated by staining each pathogen with a specific fluorophore. The limit of detection was reported 1: 10<sup>5</sup> *E. coli* O157 cells in a high background of normal K12 cells in 30 minutes. Moreover, various designs were shown for the device ranging from 4 to 96 channels to generate droplets. Although this device displayed a great potential to perform parallel emulsion PCR, it was highly depended on the multicolor flow cytometer for detection which is an expensive machine and made it unfeasible to be used in resource-limited regions such as third world countries. Also, the disposability of the device was not discussed which could drastically increase the operation and fabrication costs.

## **2.5 Summary**

This chapter provided an overview on nucleic-acid-based technology (NAT) and its key role in molecular diagnosis. A general categorization of nucleic-acid amplification methods was presented based on thermal condition of the amplification reaction followed by introducing PCR and the most recent developed isothermal methods in detail. Also, the advantages of using microfluidic devices in biomedical field were discussed by going through the recent innovations and novelties of high-throughput amplification devices in order to produce and fabricate a sensitive, disposable and inexpensive point-of-care tool to be used in resource-poor countries where early diagnosis of deadly bacteria could be a lifesaver. Finally, high-throughput devices were classified into four groups based on the

mechanism which was used to distribute the sample into various micro-chambers or micro-channels, and the advantages and disadvantages of each of them were explained.

## **Chapter 3: Device Design, Materials and Methods**

In the previous chapter, nucleic acid based diagnostic methods were discussed and the microfluidic devices that have been developed to automate and parallelize them were also detailed. Although several improvements have been made, a low cost simple method to perform DNA amplification in the field has not been achieved.

In this chapter, the design criteria and constraints for such a device for resource poor settings are detailed. Next, a design of a microfluidic device that could meet the design criteria is proposed. The device includes two components, the micro-wells and the flexible heater. First, the design of the micro-well component is discussed by introducing the design constraints, followed by the parameters which affect the signal intensity and the limiting factors using lithography method.

Then, the flexible heater design process is presented, including CAD design in AutoCAD and design simulation using COMSOL Multiphysics Software to analyse the uniformity of the temperature gradient. Then, device fabrication including the micro-well and the flexible heater components, sample preparation, experimental setup containing large field of view fluorescence detection system and image processing method using ImageJ are explained in detail.

## **3.1 Device design**

### **3.1.1. Design criteria**

The intended purpose of the device was to design a simple to use, fast, inexpensive and disposable device to perform isothermal parallel DNA amplification in order to be used in resource poor settings where there is no access to expensive instrumentation or skilled personnel.

The first criterion which was considered in designing the device was the volume of the sample which was defined according to the end application. Typical DNA based assays use a 25  $\mu\text{L}$  volume for analysis as the reagents used such as the polymerase enzymes and the primers are expensive to prepare in larger volumes or high concentrations. A pre-concentration or enrichment step as well as a purification step usually precedes the DNA amplification in order to obtain enough detectable concentration of the sample DNA. Therefore, the total micro-well volume was designed to accommodate a total volume of 25  $\mu\text{L}$ .

The next criteria to be considered was the viscosity of the sample. The viscosity of the sample is critical factor that must be considered in the filling of the microscale amplification chambers. Since pre-processing of the sample will be performed, the DNA will be suspended in a buffer solution and the typical viscosity will be similar to that of water. Therefore, DNA suspended in buffer medium was used as a sample solution.

Other important criteria in designing the device were cost and time of operation. As it was discussed in detail in chapter 2, parallel amplification strategy, performing different reactions simultaneously on one device, was implemented on many recent devices in order

to reduce the cost, the time of operation and the chance of cross contamination by decreasing the required manipulation steps [98]. Moreover, another part of the device which directly affects the final cost of the device, is the energy source required to provide the constant 65 Celsius temperature during the amplification time. Therefore, plotting method was used in order to fabricate inexpensive flexible heaters.

Finally, the simplicity of operating the device is another criterion in designing the device. An ideal microfluidic device does not require any advanced technologies or trained technicians in order to perform the device and analyse the data. In this regard, a simple segmentation method in order to generate a large number of aliquots of the sample is introduced, which eliminates the use of high-tech and expensive equipment such as micro-pumps or two phase flows.

In the next section, the schematic of the designed device is presented.

### **3.1.2. Schematic of the device**

According to the design criteria which were discussed in the previous section, a microfluidic device to perform parallel DNA amplification was designed. The device composed of two components, a micro-well array and a flexible heater. The schematic of the device is illustrated in Figure 3.1.

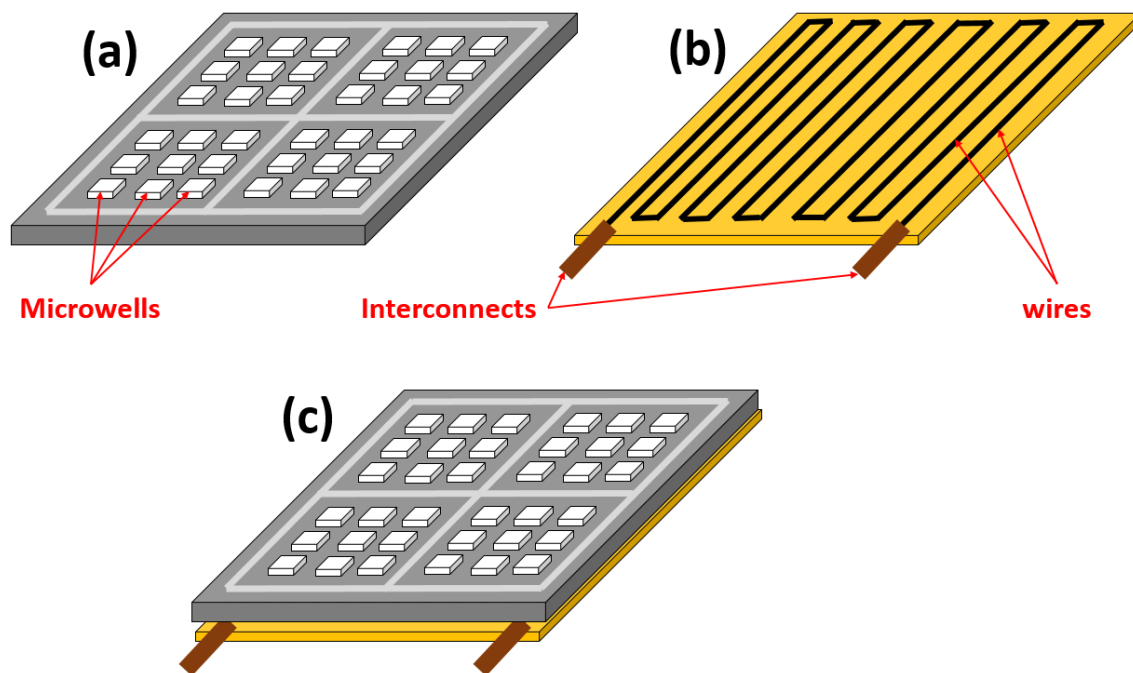


Figure 3.1 The schematic of the device. (a) The micro-well array. (b) The flexible heater. (c) The integrated device.

The device is designed to have an array of micro-wells that could partition and hold small volumes of the sample and the amplification mixture as shown in Figure 3.1a. Groups of wells are surrounded by a moat that isolate it from the next group of wells. The moat was designed so that the adjacent groups of wells could be filled with different reagents or samples without cross-contamination. Finally, a low cost flexible heaters (Figure 3.1b) were designed to be attached to the bottom side of the thin micro-well array in order to uniformly heat the wells and the samples in them to the isothermal amplification temperature.

The micro-well array uses a simple segmentation technology has been developed previously in our lab to uniformly aliquot nL-  $\mu$ L volumes of materials into the wells or the

array by simply moving the sample back and forth on top of the array. This technology has been used for cell culturing application as it is shown in Figure 3.2 [99] but not for DNA amplification. Ayyash et al used it to detect bacterial viability and drug resistance based on oxygen consumption or production of metabolites.

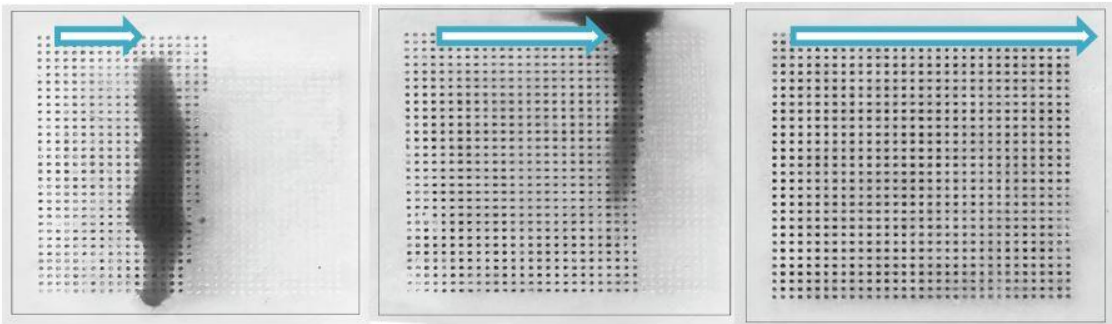


Figure 3.2 The micro-wells design for bacteria detection application where the dimension of each nano-well was  $100*100*100 \mu\text{m}$  [99].

The key element of the segmentation technology was to make the inside of the micro-wells hydrophilic and the outside hydrophobic which helped the sample to fill the micro-wells smoothly. This method was the foundation of this thesis which is described in detail in section 3.6.

This simple segmentation method could potentially be used for aliquoting precise sample volumes into multiple micro-wells for parallel amplification. However, in order to use this sample loading method for the purpose of DNA amplification, the dimensions of the wells such as the shape and the height and the spacing between them have to be determined and are optimized in section 4.2 in chapter 4, based on the requirements and constraints, such as having the minimum number of trapped bubbles and maximum difference between the positive and the negative signals.

As it was discussed in the previous section, performing parallel DNA amplification was one of the design criteria. In this regard, four separate regions were designed on the chip in order to show the ability of the device to perform parallel DNA amplification for more than one pathogen at a time. For instance, in the case of food contamination, assays for common foodborne pathogens such as *E. coli*, *Listeria*, *Salmonella* and others are conducted on the sample simultaneously along with appropriate negative control.

The designed chip could potentially parallelize those assays by immobilizing appropriate primers in the wells so that a sample could be distributed in all the wells and then parallel assays could be conducted. These four regions were separated by the means of the waste channel which was implemented in the design for two reasons, to collect any extra sample that was dispensed and to prevent the reagents from one region to get mixed with the reagents from another region during sample loading step. The efficiency of the waste channel in the design is illustrated in section 4.2 in chapter 4.

### **3.1.3. Challenges to be tackled**

In this section, two challenges which were required to be tackled in designing the micro-well component, are presented.

#### **3.1.3.1 Trapped bubbles**

Bubble formation is a big issue in most PDMS-based microfluidic systems due to the hydrophobicity of the PDMS surface and temperature or pressure gradient in channels or wells [100].

In the sample loading step, bubbles can be trapped in the micro-wells due to the presence of the surfactants and the other constituents of the DNA amplification mixture. In order to show the difference between the filling efficiency of the amplification solution and DI water, Figure 3.3 is illustrated. A micro-well component composed of micro-wells with dimensions of  $320 \times 320 \times 100 \mu\text{m}$  was filled once with methylene blue solution (0.05 M) in DI water to be able to observe the filling process with the naked eye (Figure 3.3a), and once with a positive amplification solution contained primer mix, master mix, DNA staining dye (EvaGreen 20X) along with the extracted DNA from *E. coli* STEC eae with the concentration of  $4 \times 10^6$  Copies/ $\mu\text{L}$  (Figure 3.3b). The sample loading process is described in section 3.6.

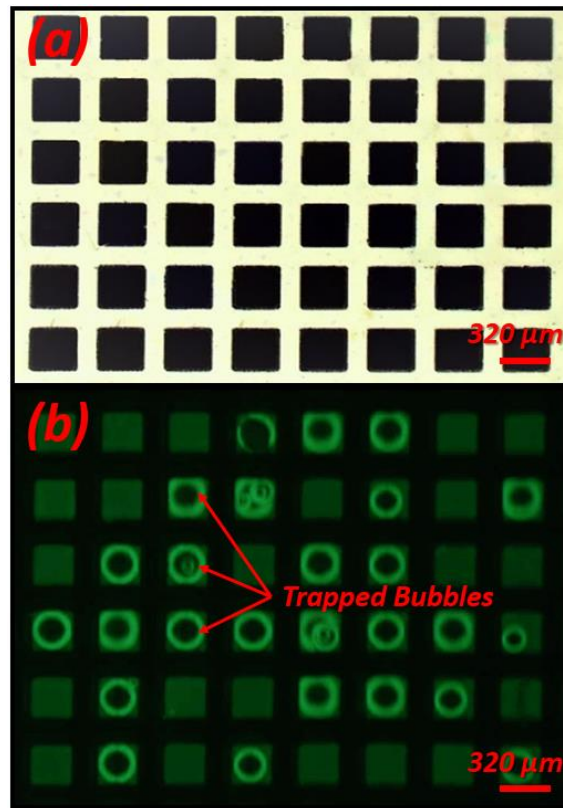


Figure 3.3 A micro-well component composed of micro-wells with dimensions of  $320 \times 320 \times 100 \mu\text{m}$  was filled (a) once with the methylene blue solution (0.05 M) in DI water

and (b) once with positive amplification solution. The high reflective edges are evident in the micro-wells with trapped bubble inside.

As it is shown in Figure 3.3a, no bubble were trapped in the micro-wells which were filled with the methylene blue solution (0.05 M) in DI water. However, half of the micro-wells in Figure 3.3b had trapped bubbles inside them. Therefore, it indicated that the bubble formation problem was due to the presence of the surfactants and the other constituents of the DNA amplification mixture. As a result, the dimensions of the micro-wells such as the shape and the height and the spacing between them are required to be optimized to achieve higher filling efficiency which are explained in section 4.2 in chapter 4.

Additionally, as it is shown in Figure 3.3b, trapped bubbles could cause high reflective edges which conceivably increases the cross-talk problem that results in high background noise [101]. Moreover, since the device is heated up to 65 Celsius to perform LAMP amplification, a trapped bubble may undergo expansion which can potentially detach the sealing of the device from the PDMS surface and provoke leakage of the sample.

Additionally, other than hydrophobicity of the PDMS, the viscosity of the sample is another factor which manipulates the filling process. Due to the presence of surfactants in the master mix which is one of the components of the amplification sample, the contact angle of the amplification solution is smaller than the DI water [100].

### **3.1.3.2 Difference between positive and negative samples**

Another challenge to be tackled in designing the micro-wells component is the capability of the device to differentiate between the amplified and unamplified micro-wells

as well as the ability to observe the real-time S-shaped amplification curve. The wells cannot be shallow as the contrast between the amplified and unamplified wells will be lower than the detection sensitivity. However, shallow wells can be filled with less solution which reduces the cost. Therefore, an optimization is needed in order to choose the appropriate height.

The difference between the positive and negative samples is directly related to the Signal to Noise Ratio (SNR). The higher SNR results in more reliable signals and lower possibility of the false positive results. According to the observations, the height of the micro-wells had the most significant effect on the signal intensity. The higher height brings about more powerful fluorescence signal. The reason behind this phenomenon is although the camera is focused on one horizontal layer inside the micro-well, somewhere between the top and the bottom surfaces, the emitted intensities from other layers accumulate and increase the gross intensity of the micro-well.

Micro-wells with different heights were fabricated to analyze the effect of the height on the intensity. The protocol developed in this regard can be found in appendix A.

Spacing between the micro-wells is a key factor in terms of crosstalk problem. The bigger spacing results in lower crosstalk problem but causes having less micro-wells in a specific area.

#### **3.1.4. Flexible heater design**

As it was described in chapter 2, the end goal of the project is to design a cheap, affordable and portable device which is disposable at the same time as well. A heat source is an inevitable part of the setup since the LAMP reaction works at 65 Celsius.

Although various options are available to use as a heat source in order to provide the required energy for the LAMP reaction, including the commercially available flexible heaters, portability of the device circumscribes the choices. One of the options is the commercially available flexible heaters, for instance Kapton® Insulated Flexible Heaters (Omega, QC, Canada) which satisfies the portability, but not the cost and disposability criteria. For instance, a 5\*5 cm Kapton heater costs CAD \$55.

Moreover, the temperature gradient is not uniform all over these kinds of heaters. A hot spot was observed at the center of temperature gradient of these heaters due to the higher heat transfer rate at the edges compare to the center of the heater. This is not an ideal heater since all the micro-wells need to be at the same range of temperature to be able to compare the results of the micro-wells together.

Based on the described reasons, the idea of designing and fabricating a cheap, portable and disposable heater was ignited with the goal of designing a flexible heater with temperature uniformity more than or equal to the commercially available heaters. Plotting method was used to make heaters which was previously developed in our lab, CAMEF, by Juncong Liu. This method is introduced in section 3.3.2.

The main criteria which were considered in designing flexible heaters, were the uniformity of the temperature gradient, the fabrication cost and the electrical power consumption which are analysed in detail in section 4.3.2 in chapter 4. The uniformity of the temperature gradient depends on the pattern of the design and the fabrication cost depends on the total length of the used micro-wire as well as the material of the micro-wire.

In the following sections, all the materials which were used in both the device fabrication as well as in the experiments and sample preparation are presented. Next, the

experimental setup is described in detail. Finally, the image processing technique is presented and the reasons behind each steps.

## **3.2 Materials & Experimental Setup**

First, materials for device fabrication are listed, followed by reagents that were used for the biochemical assays and sample preparation. Also, equipment which were used in experimental setup, are introduced.

### **3.2.1. Silicon wafer**

Silicon wafers were used as a substrate in the photolithography process to define mold for the fabrication of the micro-wells. Different sizes of wafers are available, from 1 to 12 inches (2.5 to 30.5 cm). The 3-inch (7.6 cm) silicon wafer (University Wafer, MA, USA) was selected as it was suitable to fit the design of the device.

### **3.2.2. Photoresist**

SU-8-100 (Microchem Corp, MA, USA), which is a negative photoresist, was chosen to fabricate PDMS molds. SU-8 is an epoxy-based photoresist which is commonly used in micromachining and microelectronic applications where chemical and mechanical stability are important. There are two types of photoresist, negative and positive. The former crosslinks upon exposure to UV light and becomes insoluble in the photoresist developer. While, the latter undergoes chemical modification and becomes more soluble to

its photoresist developer after exposure to UV light. A negative photoresist was chosen for making the molds as it is more long lasting and has higher structural strength as compared to the positive photoresists. Although many versions of SU-8 are available, SU-8-100 was chosen as it is capable of producing layer thicknesses between 100 to 700  $\mu\text{m}$  that is needed in this device design.

### **3.2.3. Polydimethylsiloxane (PDMS)**

PDMS (Sylgard 184 silicon elastomer kit, Dow Corning Corp, MI, USA) is a transparent polymer which is commonly used in the microfluidic field. The chemical formula is  $\text{CH}_3[\text{Si}(\text{CH}_3)_2]_n\text{Si}(\text{CH}_3)_3$ ,  $n$  being the number of monomers repetitions. The reasons behind selecting PDMS as the main material of the device in this thesis are some of its unique properties like transparency, biocompatibility, inertness, non-flammability and most importantly, the ability of PDMS to replicate features in micro/nanometer scale for rapid prototyping of microfluidic devices [102], which makes it an ideal material for biomedical research.

### **3.2.4. Sealing film**

Microseal B PCR plate sealing film (Bio-Rad Laboratories, ON, Canada) was used to seal the PDMS micro-array device. This is a commonly used clear polyester for high sensitivity optical assays. It was chosen as the sealing film because it is less water permeable compare to other sealing options and can prevent the sample evaporation due to the amplification temperature.

### **3.2.5. Micro-wire**

Different micro-wires, in terms of material (silver, copper and nichrome) and size (25 to 500  $\mu\text{m}$ ), were considered for the fabrication of flexible heaters. Smaller wires are harder to work with since the chance of breakage increases. Finally, X-Wire™ Coated Copper Bonding Wire (Microbonds Inc., ON, Canada) with wire diameter of 25 and 50  $\mu\text{m}$  was chosen as the suitable one for the fabrication of the flexible heaters using plotting method which is described in section 4.3.2.

### **3.2.6. Pressure sensitive adhesive (PSA)**

PSA film (3M, ON, Canada) was used to hold the micro-wires patterns that were created in the plotting process in place. The films are a bilayer stack of adhesive (91  $\mu\text{m}$ ) and liner (102  $\mu\text{m}$ ) and made of acrylic. This material is rated to be used for a short period of time (minutes to hours) at 148 Celsius and for longer periods of time (days to weeks) at temperatures up to 93 Celsius. It comes in standard sheet size of 60.9\*91.4 cm which is then cut to shape.

### **3.2.7. Electrical interconnects**

In order to make a rigid connection between the micro-wires that are embedded in the device and external electrical connection, a highly conductive copper electrical tape with conductive adhesive (76555A641, McMaster Carr, Cleveland, USA) was used. So, the chance of breaking the micro-wires was reduced when connecting it to the power supply. The width of the tape was 6.35 mm with the thickness of 0.09 mm. The thickness

of the copper and the acrylic adhesive layers were 0.03 mm and 0.05 mm, respectively. Also, the working temperature range of this tape was between -40 to 162 Celsius. The electrical resistance through adhesive layer with dimensions of 0.63 cm and 2.5 cm was 0.010 ohm.

### **3.2.8. Bacterial DNA**

The bacterial DNA that was used in this thesis was extracted from Escherichia Coli (E.Coli) bacteria. Various extraction methods can be used in order to extract the DNA from the bacteria which were explained in section 2.1 in chapter 2.

E. coli is a gram-negative, rod-shaped, coliform bacterium. Most strains are harmless but some can cause food-poisoning and diarrhoea. They can be commonly found in the lower intestine of humans and animals.

The serotype which was used in these experiments was the one containing the Shiga toxin eae virulence factor gene of E. coli 0157. Shiga toxin-producing Escherichia coli (STEC) strains are the main group of food-borne pathogens. Also, the protein which is responsible for the attachment of the bacteria to intestinal epithelial cells is encoded by the chromosomal gene eae, is called intimin. The stains which have this eae genes are responsible for severe diarrhea and hemolytic uremic syndrome [103]. As it was mentioned in the previous chapter, Pathogenic E. coli causes about 73,000 cases of foodborne illness each year in the U.S. Also, it can easily and economically be grown in laboratories. So, because of these reasons, it was chosen as the model to study in this thesis.

### 3.2.9. DNA staining dye

EvaGreen 20X (Biotium, CA, USA) is a green fluorescent nucleic acid dye which shows higher efficiency compare to other common dyes in different applications such as qPCR, high resolution DNA melt curve analysis (HRM) and capillary gel electrophoresis. After intercalation in dsDNA, the peak of the excitation spectrum is 500 nm and the peak of the emission spectrum is 530 nm (Figure 3.4).

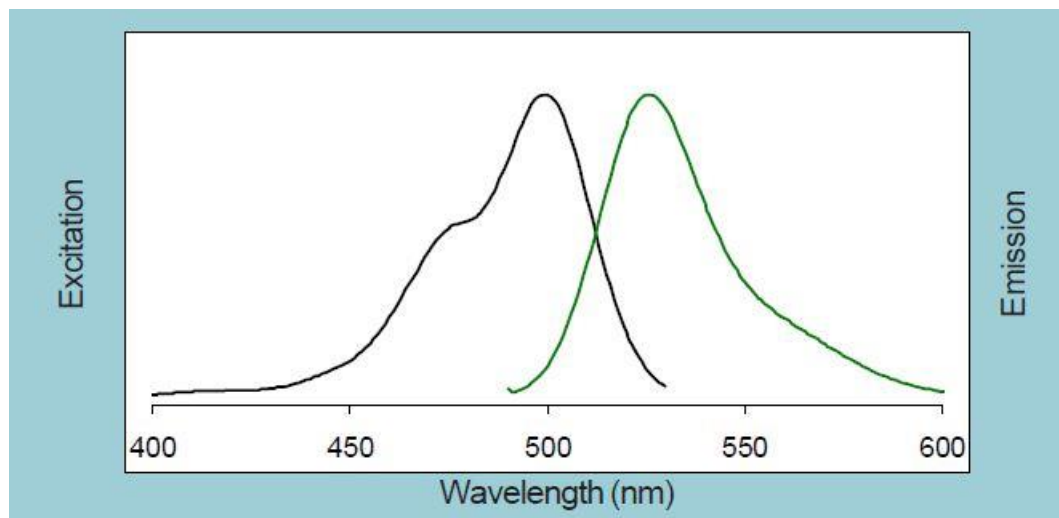


Figure 3.4 The excitation (left) and emission (right) spectra of EvaGreen dye [104].

EvaGreen is considered as a very stable dye, thermally and hydrolytically. Also, the dye is not fluorescent by itself but becomes highly fluorescent when it intercalates with dsDNA. EvaGreen Dye binds to dsDNA through a mechanism called release-on-demand. The dimeric dye molecule which may have a hairpin structure is non-fluorescent or minimally fluorescent by itself. Before the dye binds to dsDNA, there is an intermediate state called an open random conformation which can be found in lesser quantity compare to the dimeric form. After the dye binds to the dsDNA in the open random conformation,

the fluorescent intensity increases significantly. As the amplification moves forward and more dsDNA produces, this ratio changes and more open random conformation can be found which enhances the release-on-demand mechanism [105].

Moreover, another advantage of EvaGreen over other staining dyes such as SYBR Green I is that it is completely impermeable to cell membranes and also does not enhance cell mutations. Because of all these properties, it was chosen as the DNA staining dye in this thesis.

#### **3.2.10. Fluorescein dye (free acid)**

A highly concentrated solution of fluorescein dye (Sigma-Aldrich Co., ON, Canada) was used to test the filling of the device since it is auto fluorescent (no need to have double stranded molecules to get intercalated with) and soluble in water. Also, the excitation peak and the emission peak are 494 nm and 521 nm, respectively; since they are close to the excitation peak and the emission peak of the EvaGreen dye, the same detection setup was used.

#### **3.2.11. Methylene Blue**

Methylene Blue (0.05 M) (Sigma-Aldrich Co., ON, Canada) was used to add blue color to the water for the filling tests to be able to see the water with the naked eye.

### **3.2.12. Master Mix without dye**

Master Mix ISO-001nd (Pro-Lab Diagnostics, ON, Canada) was used for isothermal amplification. The master mix contains OptiGene's proprietary novel GspSSD LF DNA Polymerase as well as the deoxynucleotide triphosphates (dNTPs) and MgSO<sub>4</sub> at their optimum concentrations. This master mix does not contain any specific reverse-transcriptase (RT) enzymes. Primers, sample DNA and an intercalating fluorescent dye should be added to the master mix to perform the LAMP reaction.

### **3.2.13. Primer Mix**

The Primer Mix was provided by our collaborator in department of pathology and molecular medicine at McMaster University, Professor James Mahoney's laboratory. It had a proprietary sequence and consisted of 6 specific primers including F3 and B3 primers at 0.2 μM, FIP and BIP primers at 0.8 μM, and LF and LB primers at 0.4 μM, for detection of eae virulence factor gene of E. coli (Escherichia coli) 0157.

### **3.2.14. Film sealing roller for PCR plates**

A Film sealing roller for PCR plates (Bio-Rad Laboratories, ON, Canada) was used to properly and uniformly stick the PCR film to the PDMS device.

### 3.2.15. Power supply

A GPS-3030DD power supply (GW INSTEC, New Taipei City, Taiwan) was used as a power source to heat up the flexible heater during the experiment. It can provide voltage up to 30 volts and current up to 3 amps.

### 3.2.16. Kapton heaters

Kapton heaters, HK913 (Minco, MN, USA) were used as a reference to compare their performance with the flexible heater made by plotting method. The main used material of these heaters is Kapton with the thickness of 0.05 mm made out an etched-foil resistive heating element and is capable of tolerating 200 Celsius. The performance parameters which were considered in the comparison between these heaters were temperature uniformity, cost as well as electrical power consumption.

<b>Model</b>	<b>1 (HK913-C)</b>	<b>2 (HK913-D)</b>	<b>3 (HK913-J)</b>
<b>Resistance (<math>\Omega</math>)</b>	120	160	275
<b>Heater Size (cm<sup>2</sup>)</b>	21.3 (3.8 × 5.6)	25.8 (4.6 × 5.6)	34.2 (3.3 Radius)

Table 3-1 Kapton Heaters specifications.

### 3.2.17. Thermocouple

The 5SRTC flexible thermocouple (Omega, QC, Canada) was used to measure the temperature inside the waste channel at the proof of concept stage of the project. Its flexibility brought about easier insertion into the channel. The diameter of the thermocouple

was 0.51 mm with a Kapton insulation layer around it. Also, the maximum service temperature of the thermocouple was 260 Celsius. Additionally, the temperature sensitivity of this thermocouple was 0.6 Celsius at the temperature above 0 Celsius.

### **3.2.18. Thermometer**

The thermocouple was connected to the Fluke 50 series II thermometer (Fluke, ON, Canada) to read the working temperature inside of the waste channel with the accuracy of 0.05% + 0.3°C.

### **3.2.19. FLIR ONE thermal imaging camera**

FLIR ONE (FLIR, MA, USA) was used to determine the temperature distribution from the top surface of the flexible heater in order to compare it with the simulation results. This device works based on infrared signal detection.

### **3.2.20. ESEQuant tube scanner**

In order to validate the microfabrication amplification device and compare its performance to existing systems, an ESE-Quant TS95 (QIAGEN, Hilden, Germany) tube based isothermal amplification system was used.

This machine is capable of performing eight separate reactions simultaneously. Also, it can provide a set temperature in the range of 15 to 95 Celsius which makes it possible to

run a variety of isothermal amplification reactions. Moreover, this machine is also capable of measuring the intensity of the fluorescence in the amplification mixture in real-time.



Figure 3.5 The ESE-Quant TS95.

The ESEQuant Tube Scanner is accompanied by the Tube Scanner Studio software (version 2.07.06 - BioLight Luminescence Systems, Baden-Württemberg, Germany), which can process the data and plot intensity time curves and also other detailed analysis.

### **3.3 Device fabrication**

Fabrication of the device was a multi-step process as shown in the fabrication process flow (Figure 4.3). The device consisted of a micro-well array and a flexible heater that were fabricated separately and then integrated together at the final step. The fabrication of the micro-wells started with photolithography technique for making the master mold which

started with photoresist spinning (Figure 3.6a), followed by UV exposure through the photomask (Figure 3.6b) and developing the master mold in the SU8 developer to remove the photoresist in the unexposed regions (Figure 3.6c). The next step was PDMS casting (Figure 3.6d) and peeling off the PDMS (Figure 3.6e). The second part was the fabrication of the flexible heater using plotting technique which was performed by writing the designed pattern on PSA (Figure 3.6f) and attaching the connectors to the micro-wires (Figure 3.6g). And finally, the assembly of the device by putting the micro-well and flexible heater parts together (Figure 3.6h).

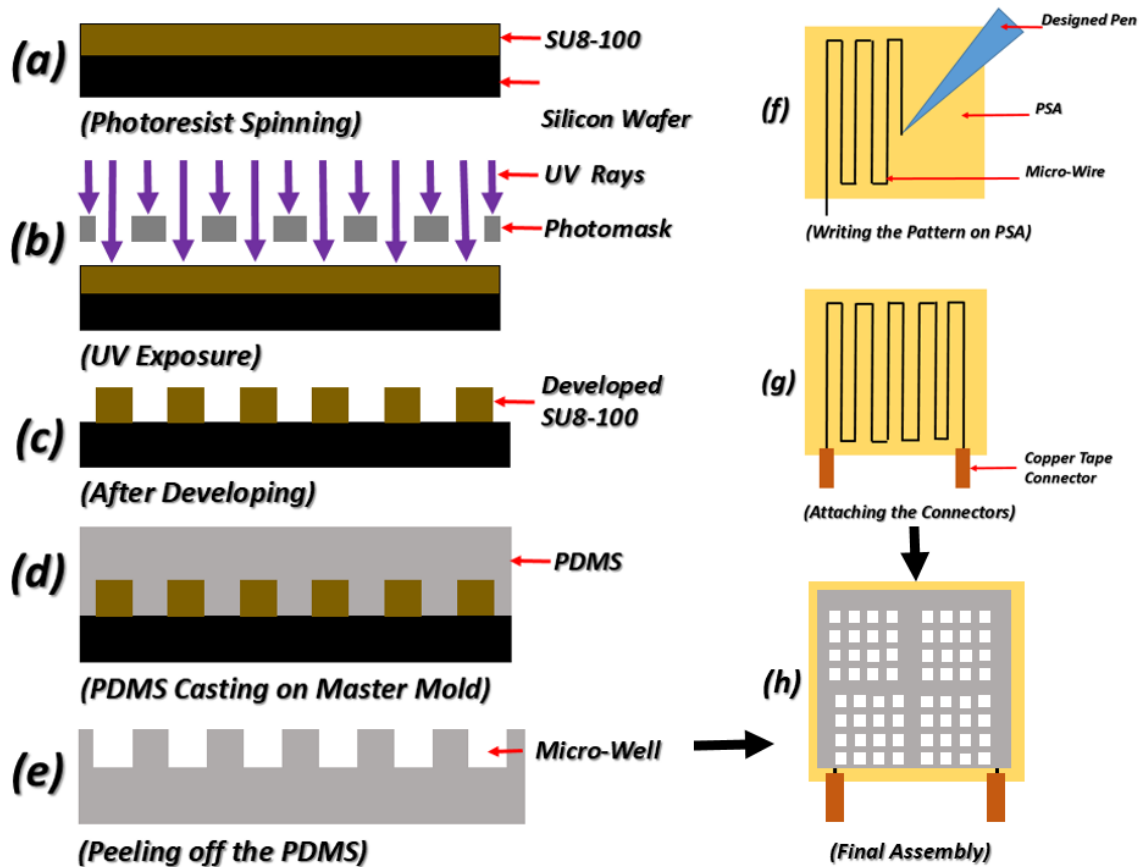


Figure 3.6 Fabrication process flow. (a) Photoresist spinning. (b) UV exposure. (c) After developing. (d) PDMS casting on master mold. (e) Peeling off the PDMS. (f) Writing the designed pattern on the PSA. (g) Attaching the connectors. (h) The final assembly.

These steps are described more in detail in the following sections.

### **3.3.1. Fabrication of the micro-well array**

The master mold to fabricate the micro-array was made using photolithography, which was firstly introduced by Xia et al [106]. Photomask with micro-array pattern was designed in AutoCAD (Autodesk Inc., San Francisco, USA) and was sent to CAD/Art Services Inc. for ultra-high-resolution printing on transparency sheet. The master mold with high-thickness features was made in clean room following the procedure which is explained in detail in Appendix A. As a brief description, first, the photoresist was spin coated on the silicon wafer (Figure 3.6a). Then, the photomask was aligned with the wafer, the photoresist was exposed to the UV light (Figure 3.6b). Finally, the photoresist was developed in SU8 developer to get rid of the unexposed area of the photoresist to UV light (Figure 3.6c).

PDMS pre-polymer contained two components, the PDMS base and the cross-linker which were mixed in the weighted ratio of 10:1. After they were mixed vigorously for 1 minute by using plain applicator sticks in a plastic beaker, the mixture was placed under the vacuum for 10 minutes to remove any trapped bubbles. Then, the uncured PDMS was poured on top of the master mold which was placed in a plastic petri dish (Figure 3.6d). Next, the petri dish was placed on a flat surface hot plate (to get uniform thickness all over the device) which was set at 80 Celsius for 2 hours. Afterwards, the PDMS was ready for peeling off. The cured PDMS elastomer was peeled off and device was cut from it (Figure 3.6e).

### 3.3.2. Plotting micro-wire integration technique for making flexible heater

The technique for fabrication of the heater was adapted from previous work developed in the lab [107]. In the following sections, this method is explained briefly, starting with pattern design in AutoCAD, writing the pattern on PSA film and finally, assembling steps.

The pattern of the micro-wire was designed in CAD based on the design criteria discussed in section 3.1.4 and saved in the .dxf format which was then transferred to the Cricut Explore One Machine (Figure 3.7).

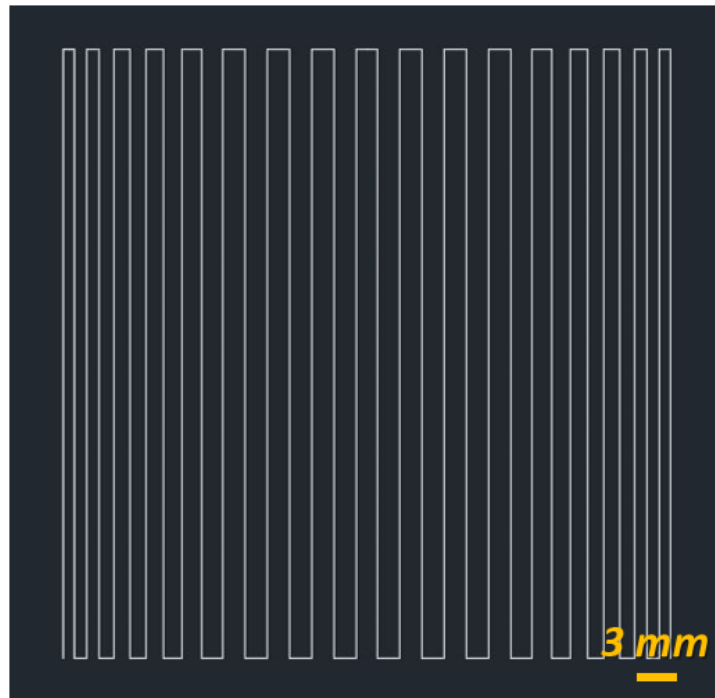


Figure 3.7 An example of a designed pattern in AutoCAD.

Next, the micro-wire was fed to the customized pen on the Cricut Explore One Machine and the pattern was written on a PSA film which was laminated on a 30.5\*30.5 cm standard grip adhesive cutting mat (Cricut Explore, Provo Craft & Novelty, Inc.). It is important to adjust the height of the pen to get the best adhesion between the micro-wire and the PSA film (Figure 3.6f).

Since the micro-wires are thin, fragile and susceptible to damage, a suitable method to interface them with external connectors was needed. For this purpose, copper tape (McMaster Carr, Cleveland, USA) was used which had an adhesive layer on one side. Thus, each end of the heater was sandwiched between two layers of copper tapes in a way that the micro-wire was in contact with the copper side of one tape and with the adhesive side of the other one (Figure 3.6g).

After connecting the copper connectors, the PSA film was cut and peeled off. Consequently, a heater on an adhesive layer was patterned which can be attached to either a thin layer of PDMS (Figure 3.8a) or another layer of PSA film (Figure 3.8b) to protect the micro-wires from breaking. The end product was a flexible heater that had some advantages over commercially available flexible heaters which will be discussed in chapter 4.

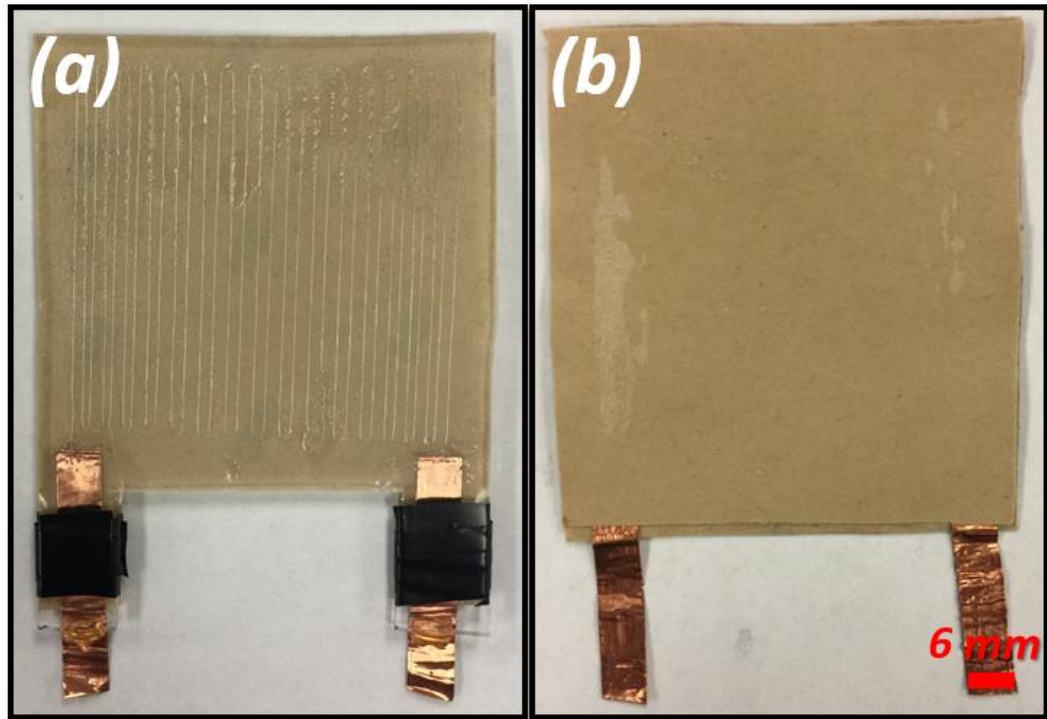


Figure 3.8 Flexible Heaters. (a) Covered with a PDMS layer to protect the micro-wires. (b) Covered with a PSA film to protect the micro-wires.

### 3.3.3. Final assembly of the device

After fabrication of the microarray and the flexible heater, they were assembled together to form the final device by aligning the center of the micro-array with the center of the flexible heater (Figure 3.6h). To achieve the perfect bonding between these two parts, either air plasma could be used if the top layer of the heater was covered with PDMS, or by using the adhesive layer of the PSA film if the top layer of the heater was covered with a PSA film. The perfect adhesion was crucial because if air bubble got trapped between them, it could affect the heat transfer from the heater into the wells and create a non-uniform temperature distribution. The integrated device is shown in Figure 3.9.

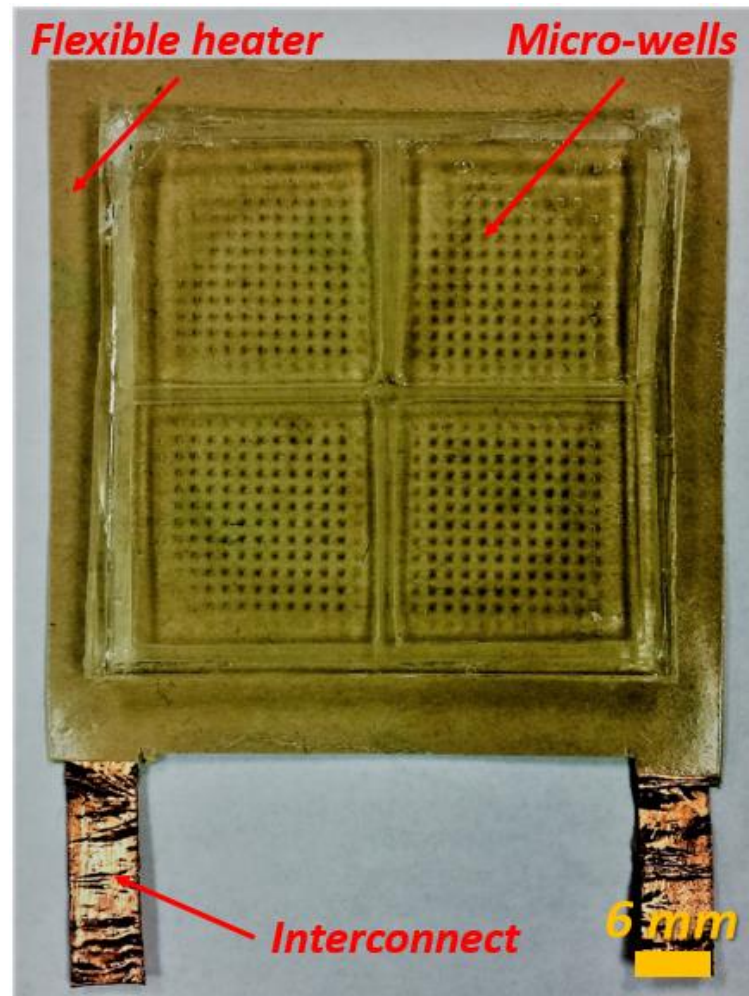


Figure 3.9 The integrated device including the micro-wells and the flexible heater made with plotting method.

## **3.4 Experimental setup**

In the following sections, the experimental setup that was used to test and characterize the device developed in this thesis is described.

### **3.4.1. The schematic of the experimental setup**

The schematic diagram of the experimental setup is shown in Figure 3.10. It consists of the device, an optical measurement unit, an electrical control unit, and the power supply. The optical measurement unit contains the required optical components for fluorescence microscopy. The power supply was used to apply current to the flexible heater in order to provide the required energy to keep the temperature of the device constant at a set value.

Also, a thermometer was used to determine the temperature using a thermocouple located in the waste channel. The electrical control unit regulates the exposure time and the period that the LED excites light in order to minimize the possibility of the photobleaching effect. Also, the pictures were saved on an SD card for further analyses on laptop.

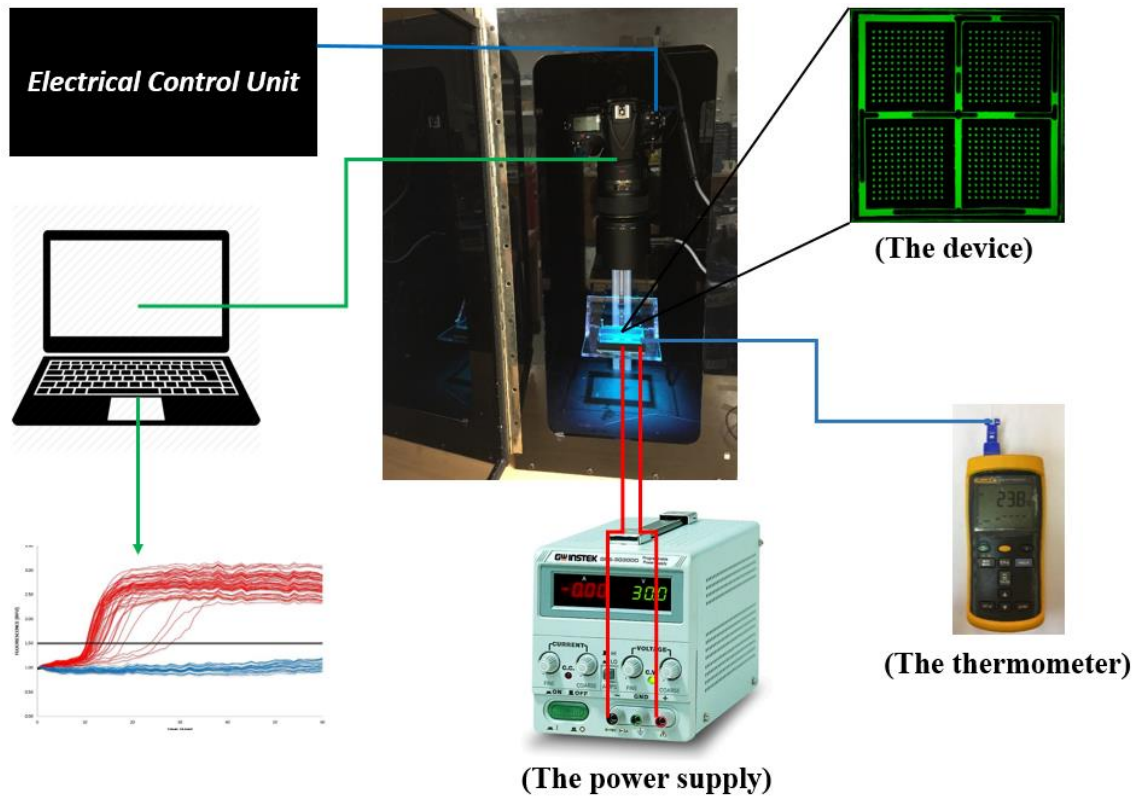


Figure 3.10 The schematic of the experimental setup.

### 3.4.2. Sample holder

A sample holder was designed according to the size of the device to hold it steady during the experiment to have a same reference point for all the images. It was designed in AutoCAD (Autodesk Inc., San Francisco, USA) and composed of two parts, the transparent laser cut part and the 3D printed part, which were put together to form the sample holder (Figure 3.11). The former (the frame) had the dimensions of 13.2 cm in length, 11.6 cm in width and 4.5 cm in height made out of a 6 mm transparent acrylic sheet. The latter (the glass slide holders) composed of two parts with the same dimensions of 8 cm in length, 7

cm in width and 1 cm in height which were 3D printed in order to hold two glass slides. As a result, the device could be sandwiched between these two glass slides. Also, the distance between the holder and the camera was adjustable in the detection system, which is introduced in the following section.

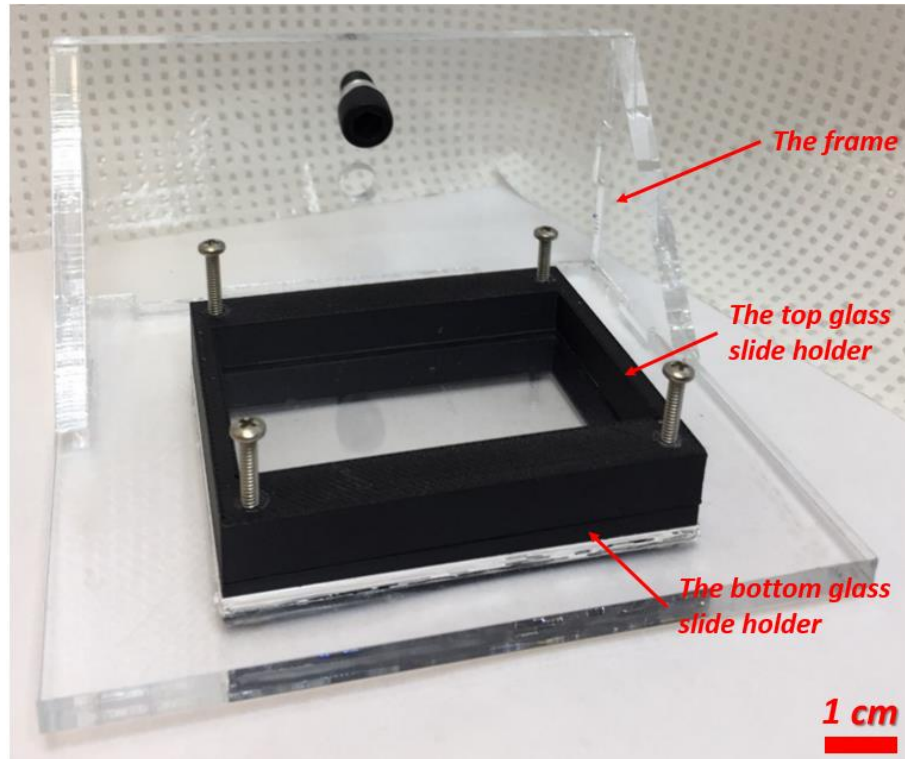


Figure 3.11 The sample holder composed of two parts, the frame and the glass slide holders.

### 3.4.3. Large field of view fluorescence detection system

This detection system was designed by Reza Ghaemi (another student in the lab) for large field of view fluorescent microscopy in our lab, CAMEF. It contains a DSLR camera, Nikon D810 (Nikon, Tokyo, Japan), with 36 MP resolution, a 3D printed filter

cube to hold a 492 nm excitation filter (Edmund Optics, NJ, USA), a 525 nm emission filter (Edmund Optics, NJ, USA), a 506 nm dichroic mirror (Edmund Optics, NJ, USA) and a blue LED (Edmund Optics, NJ, USA) as the source of excitation light. To reduce the interference from external light, an enclosure was designed to fit all the parts inside as it is shown in Figure 3.12. A black, non-transparent acrylic sheet was used as the material of the box and was cut by using laser cutting technique.

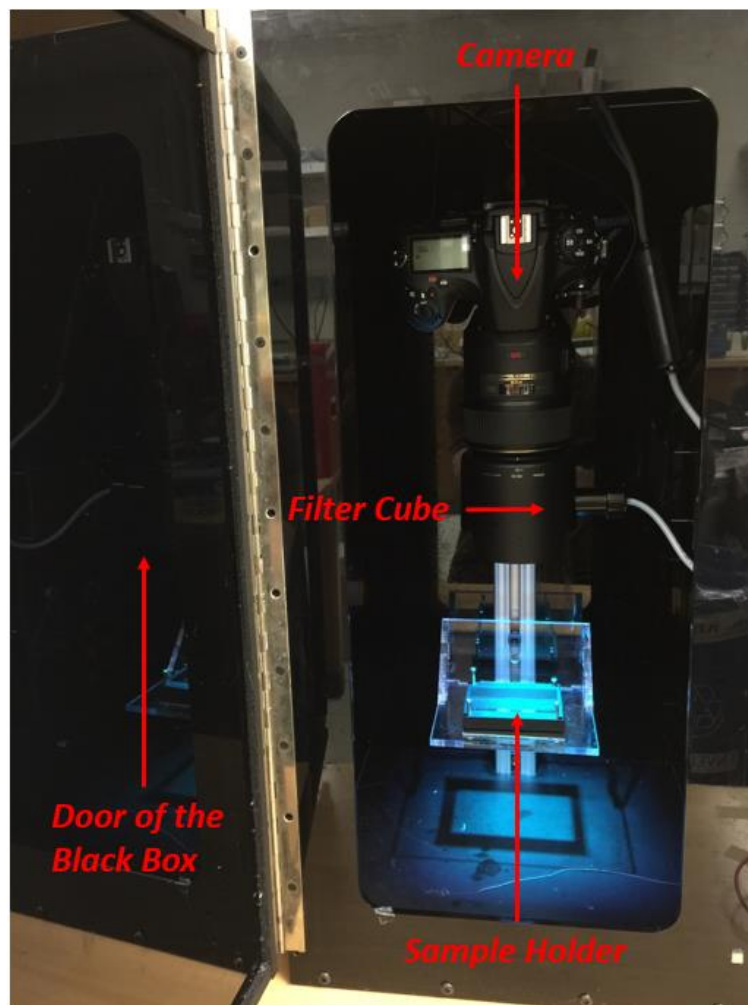


Figure 3.12 The large field of view fluorescence detection system.

A software called ControlMyNikon 5.3 Pro (Tetherscript Technology Corp.) was used to remotely control the camera to periodically take images at a set frequency so that there are no mechanical motion or misalignment between the camera and the device during the course of imaging.

#### **3.4.3.1 Electrical control unit**

An electrical control unit was designed to control the amount of time that LED is being on and off. Overexposing of the dye to the excitation light during the amplification time, can cause photobleaching of the dye which prevents recording the real time fluorescence signals. The user can set the exposure and the interval times at the beginning of the experiment. In these experiments, the exposure time was set to 8 seconds with the interval time of 1 minute. So, a picture was captured every minute. All the pictures were saved on an SD card for further analyses on a laptop using ImageJ freeware (<http://imagej.nih.gov/ij/>).

### **3.5 Sample preparation**

In this section, the protocol which was used for sample preparation is presented. All the reagents were stored in the freezer at the temperature of -4 Celsius. Before starting the sample preparation protocol, the reagents were brought out of the freezer. Between 10 to

15 minutes was required for the reagents to reach the room temperature. The reagents were mixed by using either a vortex mixer (Thermo Fisher Scientific, Massachusetts, USA) or by pipetting the reagents for few times to obtain a homogenous solution. Two different samples were used in the experiments described in the results section, positive and negative samples. Unless specified alternatively, positive samples typically had volumes of 25  $\mu\text{L}$  composed of 14.62  $\mu\text{L}$  of the Master Mix, 5  $\mu\text{L}$  of the Primer Mix, 5  $\mu\text{L}$  of the DNA template and 0.38  $\mu\text{L}$  of the EvaGreen 20X. The negative solution had the same composition, except for the DNA template part which same amount of deionized water was added instead.

### **3.6 Sample loading**

In this section, sample loading technique was described. First, the surface of the device was made hydrophilic, followed by sample loading on top of the micro-array device and sealing the device to eliminate evaporation during the amplification time.

#### **3.6.1. Autoclaving of the pipettes and the tips**

To avoid any kind of contamination, all the pipettes and tips were autoclaved before performing an experiment by using a benchtop autoclave machine (TUTTNAUER, NY, USA) located at Biointerface Institute at McMaster University.

### **3.6.2. Surface modification of PDMS**

PDMS is an inherently hydrophobic material, with a water contact angle of 95-110 degrees. This feature is not desirable in this application since it prevents sample from filling the micro-wells. If the PDMS micro-wells can be made hydrophilic, then the wells can be easily and automatically filled by simply loading the sample on top of it, and spreading it by using a glass slide.

There are different ways to make the surface of PDMS hydrophilic, such as 1) application of a hydrophilic polymer to its surface, 2) oxidization of the surface by plasma treatment or electrical discharge. It should be noted though that surface modified PDMS slowly recovers its hydrophobic properties due to the diffusion of uncross linked PDMS chains from the bulk onto the modified surface [108].

After the device was ready, it was placed in the chamber of the Oxygen Plasma Cleaner (Harrick Plasma, NY, USA) to be exposed to air plasma for 70 seconds.

After the PDMS surface was made hydrophilic, the prepared sample was loaded on top of it by using a clean pipette and tip (Figure 3.13). Then, the sample was slowly dispensed all over the device by using a clean glass slide back and forth on the device to

spread the sample and fill all the micro-wells. This process was also used to get rid of excess sample which was pushed into the waste channel.

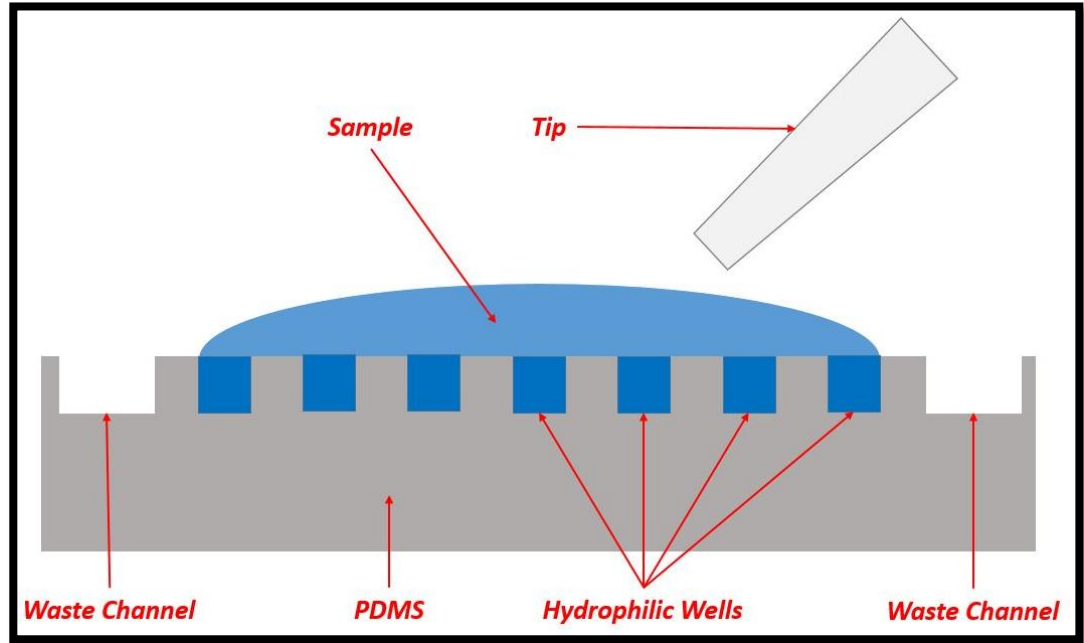


Figure 3.13 Sample loading on top of the hydrophilic PDMS surface.

### 3.6.3. Device sealing

It is crucial to seal the device to eliminate sample evaporation during the amplification time. In this regard, microseal B PCR plate sealing film (Bio-Rad Laboratories, ON, Canada), a clear polyester for high sensitivity optical assays was used to seal the PDMS micro-array device (Figure 3.14). The PCR film had been cut prior to this step to the right dimension to cover the device properly.

A film sealing roller for PCR plates (Bio-Rad Laboratories, ON, Canada) was used to properly and uniformly stick the film to the PDMS device. This process also pushed the extra sample into the waste channel.

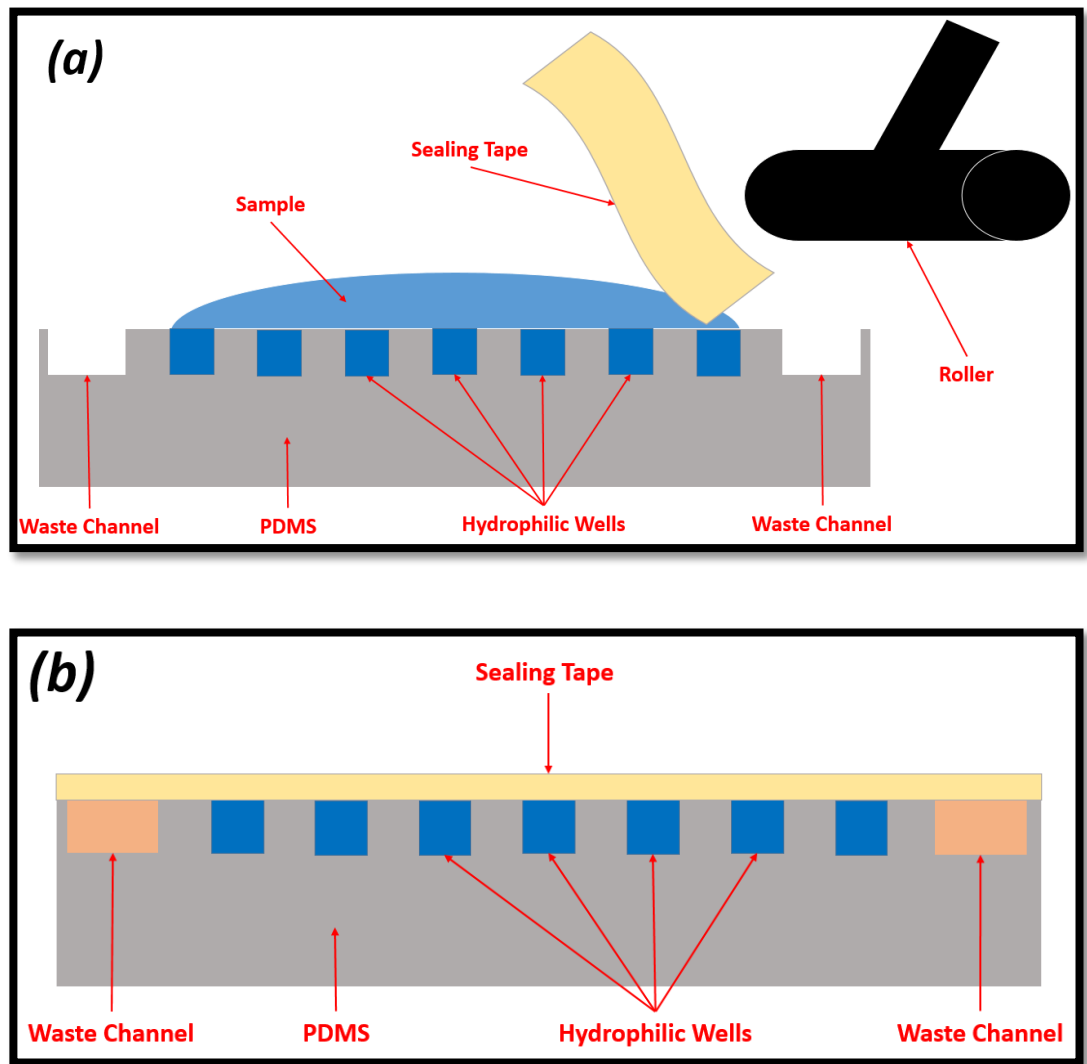


Figure 3.14 Device Sealing. (a) Before attaching the sealing tape. (b) After attaching the sealing tape.

### **3.7 Image processing method**

In this section, image processing and data analyses methods that were used to analyse the result are described. Images were saved in the raw format which gave the user more options at the time of analysis. The images were converted from the raw format to either TIFF (8 bit) or TIFF (16 bit) or JPEG format using ViewNX-I (Nikon Inc., NY, USA).

ImageJ (a freeware from National Institute of Health) was the core of the image analysis part which is a public domain software. After loading a converted picture on ImageJ, the three channels, Red, Blue and Green were split. Only the green channel was used in the analyses. This method works as an extra software filter in conjunction with hardware filters in detection setup, like the excitation and the emission filters and the dichroic mirror, to increase the sensitivity and efficiency of the analysis [109].

The software was used to extract the intensity of the green channel of the images. Then, the average intensity of each well was computed using a custom written macro. This process was performed for each of the images captured over time during the amplification process. The relative increase of the fluorescent intensity in the green channel was then computed, by subtracting the intensity at time "t" with the corresponding intensity at  $t=0$ . This calculation normalized the variation in the illumination intensity and other such environmental factors. This procedure was also performed for a negative sample where there should be no amplification. The key point in defining the threshold time was the average increase in the intensity of the negative sample which could be due to the primer dimers. A positive amplification was then defined as an event when the increase in the

intensity of a well was more than 5 standard deviations of the average increase of the intensity for the negative sample.

### **3.8 Summary**

In this chapter, the design methodology of the device, including two parts, the micro-wells part and the flexible heater, was explained. First, the design of the micro-wells was introduced by presenting the criteria, followed by design constraints and parameters and effect of each of them on the device design. Next, the device fabrication method and materials which were used, were explained completely, followed by presenting the experimental setup that contained the large field of view detection system which was designed in-house. Then, the sample preparation and loading methods were described thoroughly. In the end, the image processing methodology was introduced to make the analyses technique more clear.

In the next chapter, the characterizations of the device that was designed and fabricated are discussed including the filling of micro-wells and effect of the height and the width of the micro-wells on the fluorescence intensity, followed by flexible heaters characterization and finally, DNA amplification results.

## **Chapter 4: Results and Discussions**

### **4.1 Introduction**

In this chapter, the experiments performed to characterize and validate the microfluidic parallel DNA amplification device are described and the results obtained are presented and discussed. First, experiments characterizing the filling of micro-wells and effect of the height and the width of the micro-wells on the fluorescence intensity are discussed.

Next, various designs for flexible heaters are characterized by analysing the temperature uniformity across their surface, followed by calculating the fabrication cost and the electrical power consumption. Last but not least, DNA amplification in these wells are demonstrated and the effect of DNA concentration on the amplification time, false negative ratio and the signal intensity was analysed. Finally, parallel DNA amplification and primer mix dehydration are demonstrated.

### **4.2 Micro-wells**

In this section, the design of the micro-wells is optimized by analyzing the geometry of the micro-wells in order to select a suitable cross sectional shape. Next, the height of the micro-wells was optimized such that the intensity of fluorescent light from the positive and

negative samples can be differentiated and the typical S-shaped amplification curve can be detected. Moreover, the effect of the waste channel on the filling process is presented. Finally, the effect of the temperature on the amplification efficiency was studied in order to obtain an optimal range of temperature for designing the flexible heater.

#### **4.2.1. Shape of the micro-wells**

In this section, the effect of the shape of the micro-wells on the filling efficiency and the fluorescent intensity was determined by fabricating two shapes, cylinder and cuboid, since these shapes are suitable for microfabrication. Then, the effect of the width of the micro-well was also tested so that the best geometry in terms of filling efficiency can be chosen.

In order to determine the best shape of the micro-wells to achieve a complete filling, arrays of cylindrical and cuboidal wells with the 500  $\mu\text{m}$  dimensions (diameter for the cylinder and side for the cuboid) and 700  $\mu\text{m}$  in height, were fabricated and filled with a highly concentrated fluorescein solution ( $0.1 \frac{\text{mg}}{\text{mL}}$ ) in DI water, following the method described in chapter 3, section 3.6 (Figure 4.1). Fluorescein was used as a model dye as it had similar emission and excitation peak as the DNA tagging dye that is used in later experiments.

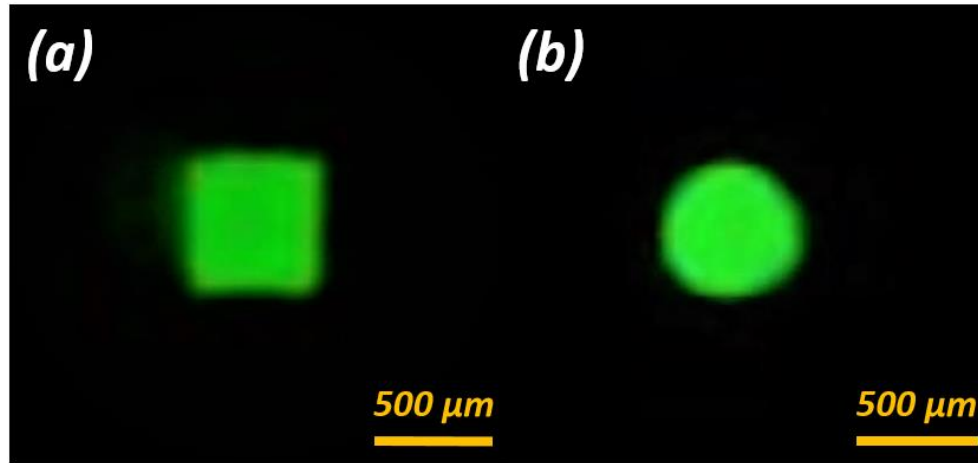


Figure 4.1 (a) Cuboid shaped wells with width of 500  $\mu\text{m}$  and height of 700  $\mu\text{m}$ . (b) Cylinder shaped wells with diameter of 500  $\mu\text{m}$  and height of 700  $\mu\text{m}$ .

Moreover, two devices with different well shapes filled with the fluorescein solution ( $0.1 \frac{\text{mg}}{\text{mL}}$ ) in DI water, are shown in Figure 4.2 in order to compare the filling efficiencies.

The filling results (Figure 4.2) showed that the cuboid design had higher filling efficiency. In particular, about 7 % of the micro-wells in the cylindrical design (10 out of 144) were filled inadequately with a bubble inside. On the other hand, all the wells in the cuboid design were filled. This experiment was performed two more times and similar results were seen.

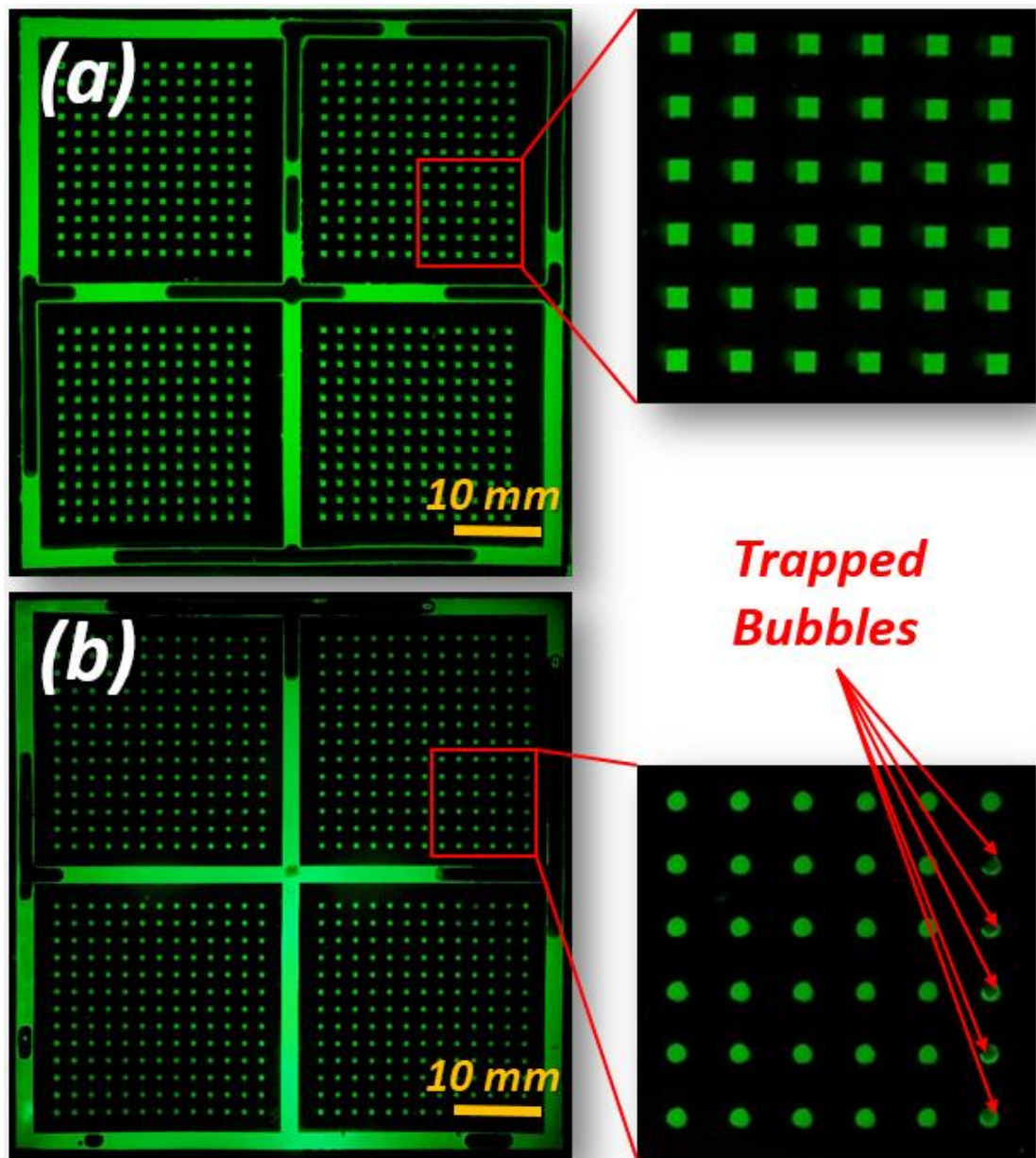


Figure 4.2 Filling comparison. (a) Cuboid design (500  $\mu\text{m}$  width, 700  $\mu\text{m}$  height). (b) Cylinder design (500  $\mu\text{m}$  diameter, 700  $\mu\text{m}$  height).

The corners in the cuboid design help the solution to smoothly fill the chamber with lower chance of having trapped bubble. Concus and Finn [110] investigated the capillary motion of a fluid in the corner of the wedge. It was shown that the droplets tend to flow into filaments in the corners which results in higher wettability and complete filling of the micro-well. Moreover, interfacial free energy between the solution and the sample could affect the contact angle and consequently the filling efficiency [111].

Therefore, between two suggested shapes, the cuboid design was chosen as the main shape of the final design due to the higher filling efficiency compare to the cylindrical design.

#### **4.2.2. Width of the micro-wells**

In this section, the effect of the width of the micro-wells on the filling efficiency was analysed in order to determine the operating range of sizes that would still have complete filling. Since according to the last section, the cuboid shape was chosen over the cylinder, different widths of cuboids were tested. For this purpose, nine different widths, ranging from 0.1 mm to 1.58 mm as it is shown in Figure 4.3, were designed and fabricated; all the designs have the same height of 100  $\mu\text{m}$ . Therefore, the aspect ratio of these designs was ranging from 0.06 to 1.

Then, after making the surface of the PDMS hydrophilic by the means of the air plasma, micro-wells were filled with around 100  $\mu\text{L}$  of methylene blue solution (0.05 M) in DI water by using a glass slide to move the solution back and forth over the array three

times which filled the wells completely, to be able to observe the filling process with the naked eye.

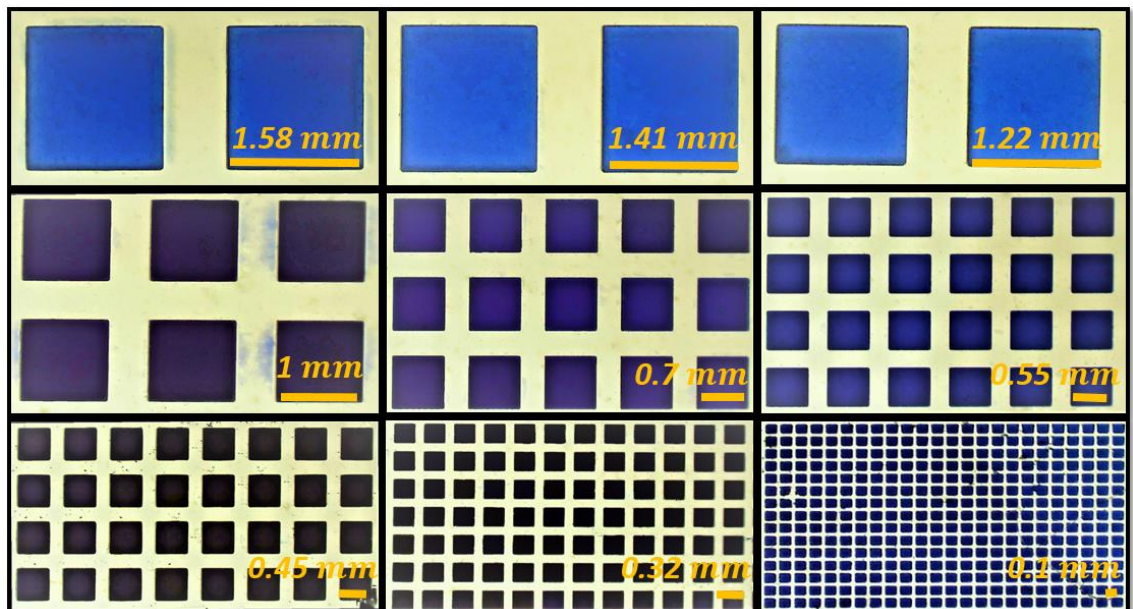


Figure 4.3 Filling efficiency of different widths of the cuboids. The widths from the biggest to the smallest size were 1.58, 1.41, 1.22, 1, 0.7, 0.55, 0.45, 0.32 and 0.1 mm. All the micro-wells above had the same height of 100  $\mu$ m.

As it is shown in Figure 4.3, all the designs showed perfect filling efficiency which indicated that no bubbles got trapped in the micro-wells. As a result, the width of the cuboid was not a limiting factor in designing the geometry of the micro-wells. However, as it was

discussed in chapter 3, the aspect ratio (width/height) of the wells have to be appropriate so that they not only fill properly but also allow sufficient contrast between the amplified and the unamplified mixtures.

#### **4.2.3. Effect of the height of the micro-wells on the intensity**

In this section, the effect of the height of the micro-wells on the intensity is studied. The intensity of the emitted light from the micro-wells depends on various parameters, such as the intensity of the excitation light, the concentration of dsDNA in the micro-well, the fluorescent dye concentration and the height of the micro-wells. Among these factors, the intensity of the light source was assumed to remain unchanged due to the design of the detection setup. The concentration of the DNA is determined by the amplification experiment and cannot be set prior.

Therefore, three designs with different heights of 100, 500 and 700  $\mu\text{m}$ , and same width of 500  $\mu\text{m}$ , were tested in order to evaluate the effect of the height of the micro-wells on the intensity. In order to compare the well arrays with these three heights, a DNA sample with the highest available concentration of  $4 \times 10^6$  *Copies*/ $\mu\text{L}$  was amplified by using ESEQuant tube scanner. This amplified solution was loaded into three devices each with the aforementioned heights. Next, fluorescent pictures were taken by using the detection setup which was developed in-house (described in section 3.4.3 in chapter 3).

The images were saved in raw format and converted into 16-bit to be analyzed. Therefore, the range of the intensity was from 0 to 65536 ( $2^{16}$ ). Also, the exposure time was set to be 8 seconds for all three images. Moreover, there were 8100 (90\*90) pixels per each micro-well.

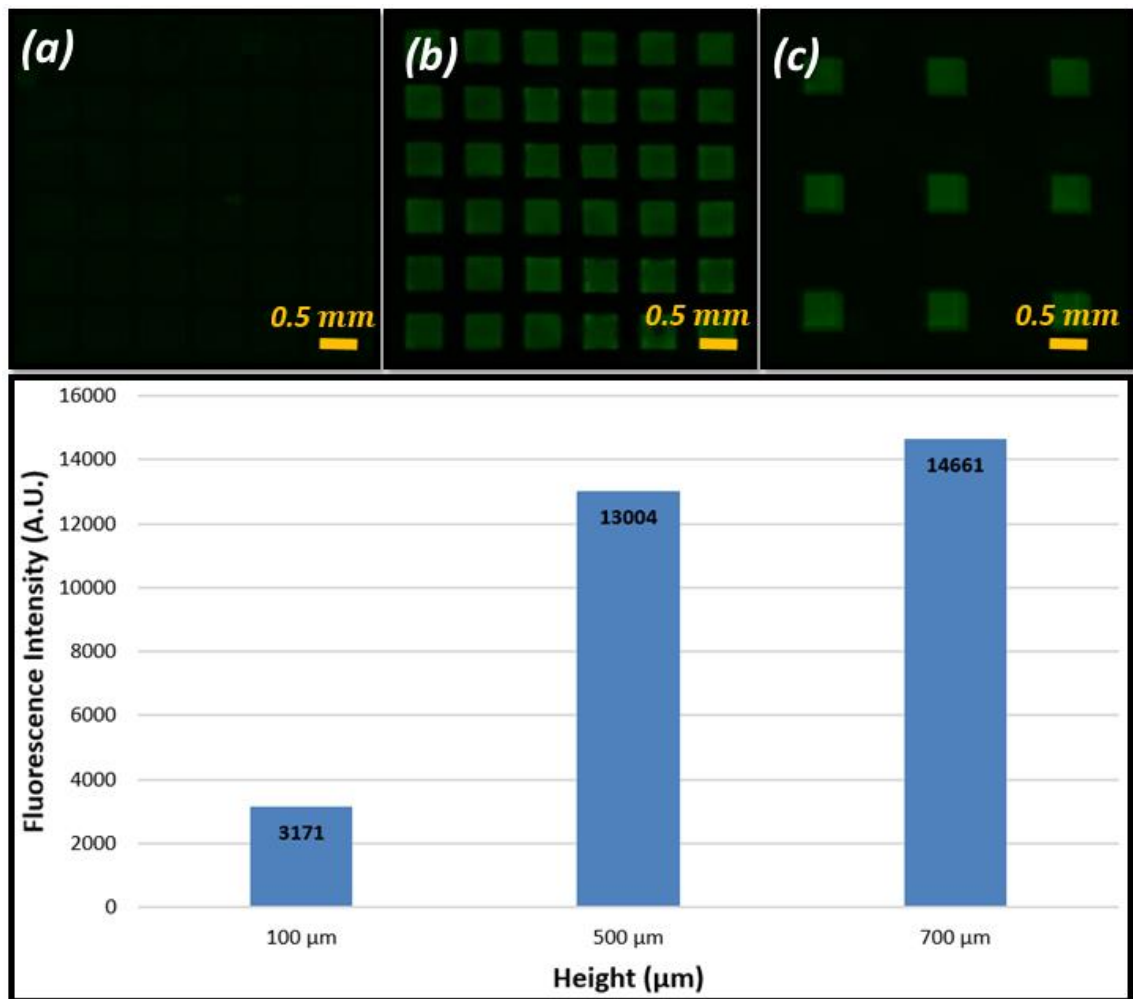


Figure 4.4 Effect of the height of the micro-wells on the fluorescence intensity for three different heights. (a) 100 μm height and 500 μm width. (b) 500 μm height and 500 μm width. (c) 700 μm height and 500 μm width.

The results (Figure 4.4) show that the intensity of the fluorescence signal increases with the height of the micro-wells. However, the increase is not linear. This is probably because the camera setup collects light both from within its depth of field (200  $\mu\text{m}$ ) and outside it. However only a smaller fraction of the light from out of the depth of field is collected and is strongly dependent on the distance from the focal plane. All the pictures were taken using a lens with 105 mm focal length. Also, the F-stop number which is an indication of the aperture was set to 4.5. A larger F-stop indicates smaller aperture. Moreover, the depth of field in front and the depth of field behind the focal plane were 100  $\mu\text{m}$ .

As it is shown in Figure 4.4, there is a rapid increase as the height of the well is increased from 100 (smaller than the depth of field) to 500  $\mu\text{m}$  larger than the depth of field and a more gradual one beyond that. Nevertheless, since the 700  $\mu\text{m}$  produced the highest signal and still was able to be filled completely and uniformly, it was chosen as the designed height of the array.

#### **4.2.4. Effect of the waste channel on the filling process**

In order to illustrate the effect of the waste channel on the filling process, two devices were prepared, one with the waste channel between the regions and one without the waste channel between the regions. Then, different colorful solutions were prepared by

mixing DI water with food dyes. Next, the solutions with different color were filled in different regions of the device, following the method described in chapter 3, section 3.6.

As it is shown in Figure 4.5, there was no waste channel between the regions. Therefore, the colors, red and blue, were mixed in the micro-wells located at the edges and made a purple shade.

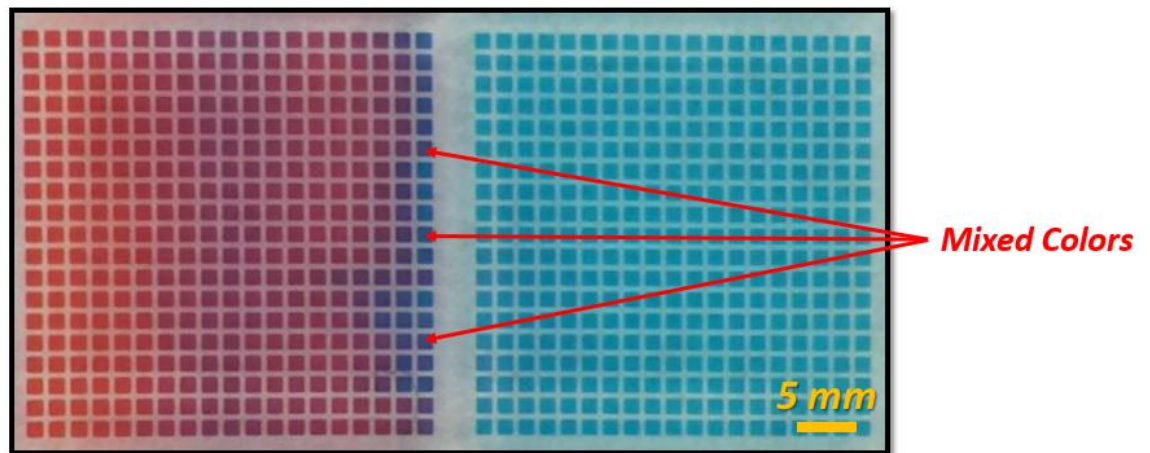


Figure 4.5 Two solutions were mixed when there was no waste channel between the regions.

On the other hand, in the presence of the waste channel, the colors, blue and yellow, did not get mixed, as it is displayed in Figure 4.6. As a result, four regions on the device can be considered independent from each other.

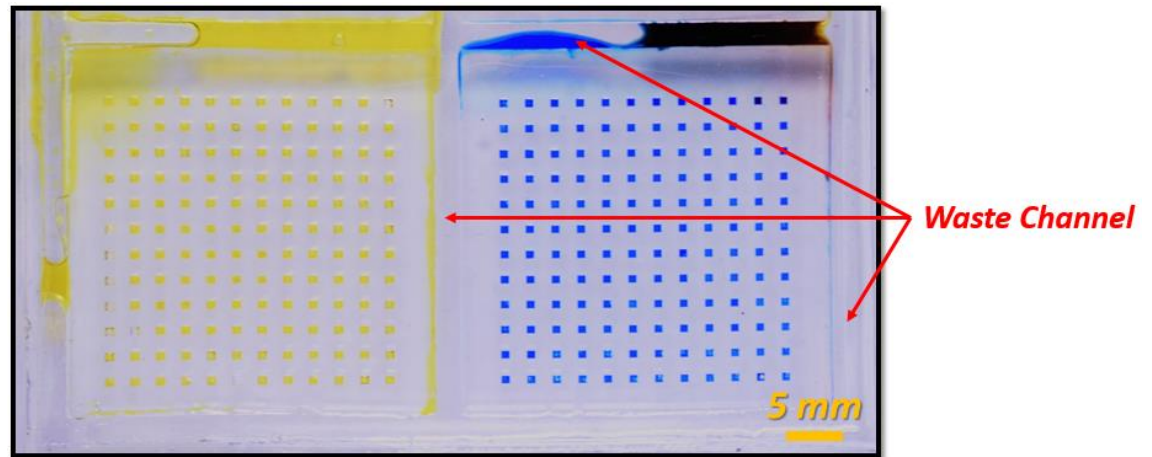


Figure 4.6 Effect of the waste channel which eliminated the samples from different regions to get mixed.

#### 4.2.5. The final design of the micro-wells part

The final design of the micro-wells part is illustrated in Figure 4.7. The design contains four separate regions to perform parallel DNA amplification reactions which are distinguished by four different food dyes. Each region has 144 (12\*12) cuboid micro-wells with the dimensions of 500\*500\*700  $\mu\text{m}$  which results in the volume of 175-nL for each micro-well.

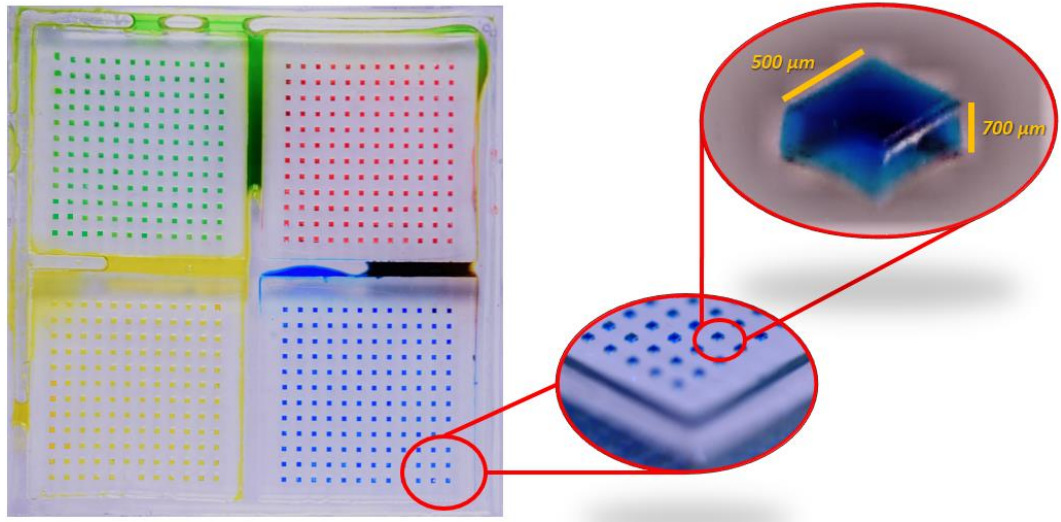


Figure 4.7 The final design of the micro-wells part which was filled with four different colors.

#### 4.3.1. Effect of the temperature on the performance of the LAMP reaction

To show the effect of the temperature on the amplification performance, a series of positive samples with the same concentration of  $4 \times 10^5 \text{ Copies}/\mu\text{L}$  were prepared and amplified at different temperatures by using ESEQuant tube scanner. The normalized real-time fluorescence intensities of the reaction mixtures during the amplification process at all the tested temperatures are shown in Figure 4.8.

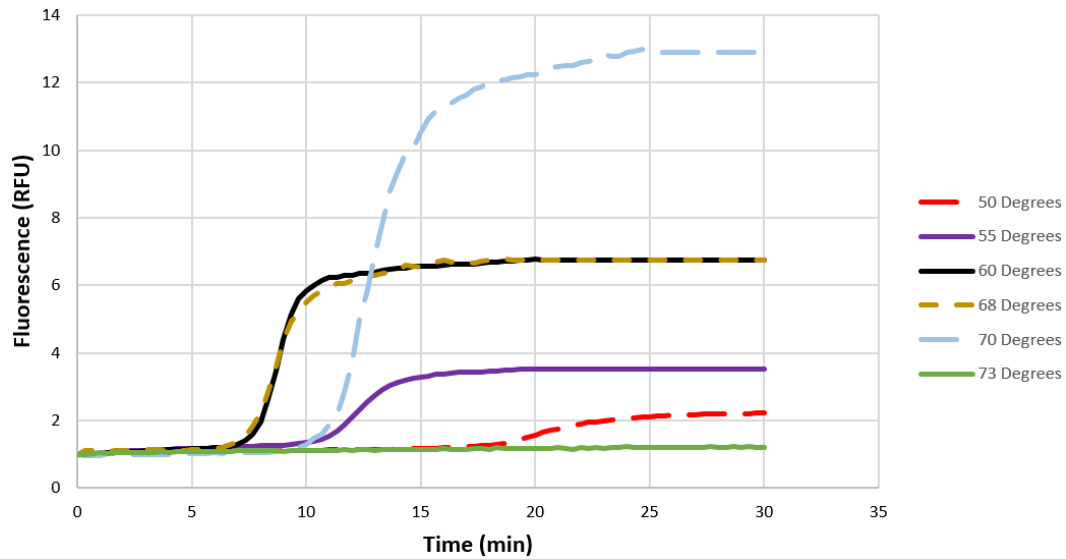


Figure 4.8 The normalized real-time fluorescence intensities of the positive sample with concentration of  $4 \times 10^5 \text{ Copies}/\mu\text{L}$  at different temperatures by using ESEQuant tube scanner.

These results show that the temperature at which the amplification is performed has a significant effect on the amplification process. As it is illustrated in Figure 4.9, the amplification temperature has a significant effect on the time at which the amplification process is completed.

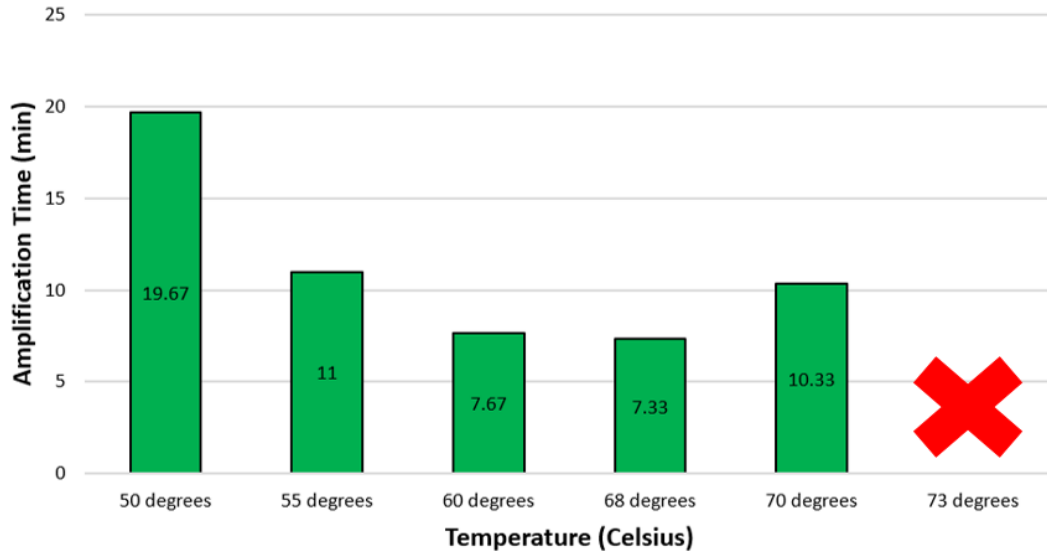


Figure 4.9 Amplification times of the positive sample with concentration of  $4 \times 10^5$  Copies/ $\mu\text{L}$  at different temperatures by using ESEQuant tube scanner.

As a result, the LAMP reaction works in the range of 50 to 70 degrees Celsius but with varying efficiencies. The prescribed amplification temperature is 65 Celsius since the efficiency of the enzymes is the highest at this temperature. The experiments reveal that a temperature range between 60 to 68 Celsius is optimal for amplification and produces similar amplification times and intensities that are only dependent on the concentration of the DNA present in the sample. On the other hand, as it is shown above, the LAMP reaction does not work beyond 73 Celsius since enzymes lose their functionality in that temperature which prevents the amplification reaction to happen. Therefore, it is essential to keep the temperature constant in the optimal range of 60 to 68 Celsius. This range of temperature was used in order to design the flexible heater in the following section.

### **4.3 Flexible heater**

As it was discussed in chapter 3, various options are available to use as a heat source in order to provide the required energy for the LAMP reaction, including the commercially available flexible heaters. These heaters are small and portable but are expensive and therefore may not be suitable for incorporation in a disposable device. The requirement for their use in this application is the uniformity of the temperature gradient which was the main motivation to fabricate flexible heaters by using plotting method.

In this section, various commercial heaters are evaluated so that their performance can be compared with the custom fabricated one in this thesis. The main performance criteria were the uniformity of the temperature gradient, fabrication cost and electrical power consumption. A new approach to fabricate flexible heaters using a new plotting method was developed and the heaters were characterized for this application.

#### **4.3.1. Commercially available heaters**

In this section, the temperature gradient of three commercially available flexible heaters were characterized in order to determine the suitability for heating the micro-well array. The heaters were connected to the power source, GPS-3030DD power supply (GW INSTEC, New Taipei City, Taiwan), and an appropriate voltage was applied across it such that the temperature gradient stayed between 60 to 68 Celsius as it was discussed in the previous section. The temperature of the heater is continuously imaged using an infrared thermal camera (FLIR ONE - FLIR, MA, USA). The calibration of the infrared thermal camera can be found in appendix E. It was found that the temperature on the entire surface of the heater stabilizes after 1 minute. Therefore, images of the temperature distribution was taken at this time.

Heater	1 HK913-C	2 HK913-D	3 HK913-J
Electrical Resistance (ohm)	120	160	275
Voltage (volts)	12.7	15.7	26
Current (ampere)	0.109	0.104	0.099
Electrical Power consumption (watts)	1.38	1.63	2.57

Table 4-1 Applied voltages and currents to Minco heaters in order to reach the temperature gradient of 60 to 68 Celsius across the heater.

As it is shown in Figure 4.10, three heaters were analysed which were different in terms of geometry and electrical resistance. To make a rational comparison between the heaters, the largest usable area was selected in a way that all of them had the same range of minimum and maximum temperatures of 60 and 68 Celsius, respectively, since this is the acceptable temperature range for the amplification according to the section 4.2.6. Then, the maximum (red triangle) and the minimum (blue triangle) temperatures were calculated in the selected area. For the sake of comparison, all the results are summarized in the table 4-2.

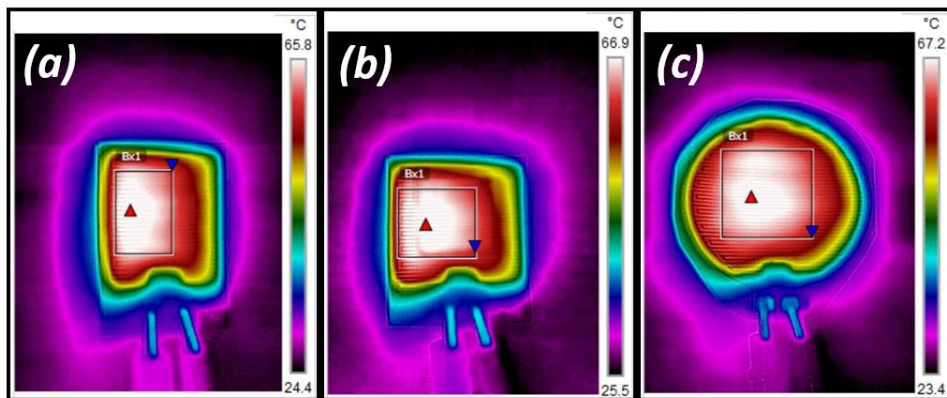


Figure 4.10 Temperature gradient of three commercial heaters made by Minco Company which were analysed with FLIR Tools software. (a) 120 ohm. (b) 160 ohm. (c) 275 ohm.

<b>Model</b>	<b>1 (HK913-C)</b>	<b>2 (HK913-D)</b>	<b>3 (HK913-J)</b>
<b>Resistance (<math>\Omega</math>)</b>	120	160	275
<b>Total Heater Area (cm<sup>2</sup>)</b>	21.3 (3.8 × 5.6)	25.8 (4.6 × 5.6)	34.2 (3.3 Radius)
<b>Largest Usable Area (cm<sup>2</sup>)</b>	4 (1.7 × 2.4)	6 (2.6 × 2.3)	8.7 (3 × 2.9)
<b>Usable Area (Percentage)</b>	19	23	25
<b>Maximum Temperature (Celsius)</b>	67.7	68.8	68
<b>Minimum Temperature (Celsius)</b>	60	60	60
<b>Average Temperature (Celsius)</b>	65.1	65.8	65.9

Table 4-2 Results of the temperature gradient analyses for three commercially available heaters.

As it is shown in table 4-2, only a portion of the heater area achieves the temperature range that is required for amplification to occur. Comparing the usable area percentage between heater 1, 2 and 3, it can be seen that by increasing the total area of the heater, the usable area percentage increases in a nonlinear pattern. However, the electrical power consumption increases at the same time by increasing the total area of the heater which results in more wasted energy. The electrical power consumption is discussed more in detail in section 4.3.4.

The non-uniformity of the temperature over the surface of the commercial heater was due to the higher heat transfer rate at the edges compare to the center of the heater. To solve this problem, either a heat spreader was required or a more uniform heater was needed to be designed and fabricated which is the subject of the next section.

#### **4.3.2. Heaters made with plotting method**

Flexible heaters were custom made using the plotting method described in chapter 3 in order to provide a more uniform temperature distribution.

From the previous experiments on commercial heaters, it was observed that the temperature at the center of the heater was higher and it gradually decreased towards the edges. This effect was due to the heat transfer from the edges to the ambient by convection. Therefore, designs of heaters that would compensate for the temperature gradient by distributing the heat more uniformly, were made as shown in Figure 4.11. This was achieved by varying the spacing between the heater wires from the center where they are less closely packed to the edges where they are more closely packed.

These designs were first simulated and tested in COMSOL Multiphysics Software (simulation detail can be found in appendix B) and those designs that showed significant improvement over the commercial heaters were fabricated and tested.

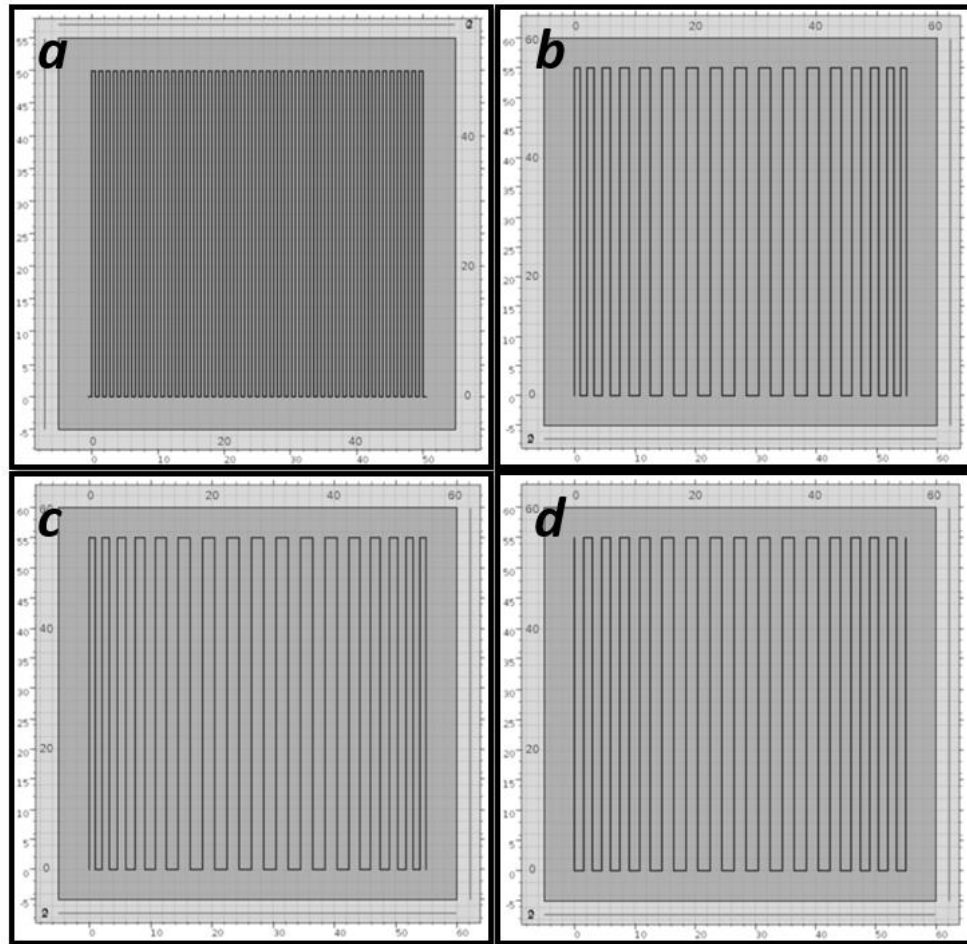


Figure 4.11 The schematic of all the designs. (a) **Design 1**: Constant spacing, 0.5 mm, made out of 50  $\mu\text{m}$  silver wire. (b) **Design 2**: Gradually increased spacing from 1 mm at the edges to 2 mm at the middle made out of 50  $\mu\text{m}$  silver wire. (c) **Design 3**: Gradually increased spacing from 1 mm at the edges to 2 mm at the middle made out of 25  $\mu\text{m}$  copper wire. (d) **Design 4**: Gradually increased spacing from 1.5 mm at the edges to 2 mm at the middle made out of 50  $\mu\text{m}$  silver wire.

After the heaters were fabricated, an analysis similar to the previous section were performed on these heaters by selecting the largest usable area in a way that all of them had

the same range of temperature which was between 60 to 68 Celsius due to the working temperature range of the LAMP reaction.

Design 1 had a constant spacing, 0.5 mm, between the micro-wires and was simulated using COMSOL Multiphysics Software. The detail information about the simulation can be found in appendix B. This design was made to mimic the designs found in commercial heaters. The simulation result (Figure 4.12) showed a hot spot at the center of the heater which was similar to the experimental results of the temperature distribution on commercially available heaters. This result was expected as the heat generation in the area is uniform while the heat transfer due to convection at the edges is higher. This design and simulation exercise confirms the observation seen in commercial heaters and therefore was not found suitable for fabrication and further testing.

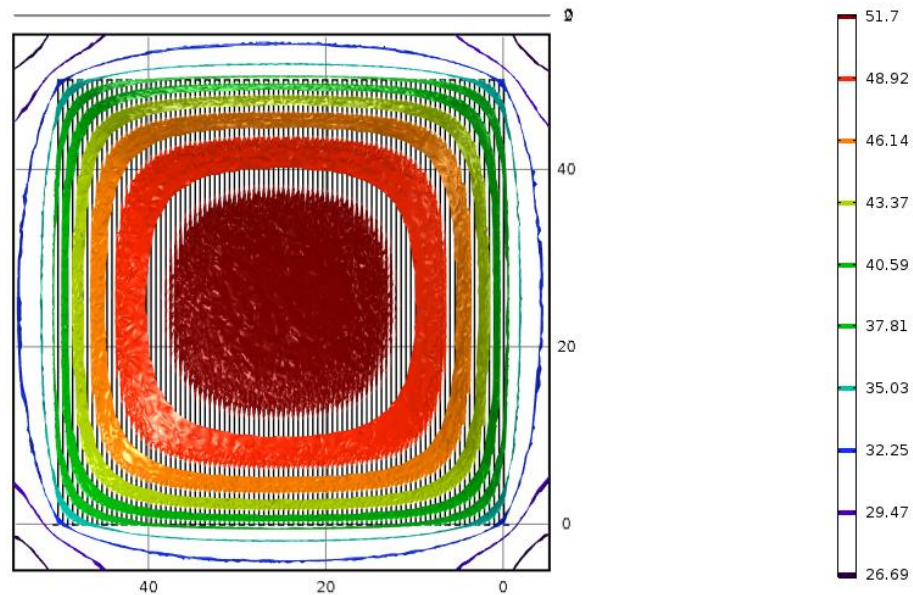


Figure 4.12 Simulation result of **Design 1** with the constant spacing, 0.5 mm, made out of 50  $\mu\text{m}$  silver micro-wire.

In order to reduce the variation of temperature at the edges and to provide a high uniformity in temperature distribution, other designs (Figure 4.9b, Figure 4.9c and Figure 4.9d) were developed that used non-uniform distribution of spacing between the micro-wires to provide a gradient in heat generation capacity to compensate the effects of heat transfer.

The specification of these designs are presented in the table 4-3. These designs varied in terms of the spacing pattern, material of the used micro-wires and the size of the micro-wires in order to analyse the effect of each factor on the temperature gradient.

<b>Design</b>	<b>2</b>	<b>3</b>	<b>4</b>
<b>Micro-Wire Size (<math>\mu\text{m}</math>)</b>	50	25	50
<b>Micro-Wire Material</b>	silver	copper	silver
<b>Spacing* (mm)</b>	1: 0.1: 2	1: 0.1: 2	1.5: 0.1: 2
<b>Resistance (<math>\Omega</math>)</b>	15.3	80	15

Table 4-3 Design specification of the 3 fabricated heaters. (\*) Minimum spacing at the edge: Spacing increment: Maximum spacing at the middle.

The simulation results of these 3 heaters are illustrated in Figure 4.13, Figure 4.14 and Figure 4.15.

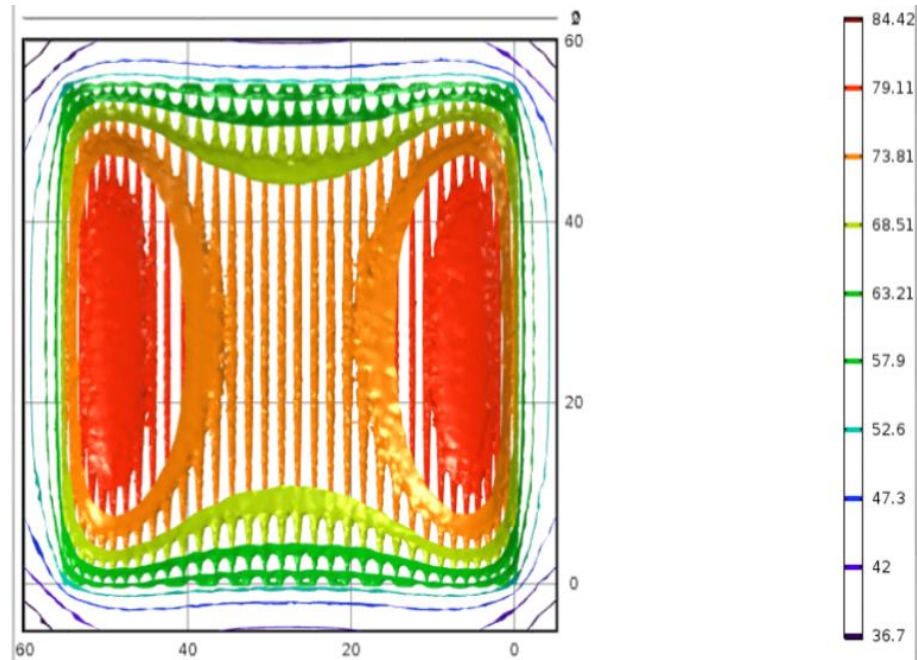


Figure 4.13 Simulation result of **Design 2** with variable spacing from 1 mm to 2 mm made out of 50  $\mu\text{m}$  silver micro-wire.

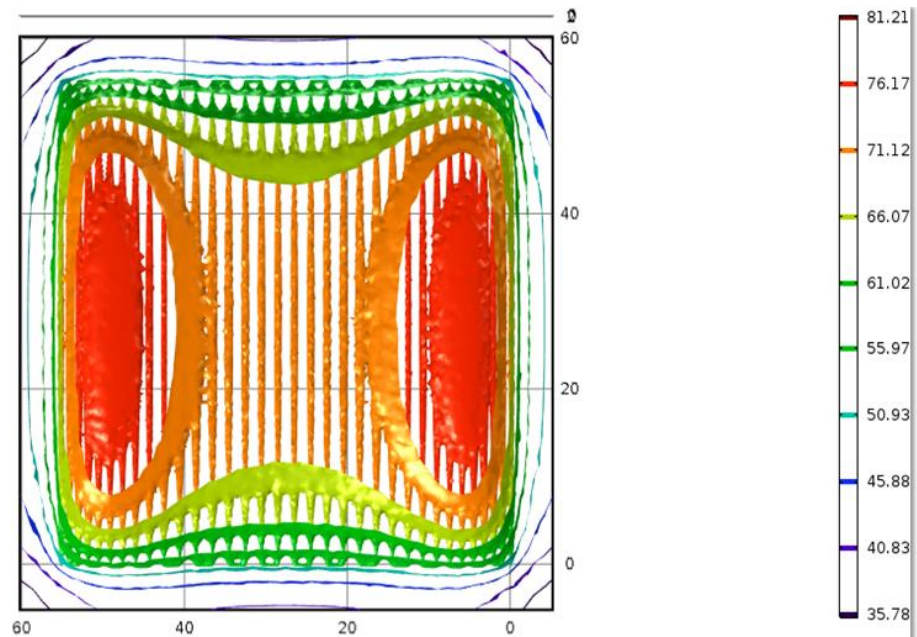


Figure 4.14 Simulation result of **Design 3** with variable spacing from 1 mm to 2 mm made out of 25  $\mu\text{m}$  copper micro-wire.

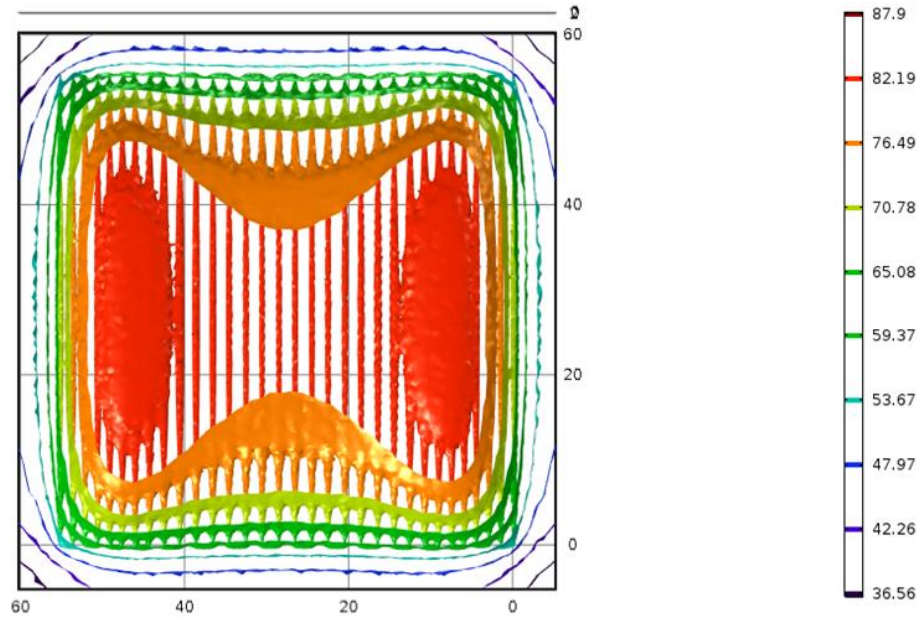


Figure 4.15 Simulation result of **Design 4** with variable spacing from 1.5 mm to 2 mm made out of 50  $\mu\text{m}$  silver micro-wire.

Design 2 (Figure 4.13) showed more uniformity at the middle of the device compared to Design 1 in the simulation due to higher convection effect at the edges which indicated that variable spacing between the micro-wires could increase the temperature uniformity.

Design 3 (Figure 4.14) was similar to Design 2 except for the used micro-wires in order to analyse the effect of the wire on the temperature uniformity. As it is summarized in the table 4-4, temperature uniformity increased 6 percentage. Moreover, electrical resistance increases as the area of the wire decreases which is described in detail in section 4.3.4.

Design 4 (Figure 4.15) was tested to analyse another spacing variation in comparison with Design 2 and Design 3. As it is summarized in table 4-4, the small spacing variation between design 2 and 4 did not have any effect on the usable area percentage where both designs had 36 percentage usable area.

The fabricated heaters based on the three designs were experimentally tested and the temperature distribution obtained is shown in Figure 4.16. Also, the largest usable area, the usable area percentage, and maximum and minimum temperatures obtained were summarized in the table 4-4.

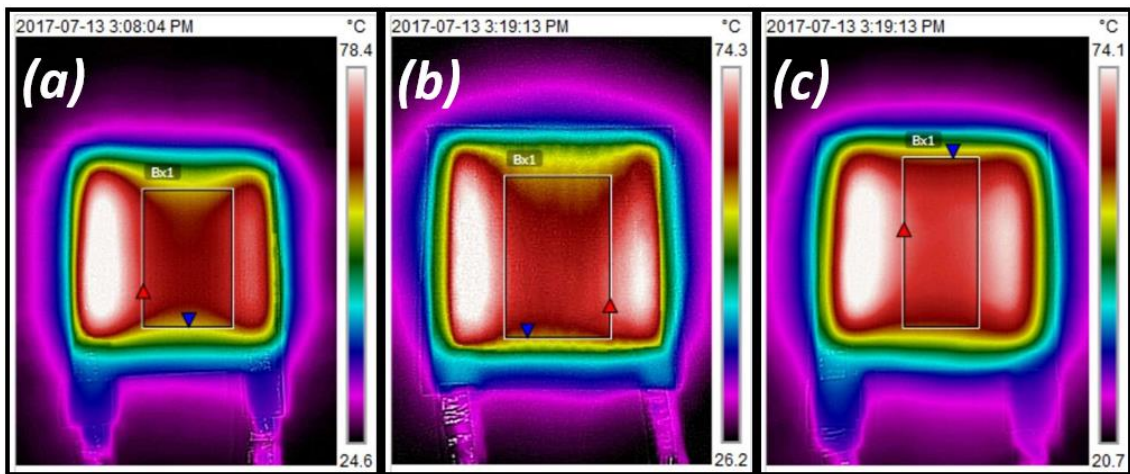


Figure 4.16 Real temperature gradients of the heaters made by plotting method. (a) **Design 2**: Gradually increased spacing from 1 mm at the edges to 2 mm at the middle made out of 50  $\mu\text{m}$  silver micro-wire. (b) **Design 3**: Gradually increased spacing from 1 mm at the edges to 2 mm at the middle made out of 25  $\mu\text{m}$  copper micro-wire. (c) **Design 4**: Gradually increased spacing from 1.5 mm at the edges to 2 mm at the middle made out of 50  $\mu\text{m}$  silver micro-wire.

<b>Design</b>	<b>2</b>	<b>3</b>	<b>4</b>
<b>Heater Area (cm<sup>2</sup>)</b>	30.2 (5.5 × 5.5)	30.2 (5.5 × 5.5)	30.2 (5.5 × 5.5)
<b>Largest Usable Area (cm<sup>2</sup>)</b>	10.8 (2.7 × 4)	12.8 (2.9 × 4.4)	10.8 (2.2 × 4.9)
<b>Usable Area (percentage)</b>	36	42	36
<b>Maximum Temperature (Celsius)</b>	68	68	68
<b>Minimum Temperature (Celsius)</b>	60	60	60

Table 4-4 Design and performance parameters of three different heaters made by plotting method.

As a result, the heaters made by plotting (Design 3) showed higher usable area percentage, 17 % higher, compare to the commercially available flexible heaters (Heater model 3).

#### **4.3.3. Cost analysis**

Another important parameter of interest, especially in a disposable application is the cost of the heaters. In this section, detailed cost analysis is shown between the heaters made using the plotting method and compared to the cost of the commercially available heaters. The cost of commercially available heaters is relatively high primarily due to the methods used for their manufacture. Typically, a photopattern is used to delineate the heater pattern onto a metal foil and then etching is performed to produce the shape. These processes are time consuming, require expensive chemicals and also lead to production of metal and chemical waste that eventually leads to the higher cost.

The prices of the commercially available heaters are summarized in the table 4-5 for few heaters from two companies, Minco and Omega. The high cost of these heaters make them unsuitable for applications where the device is used once and disposed off.

<b>Model</b>	<b>Area (cm<sup>2</sup>)</b>	<b>Resistance (<math>\Omega</math>)</b>	<b>Price (CAD)</b>	<b>Price/Area (CAD/cm<sup>2</sup>)</b>
<b>Omega KHLV 101/5</b>	6.25 (2.5 × 2.5)	11	48	7.7
<b>Omega KHLV 103/10-p</b>	19 (2.5 × 7.6)	40	54	2.8
<b>Omega KHLV 202/5-p</b>	25 (5 × 5)	108.6	55	2.2
<b>Omega KH 303/10-p</b>	57.8 (7.6 × 7.6)	153.7	61	1.1
<b>Minco HK913-C</b>	21.3 (3.8 × 5.6)	120	61	2.9
<b>Minco HK913-D</b>	25.8 (4.6 × 5.6)	160	61	2.4
<b>Minco HK913-J</b>	34.2 (3.3 Radius)	275	63	1.8

Table 4-5 Summarized price information of flexible heaters from two companies, Minco and Omega.

On the other hand, heaters made by plotting method consists of three materials, PSA film as a substrate, micro-wires and copper tapes for connections as it was explained in section 3.2 in chapter 3. The most expensive of these three materials is the micro-wire. Also, the price of the micro-wire depends on the main material of the micro-wire and its

purity, the diameter of the micro-wire and if there is any heat treatments done on the material.

Other than the price of the micro-wire which is indicated in the table 4-5, the price of PSA film and the copper tape are needed to be considered to estimate the cost of each heater. A big roll of PSA film with dimensions of  $30.5\text{ cm} * 55\text{ m}$  costs CAD 475. So, a  $6\text{ cm} * 6\text{ cm}$  PSA film costs 10 cents. Also, since two PSA film of this size were used to fabricate the heater, one as a substrate and one as a protector cover, it resulted in 20 cents. Moreover, a copper tape roll of  $16.5\text{ m}$  costs CAD 18. Each heater needs around  $15\text{ cm}$  of this tape which costs about 15 cents. As a result, except the cost of the micro-wires, each heater costs 35 cents (20 cents for the PSA film and 15 cents for the copper tape).

The prices of micro-wires from two companies, Surepure Chemetals (NJ, USA) and The Vape Mesh Company (Cheshire, UK), with different sizes and materials are summarized in the table 4-5 in appendix C. As a result, the price of the micro-wires per meter covers a wide range, from CAD 0.04 to CAD 13.8, which could significantly alters the price of the whole heater.

From the industrial point of view, Nichrome which is an alloys of Nickel, Chromium and sometimes Iron, is used in many heating applications. In the heating up process, most metals oxidize fast and become brittle and vulnerable to breakage. However, when heating up the Nichrome, a thin layer of chromium oxide forms on the outer layer of the wire and prevents further oxidization which makes Nichrome a perfect candidate for this application. Also, according to the table 4-4, NiCR80/20 with the size of  $50\text{ }\mu\text{m}$  in diameter from the Vape Mesh Company has the lowest price among all the presented micro-wires (CAD 0.04 per meter). However, at the time of the experiments, this wire was out of stock. Therefore, the result test of this wire is not presented. Additionally, in terms

of the price, the Surepure Chemetals (3618) copper wire with the size of 76  $\mu\text{m}$  in diameter is another good candidate (CAD 0.06 per meter).

Four different designs were illustrated in Figure 4.11 previously. To be able to calculate the cost of the used micro-wires in each one, the length of the pattern is needed. For this purpose, the detailed information of each design is summarized in the table 4-6 below.

<b>Design</b>	<b>1</b>	<b>2</b>	<b>3</b>	<b>4</b>
<b>Length of the pattern (m)</b>	5.1	1.9	1.9	1.8
<b>Estimated cost of used micro-wire (CAD)*</b>	0.2	0.08	0.08	0.07
<b>Final cost (CAD)**</b>	0.55	0.43	0.43	0.42
<b>Price/Area (CAD/cm<sup>2</sup>)***</b>	0.018	0.014	0.014	0.014

Table 4-6 The estimated final cost of four different patterns. (\*) NiCR80/20 with the size of 50  $\mu\text{m}$  in diameter from the Vape Mesh Company (CAD 0.04 per meter). (\*\*) Additional 35 cents for the PSA film and copper tape. (\*\*\*) The area of all the heaters are 30.2  $\text{cm}^2$ .

As a result, the final price of fabricating heaters using plotting method is considerably cheaper (almost 100 times) than buying the commercially available heaters.

#### **4.3.4. Electrical power consumption**

Another important factor in analyzing the performance of the heaters is the electrical power consumption which can be calculated by the formula below where P is the power in watts, V is the electric potential in volts, I is the current in amperes and R is the electrical resistance in ohm:

$$P = V \times I = R \times I^2 = \frac{V^2}{R}$$

Moreover, the electrical resistance of a wire can be expressed with the formula below where  $\rho$  is the resistivity of the material in  $ohm \times m$ , L is the length of the wire in meter and A is the area of the cross section in  $m^2$ :

$$R = \rho \frac{L}{A}$$

Based on these formula, the electrical power consumptions of all the mentioned heaters including three flexible heaters from Minco and three fabricated heaters using plotting are calculated and shown in the table below. All the numbers are based on generating the same range of temperature (65 Celsius) at the center of the heater.

<b>Heater</b>	<b>Heater 1</b>	<b>Heater 2</b>	<b>Heater 3</b>	<b>Design 2</b>	<b>Design 3</b>	<b>Design 4</b>
<b>Electrical Resistance (<math>\Omega</math>)</b>	120	160	275	15.3	80	15
<b>Voltage (V)</b>	12.7	15.7	26	10	17.1	10
<b>Current (I)</b>	0.109	0.104	0.099	0.535	0.200	0.560
<b>Electrical Power consumption (W)</b>	1.38	1.63	2.57	5.35	3.42	5.6

Table 4-7 The electrical power consumptions of all the mentioned heaters.

As a result, the electrical power consumption of Minco heaters are lower than the heaters made by plotting method. However, the reason is the material of the used micro-wires in fabrication which were copper and silver. By changing the material to Nichrome, it could be expected that the electrical resistance increases significantly since the resistivity of the Nichrome is 58 times higher than the annealed copper. Therefore, the current would

decrease drastically and in order to produce the same temperature, higher voltage is required. So, more studies are needed to optimize the power consumption.

In conclusion, the fabricated heaters using plotting method were compared to the commercially available heaters in terms of the uniformity of the temperature gradient, fabrication cost and electrical power consumption. The first two criteria showed better results especially the fabrication cost. On the other hand, the electrical power consumption was lower in the commercially available heaters. However, as it was mentioned earlier, more studies are needed to optimize the pattern of the heater and the used material of the micro-wires.

## **4.4 DNA amplification**

In this part, the result of the DNA amplification, which is the main focus of this research, is presented. First, DNA amplification in the integrated microfluidic device is illustrated, followed by amplification characterization and discussion. Also, the capability of the device to perform parallel DNA amplification and on chip reagent storage are presented.

### **4.4.1. Demonstration of amplification in the integrated microfluidic device**

In this section, experiments were performed on the micro-well array device with integrated heaters to show that it could be used to amplify DNA. The micro-well array consisted of wells with dimensions of  $500*500*700 \mu\text{m}$  and flexible heaters made with plotting method using Design 3, were made and integrated together as it was explained in section 3.3 in chapter 3.

Positive and negative DNA samples were used. The positive sample contains primer mix, master mix, DNA staining dye (EvaGreen 20X) along with the extracted DNA from *E. coli* STEC eae with the highest available concentration of  $4 * 10^6$  *Copies*/ $\mu$ L. The negative sample did not contain the DNA template; instead it has DI water added to primer mix, master mix and DNA staining dye (EvaGreen 20X). The amplification was performed for an hour to ensure that the amplification reaction has reached completion. Fluorescent images of the array before and after the amplification was taken and compared.

A positive sample was prepared and loaded into the device, as it was explained in section 3.6 in chapter 3. Also, the thermocouple was implanted into the waste channel carefully in order to monitor the applied temperature by using the Fluke 50 series II thermometer. Next, the integrated device was put on the sample holder and connected to the GPS-3030DD power supply. Then, the device was heated up to 65 Celsius by applying proper current and voltage (0.225 A and 18 V) to the device. It took 3 minutes to reach to 65 Celsius from the room temperature. After the temperature was steady, an initial fluorescent image was taken by using the fluorescence detection setup described in section 3.4.3 in chapter 3.

Next, the amplification was performed for 60 minutes at 65 Celsius. Afterwards, another fluorescent image was taken in order to compare the before and after amplification fluorescent signals. It is important to mention that both pictures were taken at 65 Celsius in order to ensure that the intensity values are comparable. It should be noted that the fluorescence intensity of the dye is temperature dependent and decreases with the increase in temperature.

The same experiment procedure was performed on the negative sample which contained primer mix, master mix, dye and DI water, instead of the DNA template. It was expected that there would be no significant change in the fluorescence intensity after performing the amplification.

Then, the taken images were analysed according to the method described in section 3.7 in chapter 3. The quantified comparison between positive and negative amplifications are presented in Figure 4.17.

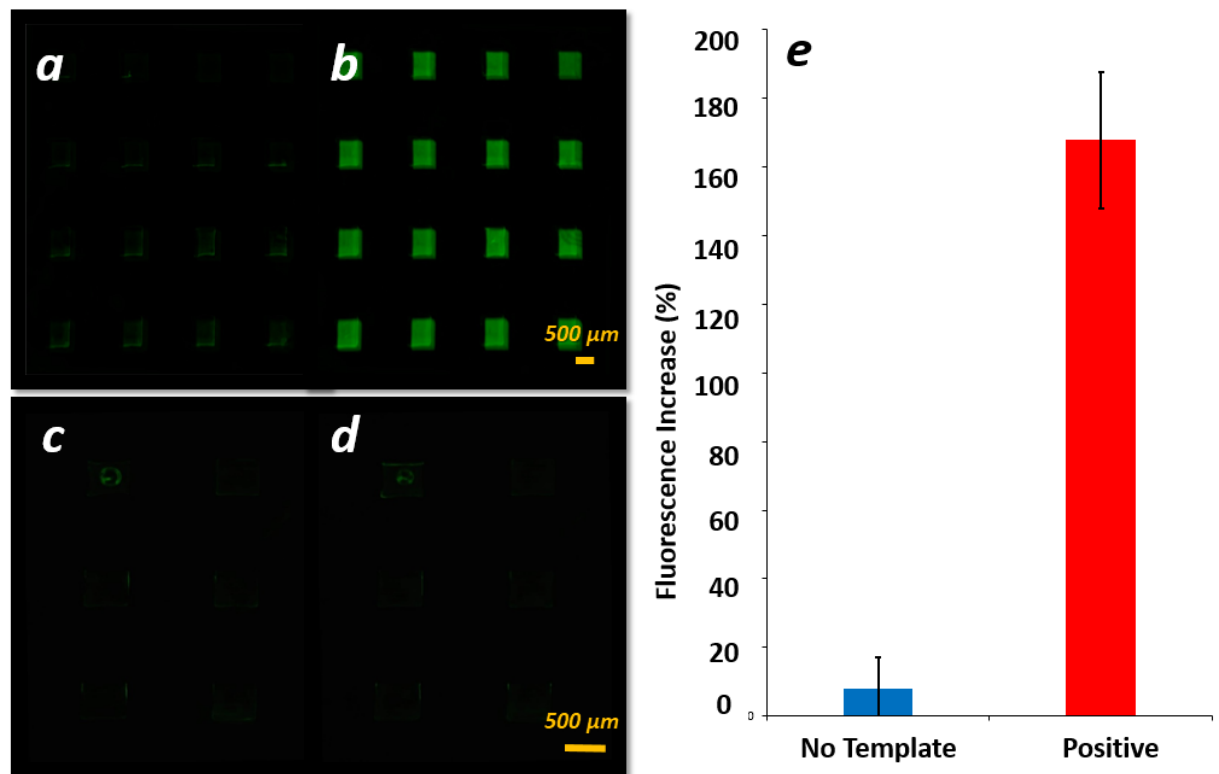


Figure 4.17 Demonstration of amplification in the integrated device. (a) Positive sample before amplification. (b) Positive sample after amplification. (c) Negative sample before

amplification. (d) Negative sample after amplification. (e) The quantified comparison between positive and negative amplifications. The average fluorescence increase percentages of the positive (red) and negative (blue) samples are shown. The initial DNA concentration of the positive sample was  $4 \times 10^6$  Copies per  $\mu\text{L}$ .

Not all the micro-wells showed similar fluorescence increments. Therefore, the average fluorescence increase percentage and standard deviation of all the micro-wells were calculated and illustrated above. The average fluorescence intensity of the positive sample started from 1800 A.U. and increased to 4800 A.U. which was 167.8 % increase with standard deviation of 19.8%. On the other hand, the average fluorescence intensity of the negative sample started from 1640 A.U. and increased to 1765 A.U. which was 8 % increase with standard deviation of 9 % which showed there was no contamination either from the device or from the solution.

This experiment demonstrated that the integrated device was capable of amplifying the DNA in multiple micro-wells simultaneously. It was also able to show a significant difference between the positive and negative samples as expected.

In order to analyse the spatial variation between the micro-wells, a few randomly selected micro-wells spread throughout the array chip were analysed. Then, the fluorescence increase between before and after the amplification, and amplification times (as discussed in chapter 3) were calculated and summarized in Figure 4.18.

Comparison of the intensities of some of the individual micro-wells in the positive amplification test showed that the change in intensities before and after the amplification, and amplification times were not the same in all the micro-wells. The mean value of the fluorescence increases of all the selected micro-wells was 210 percentage with standard deviation of 64 percentage. Similarly, the mean value of the amplification time of all the

selected micro-wells was 16 minutes with standard deviation of 4.5 minutes. The reasons behind the spatial variation could be because of filling variation, interaction between the molecules and the PDMS surface, temperature non-uniformity throughout the device or non-uniformity of the excitation light throughout the device. In the next paragraphs, the effect of these factors are analysed.

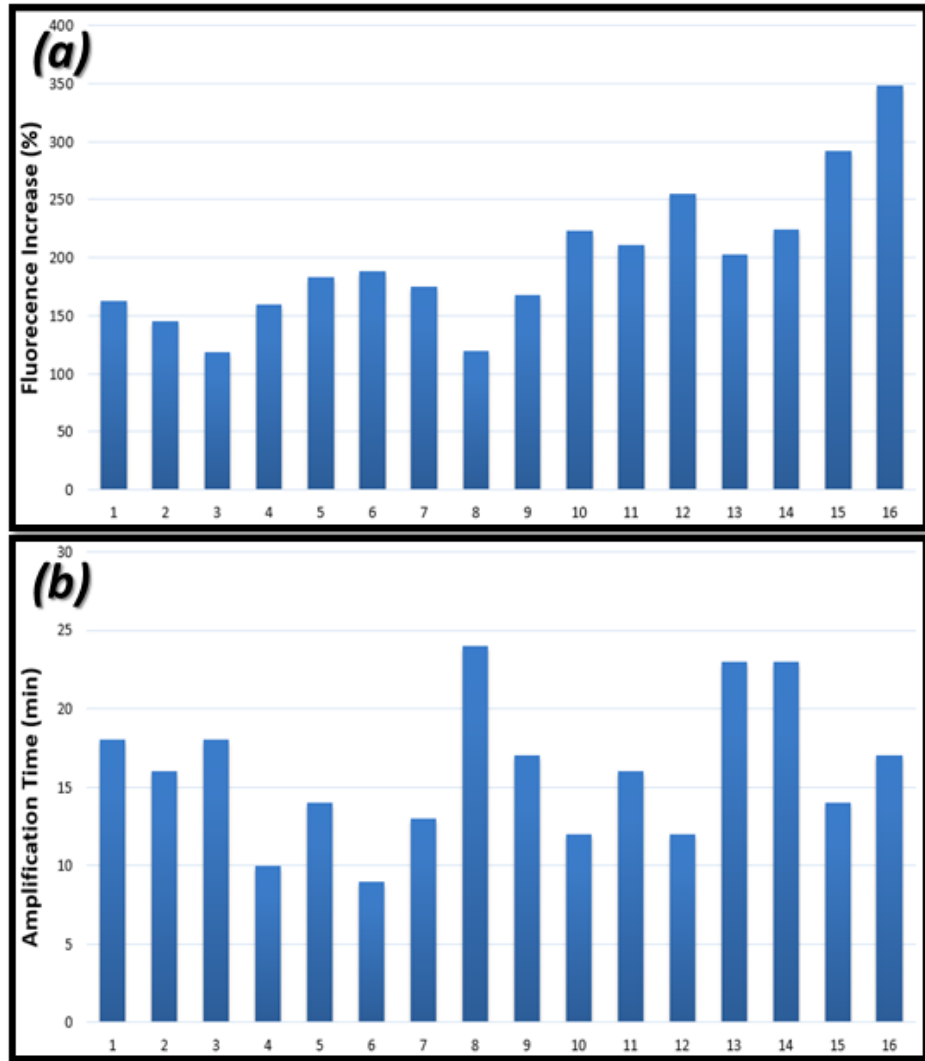


Figure 4.18 The spatial variation of the micro-wells at multiple random locations spread throughout the array chip. (a) Fluorescence increase distribution. (b) Amplification time distribution.

In order to analyse the filling variation hypothesis on the spatial variation in fluorescence increase, the fluorescence intensity distribution of the above amplified device was compared to the fluorescence intensity distribution of the device which was filled with a highly concentrated fluorescein solution ( $0.1 \frac{mg}{mL}$ ) in DI water, following the method described in chapter 3, section 3.6. The device filled with the amplified mixture had the mean fluorescence intensity of 11213 A.U. with standard deviation of 1619 A.U. Also, the device filled with the highly concentrated fluorescein solution had the mean fluorescence intensity of 63982 A.U. with standard deviation of 1501 A.U.

The key factor to compare these two distributions is the coefficient of variation (CV) which is defined as the ratio of the standard deviation to the mean, which is a parameter to measure relative variability. The solution in the amplified device had the CV of 14 % and the solution in the fluorescein device had the CV of 2 %. This result showed that the spatial variation in fluorescence increase was due to the non-uniform amplification issue and not because of any filling problems.

As it was mentioned earlier, another reason behind spatial variation between micro-wells could be a slight temperature non-uniformity throughout the device. In order to analyse the temperature variation between the randomly selected micro-wells throughout the device, the infrared thermal image of the device taken with FLIR ONE camera is shown in Figure 4.19a indicating the location of the selected micro-wells. Also, the temperature distribution of the randomly selected micro-wells is shown in Figure 4.19b.

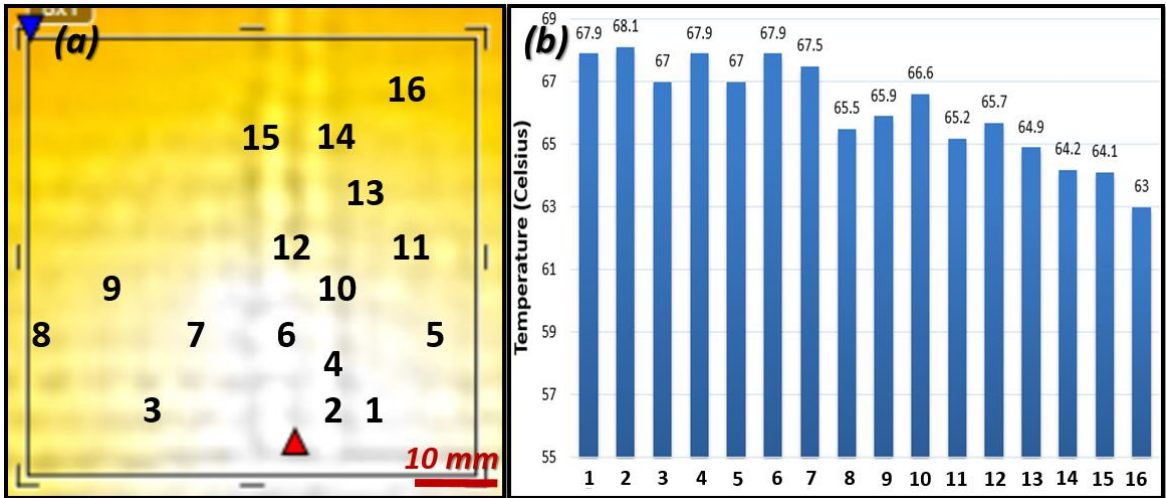


Figure 4.19 (a) The infrared thermal image of the device taken with FLIR ONE camera indicating the location of the randomly selected micro-wells. (b) The temperature distribution of the randomly selected micro-wells.

The temperature of these 16 micro-wells ranged from 63 Celsius to 68.1 Celsius with mean value of 66.1 Celsius, standard deviation of 1.6 Celsius and coefficient of variation (CV) of 2.4 %. Also, the minimum temperature (blue triangle) and the maximum temperatures (red triangle) in the selected area in Figure 4.19a were 60 Celsius and 68.2 Celsius, respectively, which were in the desired range of required temperature for LAMP reaction described in section 4.2.6.

Next, the relationship between the fluorescence increase percentages and the temperatures (Figure 4.20a), as well as the relationship between the amplification times and the temperatures (Figure 4.20b) are illustrated.

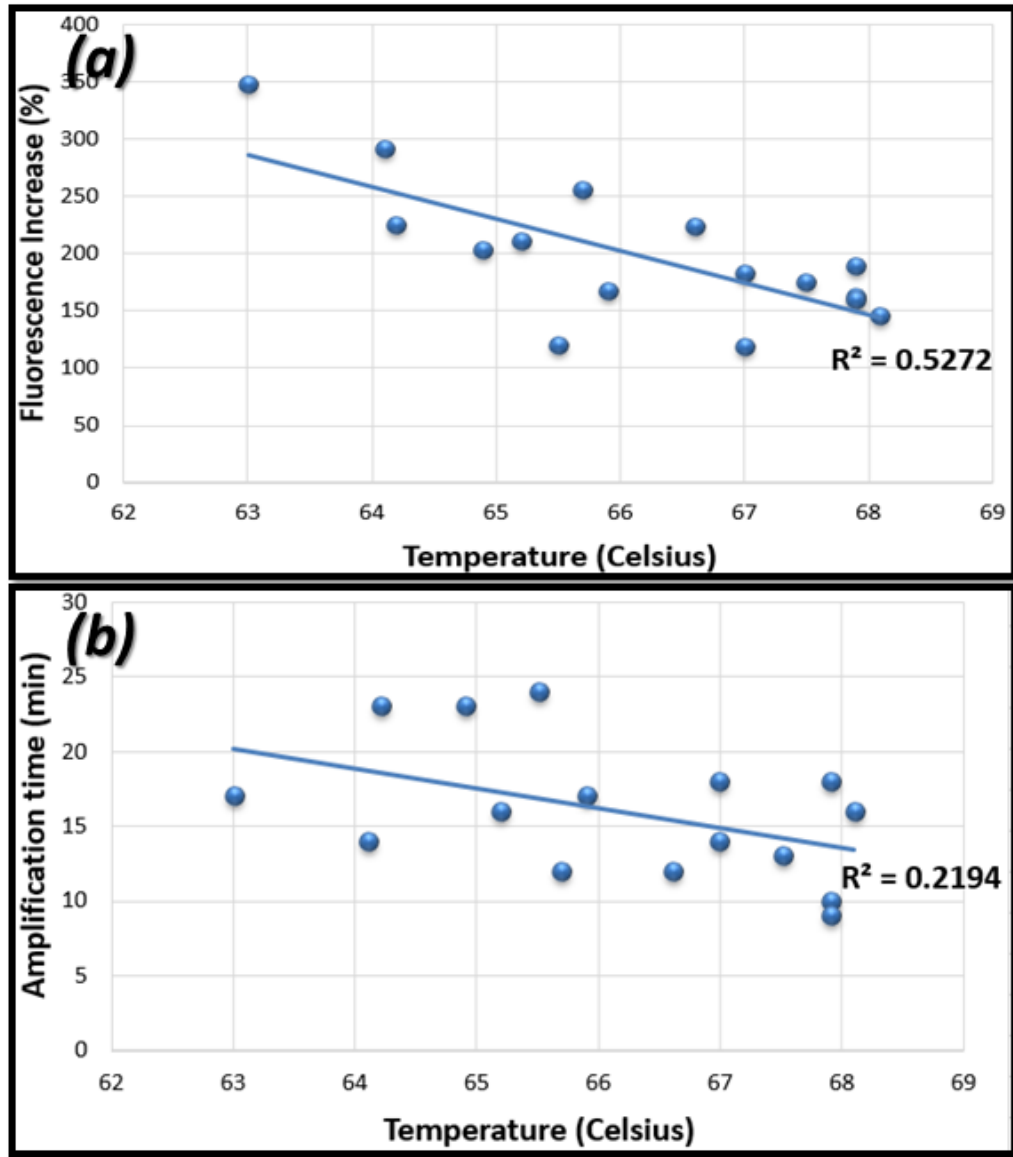


Figure 4.20 (a) The relationship between the fluorescence increase percentages and the temperatures. (b) The relationship between the amplification times and the temperatures.

As it is shown in Figure 4.20a, there was a weak linear equation between the fluorescence increase percentages and the temperatures with the coefficient of determination (R-Squared) of 0.5272. Moreover, according to the Figure 4.20b, no specific

relationship was detected between the amplification times and the temperatures of the micro-wells. The coefficient of determination (R-Squared) was 0.2194 which indicated that there is no linear relationship between them. Also, as it was illustrated in section 4.2.6, LAMP reactions performed by using ESEQuant tube scanner, showed similar efficiencies and amplification times in this range of temperature (60 to 68 Celsius). However, designing a heater with more uniform temperature gradient can decrease any possible effect of temperature non-uniformity on the performance of the LAMP reaction.

Other than these analysed parameters, the filling variation and the slight temperature non-uniformity, the non-uniformity of the excitation light throughout the device could be another source of spatial variation between the randomly selected micro-wells. Although the effect of the non-uniformity of the excitation light was eliminated through the method which was used to normalize the data explained in section 3.7 in chapter 3 (each micro-well was normalized to its initial fluorescence value), it still could affect the intensity of the emitted light from the micro-wells which could directly alter the amplification times and fluorescence increase.

Therefore, the combination of the effects of all the analysed factors together could possibly cause the spatial variation between the micro-wells.

The next sections will illustrate the real-time amplification measurement and investigate the accuracy and the reliability of the amplification process in this device.

#### **4.4.2. Real-time amplification measurement from the device**

In this section, experiments were performed on the micro-well array device with integrated heaters to show the real-time amplification measurement from the device.

Positive and negative DNA samples were used. The positive sample contains primer mix, master mix, DNA staining dye (EvaGreen 20X) along with the extracted DNA from E. coli STEC eae with the concentration of  $4 * 10^6 \text{ Copies}/\mu\text{L}$ . The negative sample does not contain the DNA template; instead it has DI water added to primer mix, master mix and DNA staining dye (EvaGreen 20X).

A positive sample was prepared and loaded into the device, as it was explained in section 3.6 in chapter 3. Also, the thermocouple was implanted into the waste channel carefully in order to monitor the temperature by using the thermometer. Next, the integrated device was put on the sample holder located in the detection system black box and connected to the power supply and was heated up to 65 Celsius by applying proper current and voltage (0.225 ampere and 18 volts). It took 3 minutes to reach to 65 Celsius from the room temperature. After the temperature was steady, the fluorescence images were taken periodically with the interval time of 1 minute as it was explained in section 4.3 in chapter 4.

Moreover, the exposure time was set to 8 seconds. The amplification was performed for an hour and the pictures were saved on an SD card for further analyses on laptop. Similar experiment was performed on another device by loading the negative solution in the device in order to compare the positive and negative results quantitatively.

Afterwards, the images from two separate experiments were processed and analyzed as described in section 3.7 in chapter 3 using ImageJ software and Microsoft Excel to obtain quantitative measurement of the intensities in each micro-well.

The fluorescent intensities of several wells in the device and their change with respect to time are plotted in Figure 4.21. It shows the characteristic S-shaped curve that is observed in real-time amplification of DNA.

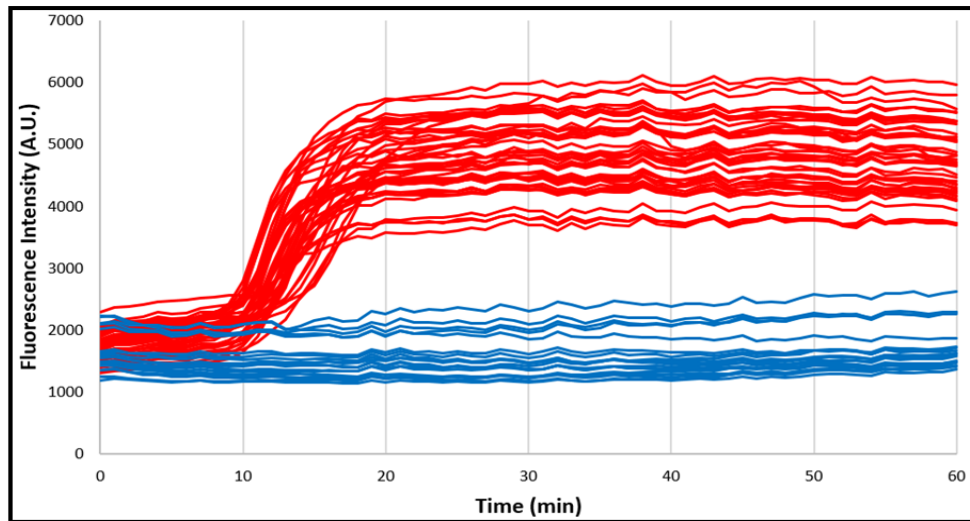


Figure 4.21 The real-time amplification curves of the highly concentrated positive solution (red lines) and the negative control (blue lines).

For the positive sample (red lines), the initial intensities were between 1309 A.U. and 2333 A.U. with the mean and the standard deviation of 1802 A.U. and 239 A.U., respectively, which resulted in the CV of 13.2 %. The final intensities were between 3703 A.U. and 6073 A.U. with the mean and the standard deviation of 4809 A.U. and 609 A.U., respectively, which brought about the CV of 12.7 %.

For the negative sample (blue lines), the initial intensities were between 1198 A.U. and 2232 A.U. with the mean and the standard deviation of 1639 A.U. and 330 A.U., respectively, which resulted in the CV of 20.1 %. The final intensities were between 1370

A.U. and 2622 A.U. with the mean and the standard deviation of 1742 A.U. and 360 A.U., respectively, which brought about the CV of 20.6 %.

In order to compare the results of all the micro-wells together, a proper normalization method was required. Therefore, intensity profile of each micro-well was normalized to its first value by dividing all of them to the first value. As a result, each line started from 1 and it was easier to follow the trend (Figure 4.22). Each red line presents one micro-well in the device which contained the positive sample. Also, blue lines signify the micro-wells in the negative experiment as a reference point for the sake of comparison. As it was expected, the red lines followed the typical S-curve amplification pattern and the blue lines stayed below the threshold value and showed no contamination in 60 minutes of the amplification time.

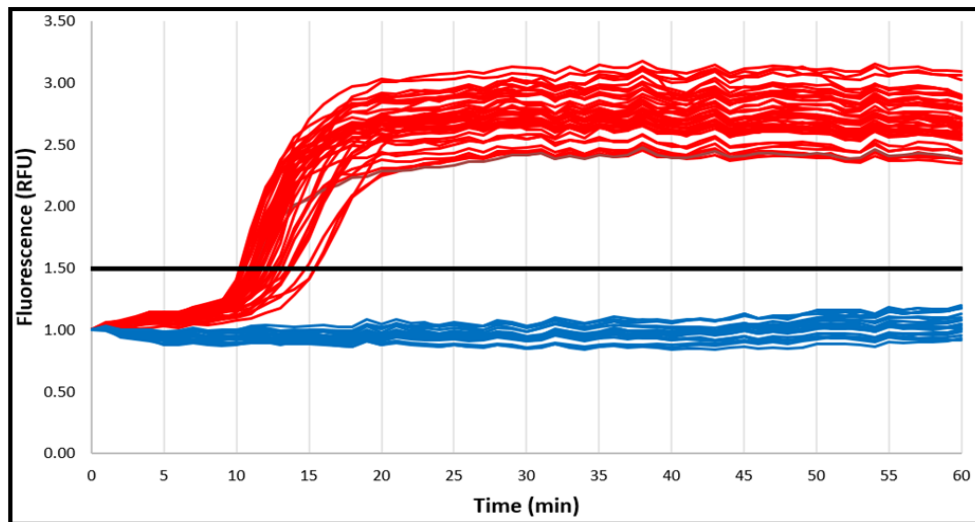


Figure 4.22 The normalized real-time amplification curves of the highly concentrated positive solution (red lines) in comparison with the negative control (blue lines).

The amplification time of the positive experiment was calculated based on the mean value of the amplification times of all the micro-wells as it was described in section 3.7 in chapter 3. Therefore, the amplification time of the positive experiment was 11.8 minutes with standard deviation of 1.4 minutes which resulted in the CV of 11.8 %. Moreover, the reasons behind spatial variation between the micro-wells were analyzed in the previous section.

As it was emphasized in chapter 2, performing the amplification in the array format increases the reliability of the results compare to the conventional methods where a single vial was used for the amplification. Moreover, this method helps to quantify the initial concentration of the DNA template by digitizing the solution into nL volumes. Additionally, digitization decreases the false positive results by reducing the chance of amplifying any possible cross contaminations.

#### **4.4.3. Repeatability**

In terms of reliability of the results in order to use them for quantification of the initial solution, different concentrations of DNA template were tested at least three times on three separate devices. In Figure 4.23 amplification results of two close concentrations,  $700000 \text{ Copies}/\text{micro-well}$  and  $70000 \text{ Copies}/\text{micro-well}$ , are shown. The error bars are one standard deviation from the mean.

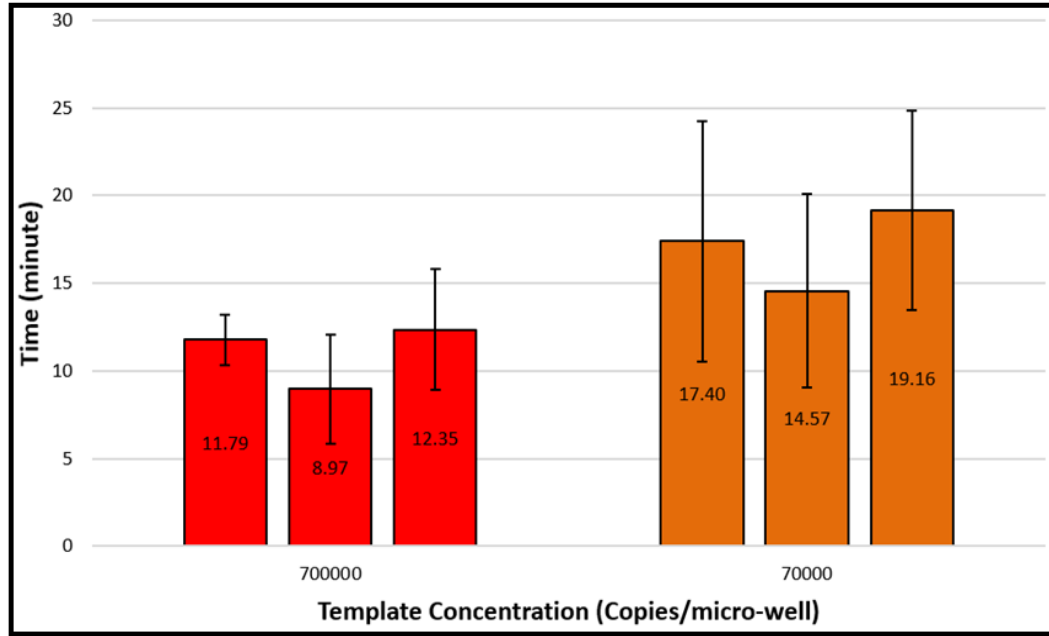


Figure 4.23 Repeatability analyses of two different DNA concentrations with 10 folds difference.

Although there was just 10 fold difference between the concentrations that were shown above, the results were distinguishable. The first group was the combination of all the data from three experiments with concentration of  $(700000 \text{ Copies}/\text{micro-well})$  and the second group was the combination of all the data from three experiments with concentration of  $(70000 \text{ Copies}/\text{micro-well})$ . The average amplification time and standard deviation of the first group were 11.6 minutes and 3.2 minutes, respectively. Also, the second group had the average amplification time of 16.7 minutes and standard deviation of 6.3 minutes. Therefore, the device is capable of quantifying the sample concentration and differentiate between two samples even with just 10 folds difference.

The next sections will characterize the device in more detail by investigating the effect of initial concentration of the DNA solution on the amplification time and the false negative ratio as well as the fluorescence increase between before and after the amplification.

#### **4.4.4. Amplification characterization**

In this section, amplification characterization is presented by showing the relationship between the amplification time and the initial concentration of the sample, the relationship between the false negative ratio and the initial concentration of the sample, the relationship between the fluorescent increase percentage and the initial concentration of the sample, followed by illustrating the capability of the device to perform parallel DNA amplification as well as the capability of the device for reagents storage prior to sample loading.

##### **4.4.4.1 Effect of the initial DNA concentration on the amplification**

In this section, the effect of the initial DNA concentration on the amplification is analyzed. The initial DNA concentration directly affects the amplification time, the false negative ratio and the fluorescence increase between before and after amplification. In this regard, serially diluted concentrations of the template target (*E. coli*) were prepared and tested in separate devices.

It was shown that the fecal samples from the infected individual can contain between  $10^6$  to  $10^9$  CFU/gram of *E. coli*. Based on this range of concentration, serially diluted concentrations of *E. coli* were prepared. The highest DNA concentration was  $\sim 4 \times$

$10^6$  Copies/ $\mu\text{L}$ . Then, serially diluted DNA concentrations were prepared by mixing DI water and DNA template with the volume ratio of 10 to 1 in order to decrease the DNA concentration by 10 fold every time. As a result, 8 different concentrations were prepared sequentially including  $4 * 10^6$  Copies/ $\mu\text{L}$ ,  $4 * 10^5$  Copies/ $\mu\text{L}$ ,  $4 * 10^4$  Copies/ $\mu\text{L}$ ,  $4 * 10^3$  Copies/ $\mu\text{L}$ ,  $4 * 10^2$  Copies/ $\mu\text{L}$ ,  $4 * 10^1$  Copies/ $\mu\text{L}$ , 4 Copies/ $\mu\text{L}$  and 0.4 Copies/ $\mu\text{L}$ . Next, different positive solutions which contained DNA solutions with different concentrations along with the primer mix, master mix and DNA staining dye (EvaGreen 20X) were prepared and amplified in separate integrated devices. The same methodology which was explained in section 4.4.2, real-time amplification measurement, was performed here as well in order to load the samples, apply the proper current and voltage, take the fluorescence images with the frequency of 1 image every minute and analyze the pictures using ImageJ and Microsoft Excel software. For each DNA concentration, 3 separate devices were prepared and tested. All the amplifications were performed for 75 minutes.

In order to determine the DNA concentration inside of each micro-well at any DNA concentrations in the solution, the concentration needed to be scaled down based on the volume of the micro-well which was 175-nL ( $500*500*700 \mu\text{m}$ ). For instance, for the highest DNA concentration solution,  $4 * 10^6$  Copies/ $\mu\text{L}$ , the DNA concentration inside each micro-well was equal to  $7 * 10^5$  Copies/Micro-well. The amplification times and standard deviations at different concentrations are summarized in Table 4.9.

<b>Initial concentration (Copies/<math>\mu\text{L}</math>)</b>	<b>Number of DNAs inside the micro-well (Copies/micro-well)</b>	<b>Amplification time (minute)</b>	<b>Standard deviation (minute)</b>
<b><math>4 * 10^6</math></b>	$7 * 10^5$	11	1.8
<b><math>4 * 10^5</math></b>	$7 * 10^4$	17	2.3
<b>4000</b>	700	30.9	6.3
<b>40</b>	7	39.8	9.7
<b>0.4</b>	0.07	55.3	17.5

Table 4-8 The amplification times and standard deviations of different concentrations.

Moreover, the results in Table 4-9 are illustrated in Figure 4.24.

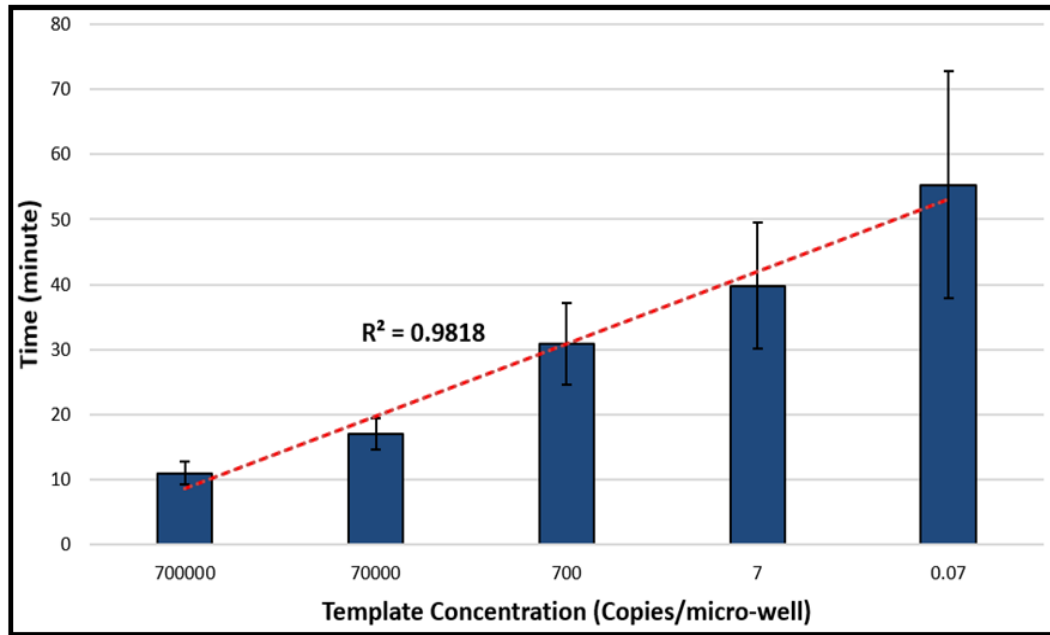


Figure 4.24 Amplification times for serially diluted concentrations.

At the highest tested DNA concentration,  $4 * 10^6$  Copies/ $\mu$ L or  $7 * 10^5$  Copies/micro-well, the amplification time was 11 minutes with standard deviation of 1.8 minutes and at the lowest tested DNA concentration, 0.4 Copies/ $\mu$ L or 0.07 Copies/Micro-well, the amplification time was 55.3 minutes with standard deviation of 17.5 minutes.

As it is shown in Figure 4.24, as the DNA concentration decreased, the amplification times increased linearly with the coefficient of determination (R-Squared) of 0.9818. This result was expected to happen since at higher DNA concentration, more number of DNAs existed in the solution which resulted in faster amplification since it passed the threshold of the detection faster. On the other hand, at lower DNA concentration, less number of DNAs in the sample brought up longer period of time in order to reach to the threshold of the detection.

Also, according to Table 4-9, the error bars increased as the DNA concentration decreased, but not as linearly as the amplification times with a calculated coefficient of determination of 0.9075. The reason could be the increase in the heterogeneity of DNA concentration distribution among the micro-wells which resulted in more diverse amplification times between the micro-wells.

Additionally, at the lowest tested DNA concentration, 0.07 Copies/Micro-well, some of the wells showed amplification while some did not since at this concentration only a few of the wells are expected to be populated with the sample DNA. This result agrees the previous reports about the ability of the LAMP reaction to amplify even a single copy of the DNA template [112][113] and confirms that this device can be used to detect even a single DNA in the sample.

For the sake of comparison, same experiments were done by using ESEQuant tube scanner. Serially diluted concentrations of the template target (E. coli) were prepared in

different tubes and amplified in one run (Figure 4.25). As it was mentioned earlier, ESEQuant tube scanner is capable of performing 8 reactions simultaneously.

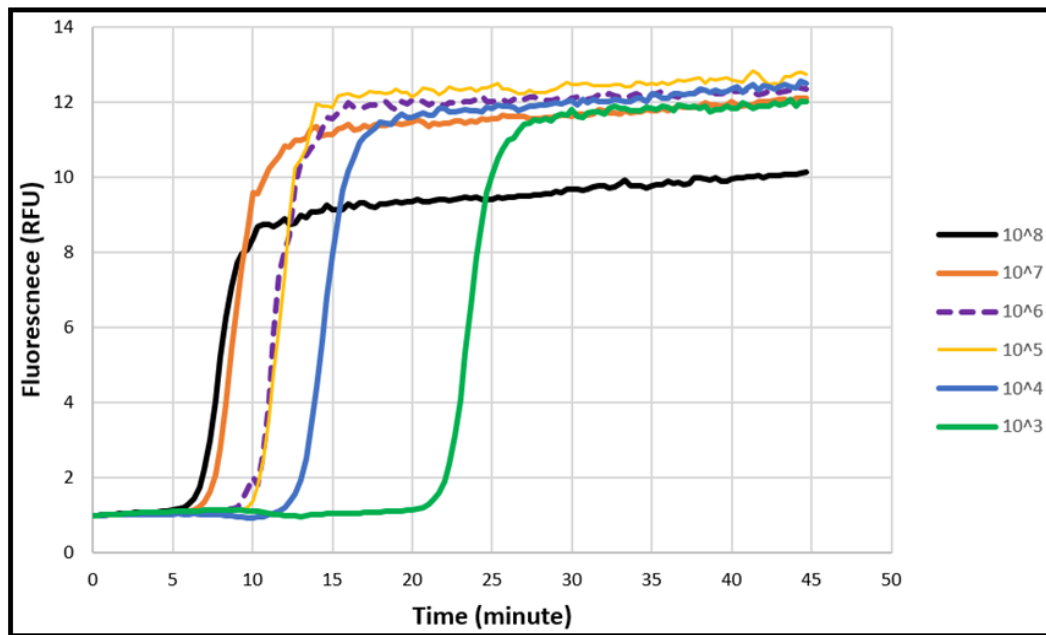


Figure 4.25 Real-time amplification profile of serially diluted concentrations by using ESEQuant tube scanner.

Moreover, the amplification time of each concentration was calculated by applying the same methodology that was used in section 4.4.2 (considering 1.5 as the threshold value). These amplification times are summarized in Figure 4.26.

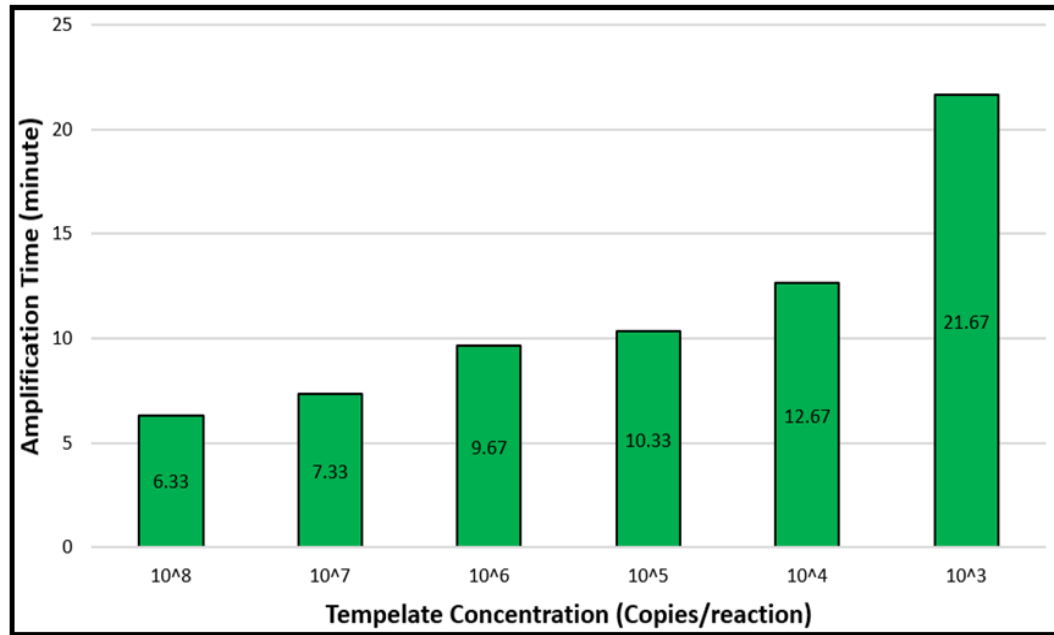


Figure 4.26 Amplification times of serially diluted concentrations by using ESEQuant tube scanner.

As a result, the comparison of the amplification times at the same concentrations between the integrated device and ESEQuant tube scanner, showed that the numbers were relatively similar which confirmed the reliability of the analyzed results.

False negative ratio is defined as the ratio of the number of micro-wells which are supposed to show amplification (since theoretically there is at least one DNA molecule inside) but do not over the total number of micro-wells which contain solution. The false

negative ratios for the serially diluted concentrations are calculated and shown in Figure 4.27.

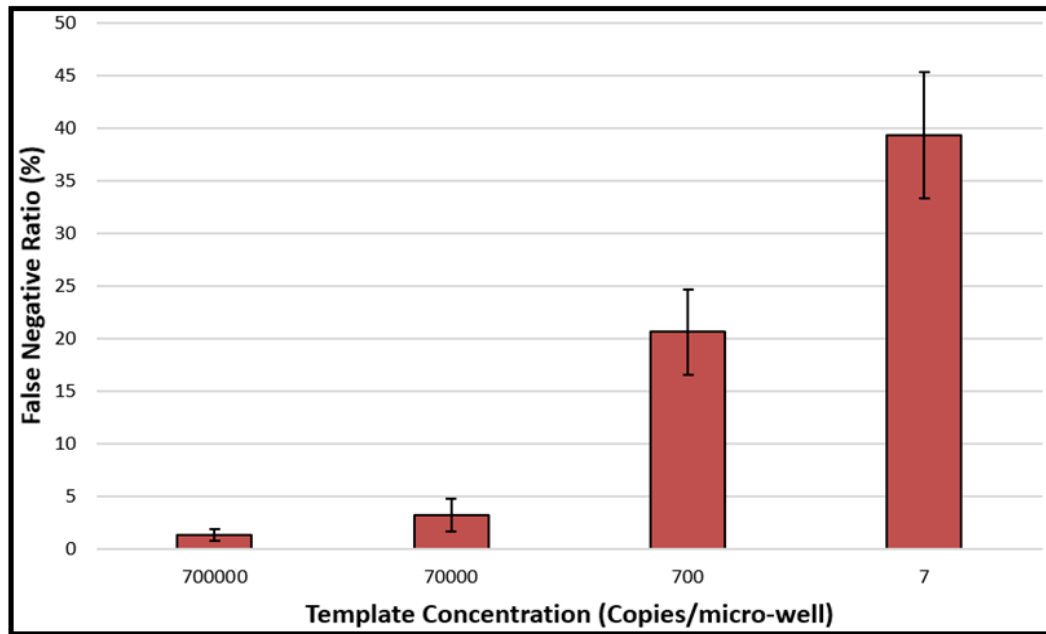


Figure 4.27 False negative ratio for serially diluted concentrations.

As it was expected, the solution with the initial concentration of 7 Copies/micro-well has significantly higher false negative ratio (39.3 %) compare to the solution with the initial concentration of 700000 Copies/micro-well (1.3 %). The reason could be the increase in the heterogeneity of DNA concentration distribution among the micro-wells as the initial concentration decreased which resulted in higher false negative ratios between the micro-wells.

Another noticeable factor in analysing the amplification data of serially diluted concentrations is the percentage increase of the fluorescence intensity which is calculated and presented in Figure 4.28 for 5 different DNA concentrations.

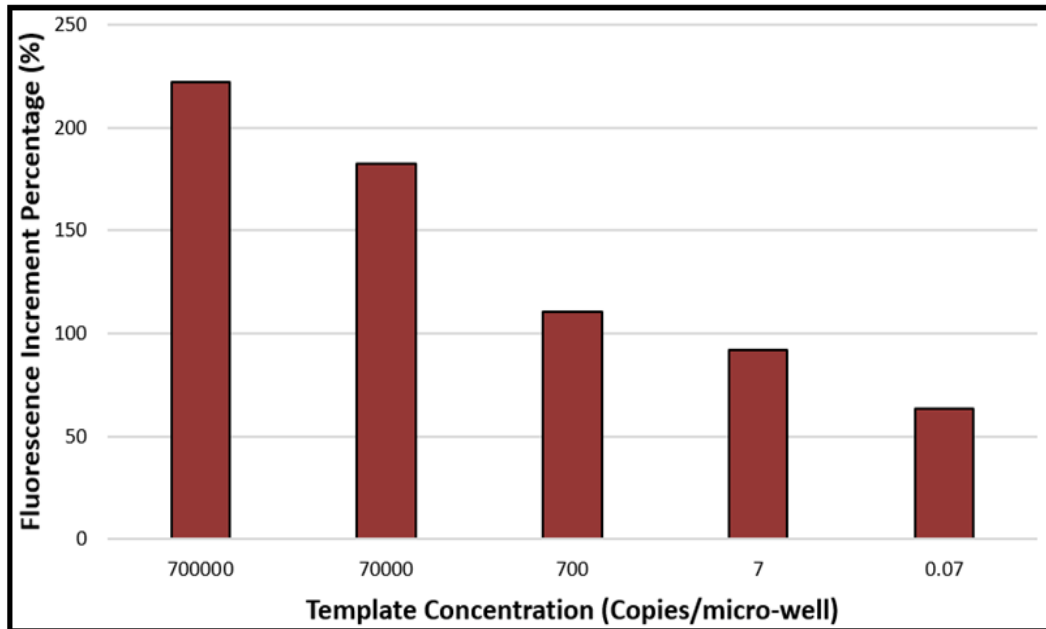


Figure 4.28 Fluorescence increase percentage for serially diluted concentrations.

As it was expected, not all the serially diluted concentrations showed similar percentage increase of the fluorescence intensity, a phenomenon which was observed in amplification of serially diluted concentrations by using ESEQuant tube scanner as well since there are limited amount of reagents (specifically dNTPs) in the solution and after

any reagents is consumed completely, the LAMP reaction stops. For instance, those amount of reagents could be used to amplify the initial DNA concentration of 7 Copies/micro-well to 1 million Copies/micro-well or it could be used to amplify the initial DNA concentration of 700000 Copies/micro-well to 10 million Copies/micro-well. Therefore, the final number of DNAs in the solution after the amplifications are different which resulted in different fluorescence intensities. As a rule of thumb, the higher the initial concentration, the higher the percentage increase of the fluorescence intensity.

#### **4.4.5. Parallel DNA amplification**

In this section, the capability of the device to perform different LAMP reactions simultaneously on the same device is illustrated which is known as parallel DNA amplification. In this regard, four different solutions were prepared including one highly concentrated positive solution of *E. coli* STEC eae with concentration of  $4 * 10^5$  Copies/ $\mu$ L, one low concentrated positive solution of *E. coli* STEC eae with concentration of 40 Copies/ $\mu$ L, one negative solution as a negative control and one positive solution which contained highly concentrated  $\lambda$  DNA (Thermo Fisher Scientific, Massachusetts, USA) with concentration of  $100 \mu\text{g}/\text{ml}$  instead of *E. coli* STEC eae to serve as the positive control.

Then, these four solutions were loaded on four different regions on the integrated device which were separated by the means of the waste channels following the

methodology which was explained in section 3.6 in chapter 3. The schematic formation of these four reactions on the integrated device is shown in Figure 4.29.

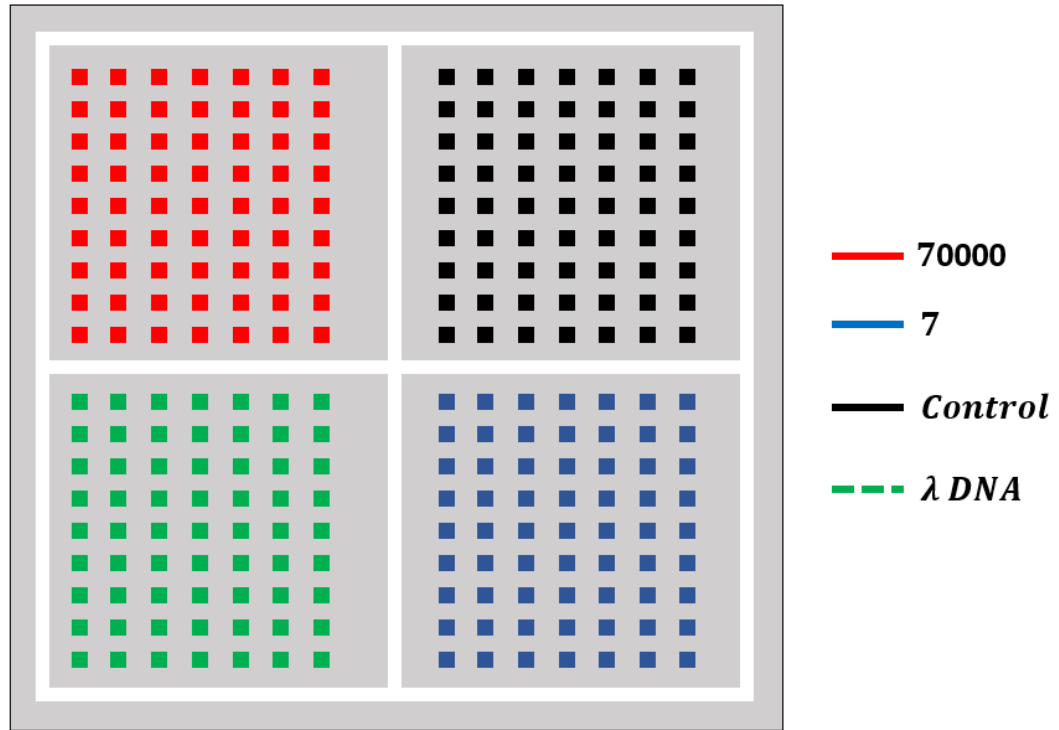


Figure 4.29 Schematic of the device for parallel DNA amplification of four different LAMP reactions including *E. coli* **70000 Copies / micro – well** solution (red), *E. coli* **7 Copies / micro – well** solution (blue), negative control solution (black) and positive control solution (green) which contained  $\lambda$  DNA with concentration of **100  $\mu\text{g}/\text{ml}$** .

Afterwards, the same procedure explained in section 4.4.2 (real-time amplification) was implemented on the integrated device. The amplification reactions were performed for 75 minutes. Next, the sequential fluorescence pictures were analyzed. The real-time amplification curves of these 4 reactions are shown in Figure 4.30. A few micro-wells from each reaction were chosen to show in the figure to make it more clear and understandable.

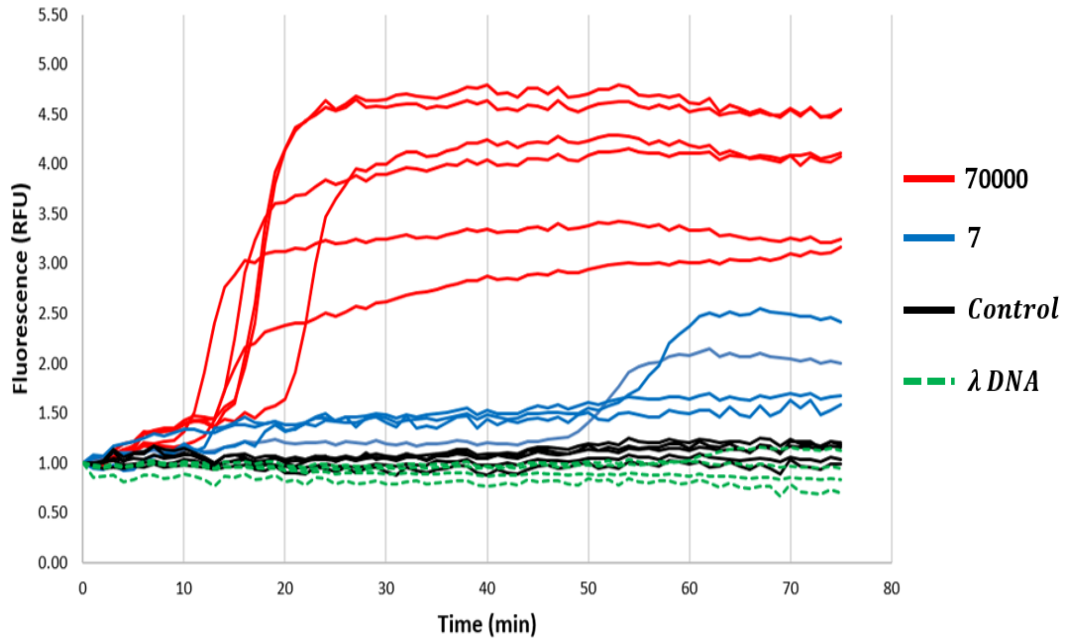


Figure 4.30 Parallel DNA amplification of four different reactions including *E. coli* **70000 Copies / micro – well** solution (red lines), *E. coli* **7 Copies / micro – well** solution (blue lines), negative control solution (black lines) and positive control solution (green dotted lines) which contained  $\lambda$  DNA with concentration of **100  $\mu\text{g}/\text{ml}$** .

As it was expected, the high concentrated template (70000 Copies/micro-well) which was displayed with red lines, was amplified faster than the others in 14 minutes. Moreover, the lower template concentration (7 Copies/micro-well) which was illustrated with blue lines, was amplified reasonably after the high concentrated template in 43 minutes. These results were in the expected ranges calculated in section 4.4.4. Additionally, the negative control solution which did not contain the DNA template and was displayed with black lines, did not show any significant fluorescence increases which indicated that

there was no contamination source. Furthermore, the positive control solution which contained highly concentrated  $\lambda$  DNA and was illustrated with green dotted lines, did not show any noticeable fluorescence increases which determined the specificity of the primers design. As it was explained earlier, the primer design for LAMP reaction is extremely specific. Therefore, the reaction just works when the primers match with the DNA template.

In conclusion, high-throughput amplification of four different samples were shown using the integrated device. This method facilitates the amplification of multiple samples or the same sample but using multiple primers while reducing the need for labor-intensive protocols. Although ESEQuant tube scanner is capable of performing multiple reactions simultaneously, it cannot prevent the false positive results if cross contamination exists in the solution. On the other hand, this technique decreases the false positive results by reducing the chance of amplifying any possible cross contaminations through sample digitization.

In the next section, the capability of the device for on chip reagent storage is illustrated.

#### **4.4.6. On Chip reagent storage**

In this section, the capability of the device for on chip reagent storage is illustrated. On chip reagent storage is useful since it eliminates or decreases the need to do sample pre-processing. For instance, after dehydration of the primer mix, a primer-less solution can be loaded into the device.

In order to dehydrate the primer mix solution on the device with the same concentration as in previous experiments, 5  $\mu$ L of the primer mix solution was added to 20

$\mu\text{L}$  of DI water to reach 25  $\mu\text{L}$  volume. Therefore, after the diluted primer mix solution was loaded into the device, the concentration of the primer mix in each micro-well remained the same as previous experiments. Next, the device was put on top of a heater which was set at 50 Celsius for 30 minutes. After primer mix solution dehydration, the device was stored in the freezer at -20 Celsius.

Next, a primer-less positive solution was prepared contained master mix, DNA staining dye (EvaGreen 20X), 5  $\mu\text{L}$  of DI water along with the extracted DNA from E. coli STEC eae with the concentration of  $4 * 10^5$  Copies/ $\mu\text{L}$ . Also, 5  $\mu\text{L}$  of DI water was added to the primer-less positive solution instead of the primer mix in order to keep the concentration of all the mentioned components the same as the previous experiments. Therefore, the volume of primer-less positive solution was 25  $\mu\text{L}$  (same volume like the original positive solution).

The devices which the primer mix was dehydrated on were kept frozen for various durations of time (2 hrs, 3 days and 5 days) prior to loading of the DNA sample and subsequent amplification in order to analyze the shelf life of frozen dried primers.

Before the primer-less solution was loaded, the device was brought out of the freezer and was defrosted at the room temperature for 10 minutes. Then, the primer-less solution was loaded into the device using the method that was explained in detail in section 3.6 in chapter 3. Next, the amplification was performed following the method which was explained in section 4.4.2. The results of these experiments are shown in Figure 4.31.

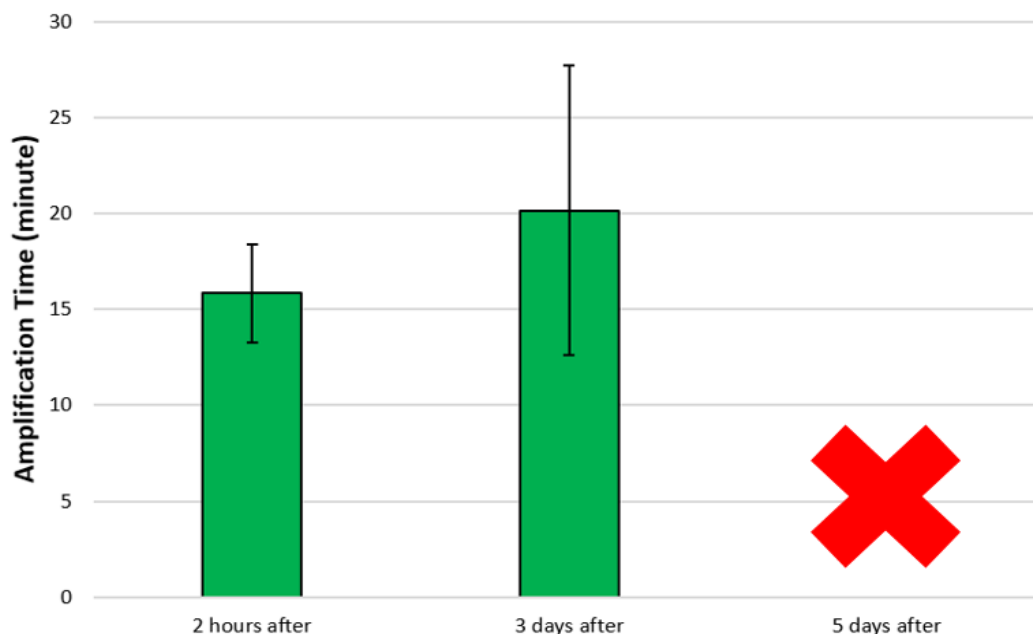


Figure 4.31 Amplification time of the primer-less positive solution with respect to time after the primer dehydration on the chip in order to analyze the shelf life of the frozen dried primers. The added DNA template had the concentration of 70000 Copies/micro-well.

As it is shown in Figure 4.31, the experiment which was performed 2 hours after the dehydration, showed amplification with the efficiency as good as the original experiment described in section 4.4.4 which had the primer mix in its solution. The amplification time was 15.8 minutes with standard deviation of 2.5 minutes. The second experiment was performed 3 days after the primer mix dehydration. Even this solution was amplified at a reasonable time of 20.1 minutes with standard deviation of 7.5 minutes, which indicated that the primer dehydration with this method worked even after 3 days. However, the amplification time and standard deviation of the second experiment were higher compare to the first experiment which revealed that the primer dehydration efficiency decreased with

respect to time. Nevertheless, the third device which was kept frozen for 5 days and then used for the amplification, did not show a successful amplification. The main reason behind this phenomenon could be loss of primers needed inclined toward the complimentary sequence and their capability to develop the dumbbell structure for LAMP amplification. In addition, T. Anchordoquy et al [114] and M. Molina et al [115] showed that stored molecules lose their molecular weight which directly affects the gene expression, with respect to time during prolonged storage.

As a solution for this problem and to prevent adsorption of the polymerase to the PDMS surface, a coating method was suggested by Zhang et al [116]. Sigmacote (Sigma-Aldrich, St. Louis, MO) was coated on the silicone surface to neutralize the molecules at the surface. It has been reported that by applying this method, the life time of the dried primers can be increased to 10 days. However, the efficiency of the amplification reaction decreases considerably [117].

## **4.5 Summary**

In this chapter, the results of different parts of the device were introduced and discussed in detail. First, the results of micro-well design were presented which covered the shape of the micro-well and its effect on the filling efficiency and the intensity of the fluorescence signal. Then, the results of designing flexible heaters using plotting method were discussed. The main criteria were the uniformity of the temperature gradient, fabrication cost and electrical power consumption which were compared to the commercially available heaters. Finally, the DNA amplification results were demonstrated by showing the proof of concept of the DNA amplification, followed by characterization of the device which started with analysing the real-time amplification curves to quantify

the initial concentration of the DNA template. The amplification times, the false negative ratios and the percentage increase of fluorescence intensity for serially diluted DNA concentrations were presented. Also, the capability of the device to perform parallel DNA amplification was presented by showing the results of four different reactions which were performed simultaneously on the same device. Lastly, the primer mix dehydration method was explained. It was shown that the primers are capable of re-suspending into the primer-less solution in order to complete a successful amplification reaction even 3 days after the dehydration.

## **Chapter 5: Conclusion and Future Work**

### **5.1 Conclusion**

Early diagnosis of diseases could increase the survival rate and decrease the cost of treatment. Nucleic-acid-based detection methods are generally considered to be more sensitive and accurate in comparison to other common techniques such as detecting by specific epitopes on the pathogen membrane or their produced toxin, as discussed in chapter 2. However, they require a number of sample preparation steps such as cell lysis, sample purification, aliquoting and mixing with the amplification reagents prior to DNA amplification. Microfluidics can be used to automate these unit operations and also provide benefits such as lower cost due to reduced reagent usage and enable faster analysis time.

In the last 20 years, scientists have tried to simplify the detection and treatment methods in order to provide more accessible and more rapid services in resource-poor areas where there are no state-of-the-art technologies available. There are two major contributions to ease the whole procedure: 1) by reducing the complexities of the biological reactions, and 2) by eliminating the use of high-tech and expensive equipment from engineering point of view. Examples of such contributions are invention and development of isothermal amplification methods and elimination of using external equipment such as pumps and temperature controllers, respectively. In this regard, microfluidic devices can play important roles by combining these two contributions in order to reduce the time and cost of the experiment, decrease the volume of the required reagents and make the procedures more automated.

In this thesis, a disposable microfluidic device to perform isothermal DNA amplification was introduced that is capable of parallel amplification of multiple samples. Loop mediated isothermal amplification (LAMP) which has been shown that is more robust and sensitive compare to polymerase chain reaction (PCR) has been implemented in this device. The integrated device composed of micro-wells and a custom fabricated flexible heater made by using plotting method. The shape and size of the micro-wells were optimized in order to reach the best possible filling efficiency, and also to be able to detect the S-shaped real-time amplification fluorescence signals by using the large-field-of-view detection setup which was designed and fabricated for this application. Moreover, the performance of the fabricated flexible heaters was analyzed and compared with the commercially available heaters in terms of temperature gradient uniformity, power consumption and cost. Additionally, it was shown that this device is capable of quantifying the concentration of the DNA template in the solution even with 10 fold difference. Finally, primer mix pre-loading was done successfully which could make the preparation steps easier in order to fill a primer-less solution into the device.

The main contributions of the thesis can be classified into four major categories. First, was the use of a simple sample segmentation technique to produce a large number of aliquots of the sample to perform parallel amplification without the use of micro-pumps or two phase flows. This method had been previously developed in our lab for the purpose of cell culturing but was not applied for amplification purposes. The geometry of the micro-wells was optimized such that they have complete filling and are able to provide sufficient contrast between amplified and unamplified samples.

The second important contribution of the thesis was the design and the fabrication of the disposable flexible heaters using a direct write process. The heaters were designed to produce a better uniformity in temperature distribution than that could be achieved with

commercial thin film heaters. It has been shown that fabricated flexible heaters by using direct write method were better than the commercially available heaters in terms of the uniformity of the temperature gradient and fabrication cost, but not the electrical power consumption. The design of the flexible heaters can be optimized further to obtain more uniform temperature gradient and also to improve the electrical power consumption by optimizing the size of the wire and its material. Moreover, implementing the direct write process reduced the fabrication cost of the whole device. In terms of the used material, 6 milliliter of PDMS was used in fabrication of each device which cost around 50 cents. Therefore, the gross cost of fabricating each device was 1 CAD or less (including the cost of the flexible heater). Consequently, this device meets the criteria of disposability of point-of-care devices in terms of the cost.

The third evident contribution was design and manufacture of the large field of view fluorescent detection setup which was designed by Reza Ghaemi (another student in the lab). Commonly available fluorescent microscopes cannot cover the area as big as the area of this device (5cm\*5cm) in one frame. Therefore, the lack of having a large field of view fluorescent microscope could be felt drastically and it was the motivation of designing one. The components of the current setup were optimized to work with EvaGreen dye as a fluorescent dye with the excitation peak of 500 nm and the emission peak of 530 nm. However, by properly changing the excitation filter, the emission filter, the dichroic mirror, and the excitation LED source this setup can be used to work with other fluorescent dyes as well.

The fourth contribution was implementing the waste channel in the design in such a way that it eliminated the samples from different regions to get mixed with each other which separates the regions, in addition to collect the extra samples. Therefore, two crucial challenges were solved by the means of the waste channel.

## **5.2 Future work**

The first parameter that can be studied further in the future is the material used to fabricate the micro-wells. Although it is common to use PDMS as the core material in fabricating the microfluidic devices, there are some challenges involved. For instance, although PDMS is a biocompatible material and has been widely used in the field of microfluidics, it can absorb the molecules at its surface which is a considerable problem. Also, PDMS is hydrophobic by nature and it needs some treatment such as using air plasma to make it hydrophilic. In this specific application, hydrophilicity of the micro-wells is the priority since it facilitates the filling process. A reasonable replacement material to use instead of PDMS is vinyl, which is one of the most widely produced synthetic plastic polymer. There are different types of vinyl available in terms of hydrophilicity and also thickness. A practical suggestion is the idea of three layers sandwich as it is shown in Figure 5.1. The bottom layer can be a thin hydrophilic vinyl, the middle layer can be a hydrophobic vinyl with specific thickness, and the top layer can be the same sealing tape that was used in these experiments.

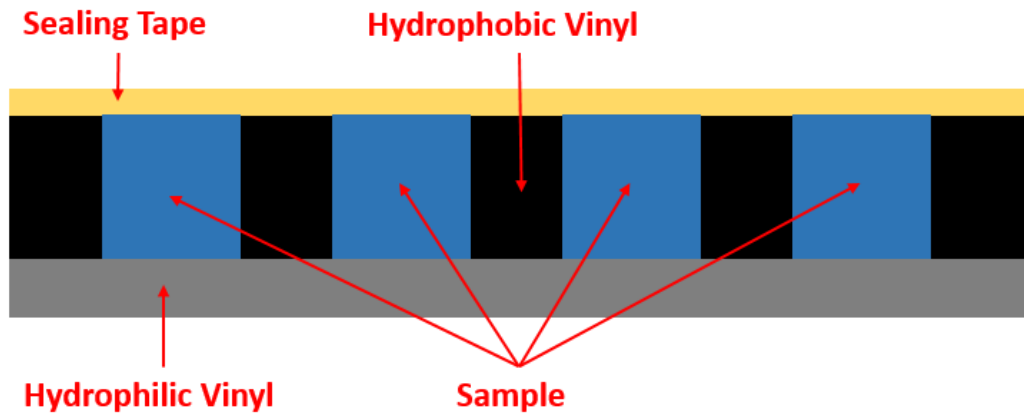


Figure 5.1 The proposal for the next generation of the device which includes a sandwich of three layers of hydrophilic vinyl, hydrophobic vinyl and sealing tape.

The critical part is cutting the hydrophobic layer of vinyl into the desired pattern to shape the arrays of micro-wells. As a proof of concept, a hydrophobic layer of vinyl with 500 micrometer thickness was cut and patterned by using the same machine as it was used in Xurography method, the Cricut Explore One Machine. Then, it was bonded to a hydrophilic layer of vinyl and was filled with Methylene Blue solution. Finally, the device was sealed using the sealing tape as it is shown in Figure 5.2.

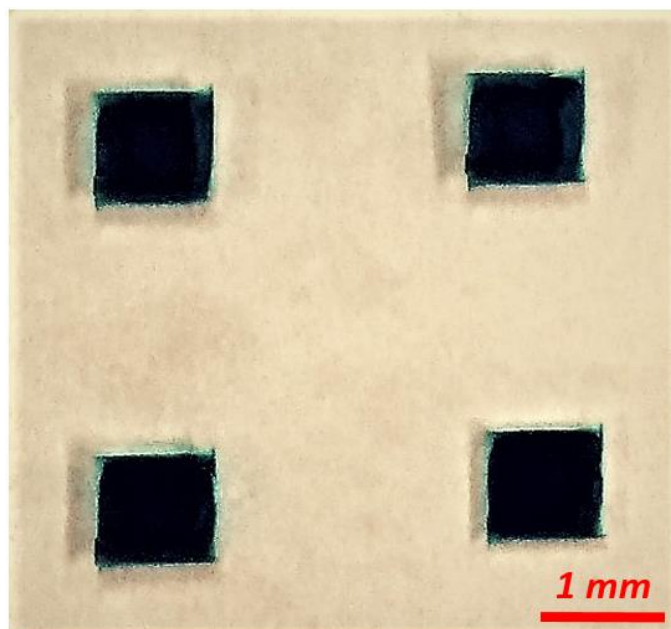


Figure 5.2 The proof of concept of the proposal for the next generation of the device.

Although the presented device in Figure 5.2 has bigger micro-wells compare to the current device, more studies are needed to be done on this part to reduce the size since there are some challenges in cutting the vinyl sheets into relatively small micro-wells. Another interesting idea is to use heat shrinkable films. In this case, bigger wells can be cut and desirable size can be reached after the shrinkage [118].

Secondly, the volume of each micro-well and the number of micro-wells can be optimized further. In microarray conformation designs, it is a privilege to have lower volume and higher number of micro-wells. In this work, these two parameters were chosen based on the fabrication constraints described in chapter 3, as well as the limit of detection (LOD) of the detection setup. One way to improve the LOD is by increasing the power of the LED light in the detection setup. Therefore, by using a more powerful LED source, the height of the micro-wells can be reduced, while getting the same real-time amplification

typical S-curve as before. Accordingly, the width of the micro-wells and the spacing between them will decrease which results in lower volume and higher number of micro-wells which are desired in the microarray conformation.

Thirdly, a better design of the flexible heater is needed. Although it was shown that the fabricated heaters by using plotting method have higher temperature gradient uniformity compare to the commercially available options, 20 percent higher, this number can be increased further to >80% percent ideally which can increase the performance of the device by providing more uniform temperature in all of the micro-wells. Other design ideas such as spiral design with variable spacing between the micro-wires can be analyzed by using the same simulation model which is described in Appendix B.

Moreover, another way to provide more uniformity to the temperature distribution can be by implementing a layer of paraffin between the flexible heater and micro-wells. This can also serve to decrease any environmental effects on the device by reducing the temperature fluctuation. Paraffin is considered as a phase change material (PCM) which has high heat of fusion. Also, paraffin solidifies and melts at the same temperature by absorbing and releasing energy as a latent heat. C. Liu et al [119] implemented the idea of using paraffin as a thermal insulator in a self-heating cartridge. However, implementing paraffin in the design can cause some problems. First of all, after paraffin melts, it can diffuse into the PDMS which is a permeable material and even get mixed with the amplification solution which could stop the LAMP reaction. Secondly, the fabrication protocol is required to change, specifically the curing time and the temperature of the PDMS since the paraffin starts melting at temperature above 65 Celsius. So, lower temperature and longer curing time is needed. Therefore, the fabrication time will increase.

Furthermore, more studies can be done on the energy source for the heater. In the presented experiments, the energy source was A GPS-3030DD power supply. However, since the consumed energy is less than 2 watts, the experiments can be run using a battery that can supply 2 watts for at least an hour. For instance, a Panasonic 9 Volt alkaline battery with the length of 5 centimeter would be a good candidate to use as the energy source. Also, another interesting idea could be connecting the device to a USB port of a laptop or a PC and use the laptop or the PC as the power supply.

The last but not least is the technique that was used to seal the device which was by hand and using a roller. This part can be investigated further to automate the sealing method. For instance, one of the feasible options would be implementing a technology such as the push click latch. In this regard, a well-designed holder needs to be fabricated to meet all the necessary criteria.

## **Appendix A: SU-8 master mold fabrication with the height of 700 $\mu\text{m}$**

1. Put the 3-inch silicon wafer in Acetone for 1 minute.
2. Put the wafer in Methanol for 1 minute.
3. Rinse the wafer with DI water for 1 minute.
4. Dry the wafer by blowing nitrogen gas.
5. Put the wafer on top of a flat hotplate at 150 Celsius for 2 minutes.
6. Put the wafer in the plasma machine which was set on 50 watts for 1 minute.
7. Put the wafer on spinner and align the center of the wafer with the center of the spinner.
8. Add 12 mL photoresist (SU-8-100) on top of the wafer.
9. Spin the wafer for 35 seconds at 450 RPM, followed by 15 seconds at 500 RPM with the acceleration rate of 100 RPM per second.
10. Prebake the wafer for 60 minutes at 65 Celsius, followed by 270 minutes at 95 Celsius.
11. Leave the prebaked wafer on a completely flat surface for 3 days which gives the photoresist enough time to flow uniformly on the surface of the wafer. Also, it should not be exposed to any lights during this period of time.
12. Align the wafer and the printed mask on the mask aligner.
13. Expose the wafer to the UV light for total exposure energy of  $800 \text{ mJ}/\text{cm}^2$ .
14. Post bake the wafer for 10 minutes at 65 Celsius, followed by 60 minutes at 95 Celsius.

15. Leave the wafer on a flat surface for 5 minutes at room temperature in order to let it cool down slowly. This step is crucial since it can prevent thermal stresses which could potentially shorten the life time of the mold.
16. Submerge the wafer into the SU-8-developer solution and slowly stir it until the features are clear.
17. Use Isopropyl alcohol (IPA) to remove the remained unexposed photoresist from the surface.
18. Re-submerge the wafer back into the SU-8-developer solution if any white spots remained.
19. Rinse the wafer with DI water and dry it by blowing nitrogen gas.
20. Hard bake the wafer at 120 Celsius for 60 minutes.

## Appendix B: COMSOL simulation setup

### 1. Model selection

- Select 3D model and add these three physics: AC/DC>Electric Currents, Shell (ecs), structural Mechanics>Shell (shell) and Structural Mechanics>Thermal Stress.
- Select study, select pre-set Studies for Selected Physics Interfaces>Stationary.

### 2. Geometry

- Set the dimension unit to millimeter (mm).
- Add a block with dimensions 65\*65\*0.09 mm with a corner at (0,0,0) (The PSA film).
- Add a xy-work plane at z=0.09 mm.
- Under plane geometry add the geometry of the designed heater. In this design, the geometry of the micro-wire pattern was composed of many connected rectangles with the width equal to the diameter of the micro-wire (0.025 mm).
- Click build all (Figure B.1).

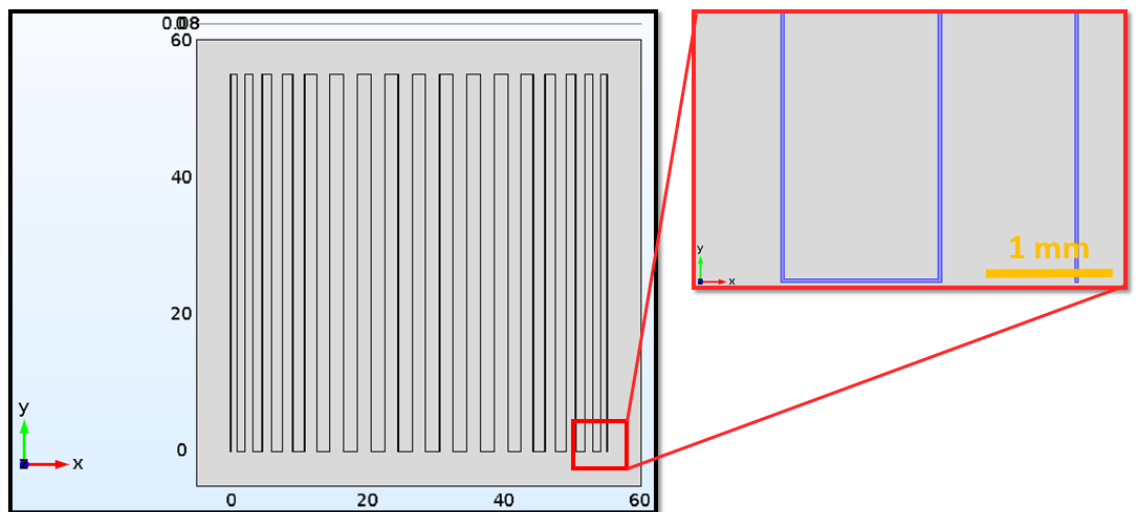


Figure B.1 The geometry of the heater.

### **3. Materials**

- Define the material of the block as acrylic plastic.
- Define the material of the micro-wires as copper.

### **4. Multiphysics**

- Select Model builder, under Multiphysics choose Boundary Electromagnetic Heat Source, go to Setting, Boundary selection and select the micro-wire pattern.
- Select Model builder, under Heat Transfer in Solids (ht), go to Physics, Click on Boundaries and select Heat flux, under select boundaries, select all the boundaries and Convective heat flux.
- Go to Physics, Click on Boundaries and select Thin layer, under select boundaries, select the micro-wire pattern and set the layer thickness to 0.025 mm.
- Select Model builder, click Electric Currents, Shell (ecs), go to Physics, under Edges choose Electric Potential, select one end of the micro-wire pattern and set the initial voltage to 18 volts.
- Go to Physics, under Edges choose Ground, select the other end of the micro-wire pattern.

### **5. Meshing**

- Set user-controlled mesh.
- Choose costume under element size. Different element sizes are required to be tested in order to show the mesh independency of the results. In this regard, 4 element sizes, 0.5 mm, 0.75 mm, 1 mm and 1.5 mm were tested and the results were compared (Figure B.3).
- Click build all.

## 6. Study

- Select Compute to solve the model.

## 7. Results

- Go to Data sets, add a surface, select the top surface of the geometry and name it 'Top'.
- One of the default plots under the results is Temperature (ht), you can find the temperature distribution of the top surface (Figure B.2).

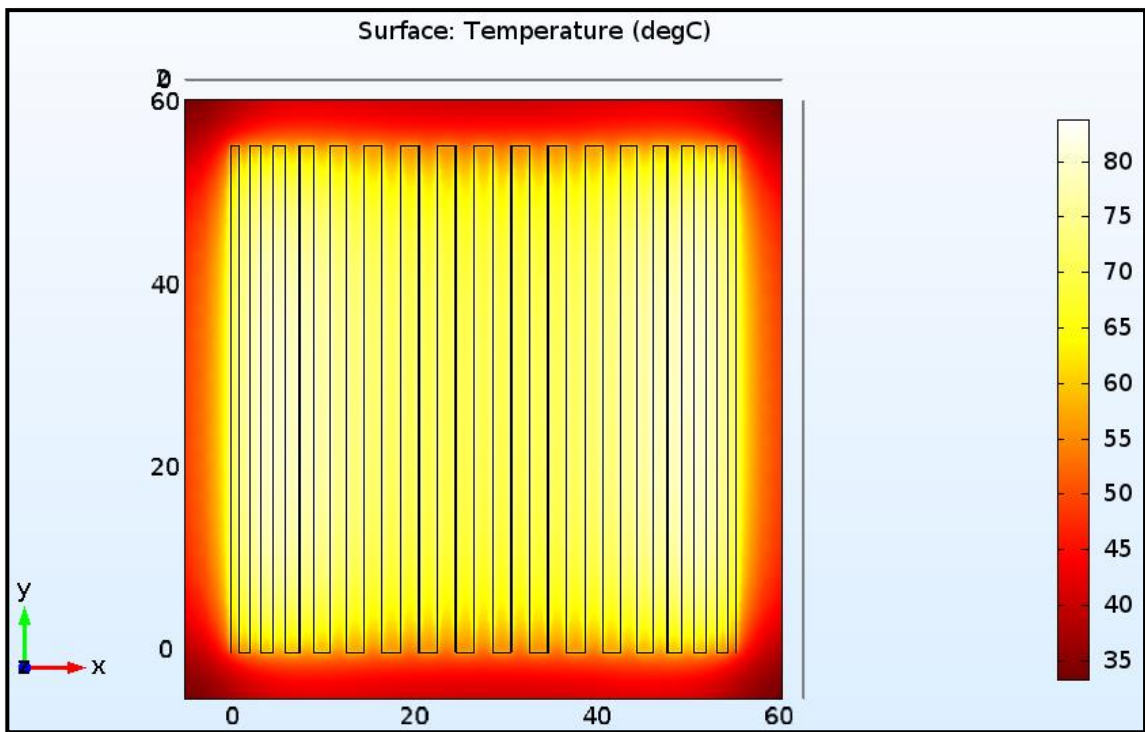


Figure B.2 The temperature distribution of the top surface.

As it was mentioned earlier, mesh independency of the results is required to be analyzed. Therefore, four different mesh sizes ranging from 1.5 mm to 0.5 mm were tested. In this regard, the temperature distribution of a vertical line located on the top surface parallel to the Y axis for four different mesh sizes were plotted in Figure B.3. The analyzed line started from the point (27.5, 10, 2) and ended up at the point (27.5, 50, 2). Therefore, the length of the line was 40 mm.

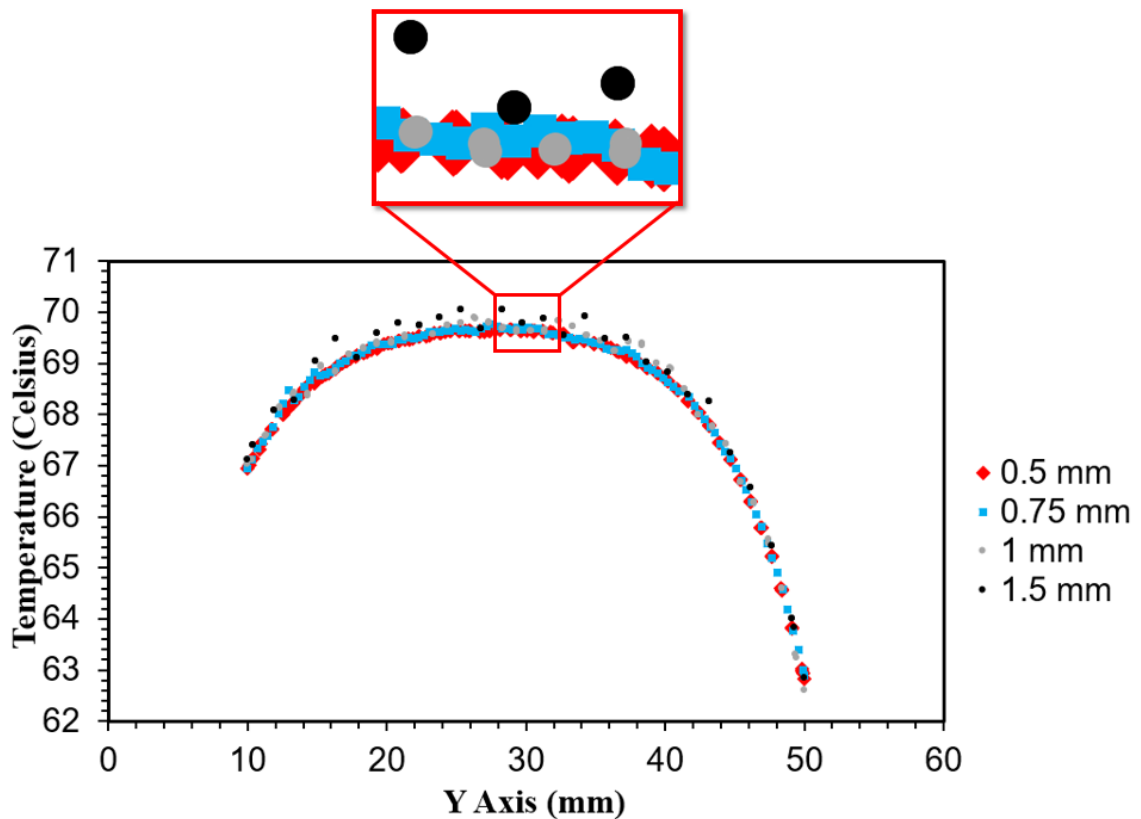


Figure B.3 Mesh independency analysis. The temperature distribution of the vertical line located on the top surface parallel to the Y axis for four different mesh sizes, 1.5 mm (black), 1 mm (grey), 0.75 mm (blue) and 0.5 mm (red).

As it is shown in Figure B.3, the temperature profiles were converging together as the meshing element size decreased. The result from 1.5 mm meshing element size was considerably different from the other three. However, not a significant difference was observed between the 1 mm, 0.75 mm and 0.5 mm element sizes. Therefore, 0.5 mm was chosen as the meshing element size in order to perform the simulation since it produced the closest result to the converging values.

## Appendix C: Detailed information for various micro-wires

Detailed information for various micro-wires from two companies, the Surepure Chemetals and the Vape Mesh Company, with different sizes and materials can be found in Table C-1.

Model	Material	Size ( $\mu\text{m}$ )	Price/Length ( $\text{CAD}/\text{meter}$ )
Surepure Chemetals (3618)	Copper	76	0.06
Surepure Chemetals (4865)	50% Copper 50% Silver	76	2.6
Surepure Chemetals (3631)	Copper	102	0.1
Surepure Chemetals (3626)	Copper	127	0.15
Surepure Chemetals (2080)	Silver	25	4.2
Surepure Chemetals (2702)	Silver	51	6.6
Surepure Chemetals (2703)	Silver	102	6.6
Surepure Chemetals (3455)	Nickel	10	13.8
Surepure Chemetals (3042)	Nickel	254	1.2
Surepure Chemetals (3042)	78% Nickel 20% Chrome	500	4.9
The Vape Mesh Company (SS317L)	Stainless Steel	50	0.04
The Vape Mesh Company (SS317L)	Stainless Steel	210	0.15
The Vape Mesh Company (Titanium Wire)	Titanium	200	0.2

<b>The Vape Mesh Company (Fecral Alloy)</b>	Fe-Cr-Al	90	0.05
<b>The Vape Mesh Company (Fecral Alloy)</b>	Fe-Cr-Al	130	0.07
<b>The Vape Mesh Company (NiCR6015)</b>	60% Nickel 15% Chrome 25% Fe	200	0.09
<b>The Vape Mesh Company (NiCR80/20)</b>	80% Nickel 20% Chrome	50	0.04
<b>The Vape Mesh Company (NiCR80/20)</b>	80% Nickel 20% Chrome	100	0.04
<b>The Vape Mesh Company (CuNi23)</b>	77% Copper 23% Nickel	200	0.15
<b>The Vape Mesh Company (Cu-31AWG)</b>	Copper	220	0.07

Table C-1 Detailed information for various micro-wires.

## Appendix D: Decrease of the fluorescence intensity phenomenon

After the sample was loaded into the device following the method described in chapter 3, section 3.6, a fluorescence picture was taken at the room temperature before starting the amplification. Then, the device was heated up to 65 Celsius and another fluorescence picture was taken. It was observed that the fluorescence intensity decreased significantly when the temperature was increased from the room temperature to 65 Celsius, as it is shown in Figure D.1 for three different heights.

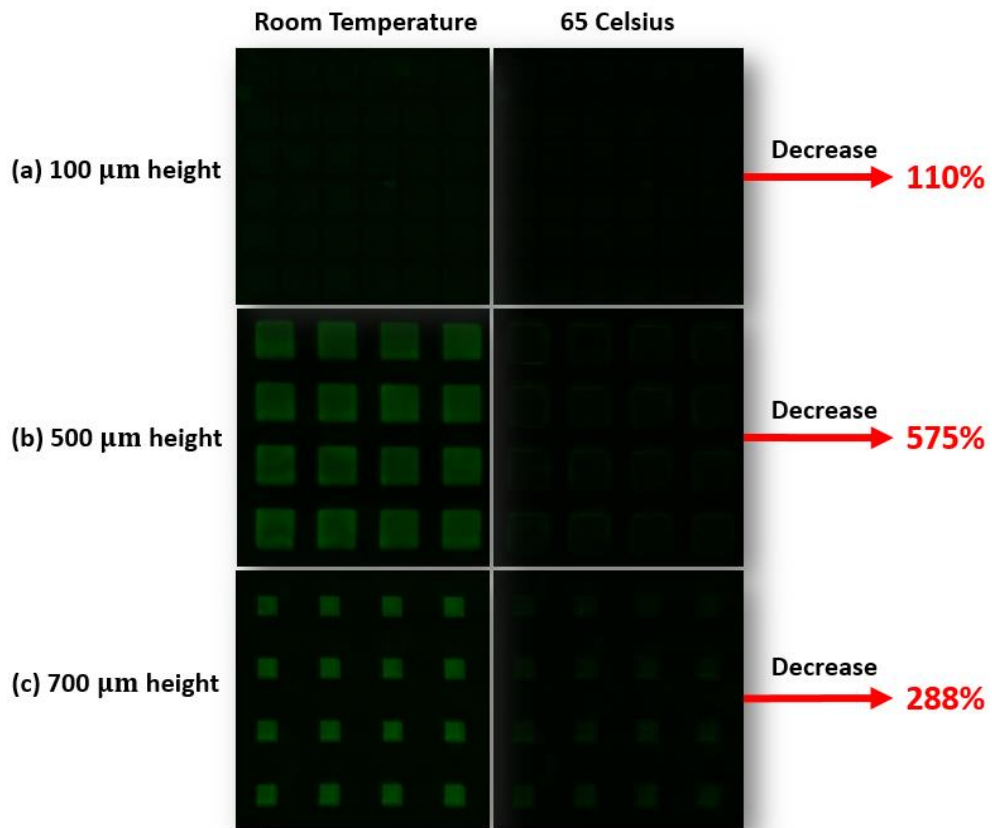


Figure D.1 Decrease of fluorescence intensity phenomenon.

The reason behind this phenomenon could be either the primer dimer or the dissociation-characteristics of double-stranded DNA during heating up process which is known as melting curve analysis. The former happens when primers bind together and make a double stranded molecule. Therefore, it gives the EvaGreen dye the chance to intercalate into the double stranded molecule and increases the fluorescence signal. The latter was due to the melting point temperature which defines as the temperature at which 50 percentage of DNAs in the sample are denatured. From the nucleobases point of view, G-C base pairs have three hydrogen bonds between them and A-T base pairs have two. Therefore, more energy is required to break down the G-C base pairs. Consequently, DNAs which have more G-C base pairs have higher melting points compare to others.

As a result, by increasing the temperature, more DNA molecules are denatured and the primer dimer phenomenon gets less effective. Therefore, lower fluorescence signal is emitted since the EvaGreen dye just emits signal when it intercalates to a double stranded molecule. As it was explained earlier, EvaGreen dye does not emit light on its own. Also, after amplification starts, the fluorescence intensity increases in an S-shape curve (typical amplification curve) till it reaches the plateau phase.

Moreover, the ESEQuant tube scanner which its result was used as a reliable reference point in these experiments, shows the amplification curve only at the set amplification temperature which means the machine waits till the temperature reaches the set point, and after the equilibrium condition is touched, it starts measuring the fluorescence intensity. Therefore, the same procedure was followed in these experiments. As a result, just the pictures which were taken at 65 Celsius were analyzed in order to generate the real-time amplification curves.

## Appendix E: Temperature calibration

In order to check the reliability of the reading temperatures from the thermocouple (5SRTC flexible thermocouple) and the infrared thermal camera (FLIR ONE), two simple tests were done. First, a mixture of water and ice were prepared. After it reached the equilibrium phase, the temperature of the mixture was measured by using the thermocouple and the thermal camera. Theoretically, this temperature is 0 Celsius. In another experiment, the temperature of a boiling water was measured by using the thermocouple and the thermal camera. Theoretically, this temperature is 99.5 Celsius considering the altitude factor (around 150 meters above the sea level). The measured temperatures are summarized in Table E-1.

	<b>Ice and Water mixture</b>	<b>Boiling Water</b>
<b>Thermocouple (Celsius)</b>	0.3	100.5
<b>Thermal Camera (Celsius)</b>	0.1	100.3

Table E-1 The measured temperatures using the thermocouple and the thermal camera.

Considering the acceptable temperature margin which was calculated in section 4.2.6 in chapter 4, the measurement errors were absolutely acceptable. Therefore, the measured temperatures were reliable.

## **Glossary**

<b>AutoCAD</b>	A computer aided design (CAD) program to create 2D or 3D designs and drafts.
<b>DI Water</b>	Deionized water is a water contains no ions such as cations and anions.
<b>DNA</b>	Deoxyribonucleic acid is a molecule contains genetic information for all the functions of living organisms and many viruses.
<b>Electrophoresis</b>	Is a separation technique based on the movement of charged particles in a fluid or gel in an electric field.
<b>Escherichia coli</b>	Also known as E. coli is a gram-negative, rod-shaped, coliform bacterium lives in the intestines of people and animals.
<b>EvaGreen Dye</b>	Is a green fluorescent nucleic acid dye which is not fluorescent by itself but becomes highly fluorescent when it intercalates with dsDNA.
<b>Fluorescein Dye</b>	An orange dye used to tag or label molecules which is fluorescent by itself and does not need to intercalate with double stranded molecules in order to be fluorescent.

<b>Loop-mediated Amplification (LAMP)</b>	Is an isothermal amplification technique which is capable of amplifying the number of DNAs or RNAs in the sample to billions in less than an hour.
<b>Negative Sample</b>	Is a solution with the volume of 25 $\mu\text{L}$ in this thesis, composed of 14.62 $\mu\text{L}$ of the Master Mix, 5 $\mu\text{L}$ of the Primer Mix, 5 $\mu\text{L}$ of DI water and 0.38 $\mu\text{L}$ of the EvaGreen 20X.
<b>Nucleic-based Acid Technology (NAT)</b>	Is a well-established technique in molecular diagnosis where the main purpose is to detect a target by the means of manipulation of biomarkers such as nucleic acids.
<b>Polydimethylsiloxane (PDMS)</b>	Is a transparent polymer with the chemical formula of $\text{CH}_3[\text{Si}(\text{CH}_3)_2]_n\text{Si}(\text{CH}_3)_3$ , n being the number of monomers repetitions. Which is commonly used in the microfluidic field.
<b>Polymerase Chain Reaction (PCR)</b>	Is the most popular non-isothermal amplification method which is capable of amplifying the number of DNAs or RNAs in the sample. It goes through thermal cycles and the number of template copies double after each cycle. PCR cycle steps are denaturation (90-95 Celsius), annealing (55 Celsius) and extension (72 Celsius).

- Positive Sample** Is a solution with the volume of 25  $\mu\text{L}$  in this thesis, composed of 14.62  $\mu\text{L}$  of the Master Mix, 5  $\mu\text{L}$  of the Primer Mix, 5  $\mu\text{L}$  of the DNA template and 0.38  $\mu\text{L}$  of the EvaGreen 20X.
- Primer** Is a necessary component of the DNA replication process. It is a short nucleic acid sequence that provides a starting point for DNA synthesis which must be synthesized by an enzyme called primase before DNA replication can occur.
- RNA** Ribonucleic acid (RNA) is a single stranded molecule transcribed from DNA, essential in various biological roles including coding, regulation, and expression of genes. Also, it is composed of a chain of nucleotides.

## References

- [1] C. M. Chang, W. H. Chang, C. H. Wang, J. H. Wang, J. D. Mai, and G. Bin Lee, "Nucleic acid amplification using microfluidic systems.," *Lab Chip*, vol. 13, no. 7, pp. 1225–1242, 2013.
- [2] A. Zieba, K. Grannas, O. Söderberg, M. Gullberg, M. Nilsson, and U. Landegren, "Molecular tools for companion diagnostics," *N. Biotechnol.*, vol. 29, no. 6, pp. 634–640, 2012.
- [3] J. M. Ghuysen and G. D. Shockman, "Biosynthesis of peptidoglycan." Dekker Inc., pp. 37–130, 1973.
- [4] P. F. Stanbury, A. Whitaker, and S. J. Hall, *Principles of fermentation technology*. Pergamon, 1984.
- [5] S. T. L. Harrison, "Bacterial cell disruption: A key unit operation in the recovery of intracellular products," *Biotechnol. Adv.*, vol. 9, no. 2, pp. 217–240, 1991.
- [6] R. H. Liu, J. Yang, R. Lenigk, J. Bonanno, and G. Piotr, "Self-Contained, Fully Integrated Biochip for Sample Preparation, Polymerase Chain Reaction Amplification, and DNA Microarray Detection," *Anal. Chem.*, vol. 76, no. 7, pp. 1824–1831, 2004.
- [7] Y. Siu Wai, L. Thomas Ming Hung, C. Hong, and H. I Ming, "A DNA biochip for on-the-spot multiplexed pathogen identification," *Nucleic Acids Res.*, vol. 34, no. 18, pp. 118–118, 2006.
- [8] A. Sale and W. Hamilton, "Effects of high electric fields on microorganismsI. Killing of bacteria and yeasts," *Biochim. Biophys. Acta - Gen. Subj.*, vol. 148, no.

- 3, pp. 781–788, 1967.
- [9] K. Mullis, F. Faloona, S. Scharf, R. Saiki, G. Horn, and H. Erlich, “Specific enzymatic amplification of DNA in vitro: the polymerase chain reaction,” *Cold Spring Harb. Symp. Quant. Biol.*, vol. 51, pp. 263–273, 1986.
- [10] M. A. Belaud Rotureau, M. Parrens, P. Dubus, J. C. Garroste, A. de Mascarel, and J. P. Merlio, “A Comparative Analysis of FISH, RT-PCR, PCR, and Immunohistochemistry for the Diagnosis of Mantle Cell Lymphomas,” *Mod. Pathol.*, vol. 15, no. 5, pp. 517–525, 2002.
- [11] T. Watkins Riedel, M. Woegerbauer, D. Hollemann, and P. Hufnagl, “Rapid diagnosis of enterovirus infections by real-time PCR on the LightCycler using the TaqMan format,” *Diagn. Microbiol. Infect. Dis.*, vol. 42, no. 2, pp. 99–105, 2002.
- [12] H. Mocharla, “Coupled reverse transcription-polymerase chain reaction (RT-PCR) as a sensitive and rapid method for isozyme genotyping,” *Gene*, vol. 93, no. 2, pp. 271–275, 1990.
- [13] Ø. Olsvik, “A nested PCR followed by magnetic separation of amplified fragments for detection of *Escherichia coli* Shiga-like toxin genes,” *Mol. Cell. Probes*, vol. 5, no. 6, pp. 429–435, 1991.
- [14] J. B. Mahony, X. Song, S. Chong, M. Faught, T. Salonga, and J. Kapala, “Evaluation of the NucliSens Basic Kit for detection of *Chlamydia trachomatis* and *Neisseria gonorrhoeae* in genital tract specimens using nucleic acid sequence-based amplification of 16S rRNA,” *J. Clin. Microbiol.*, vol. 39, no. 4, pp. 1429–35, 2001.
- [15] J. Mahony, S. Chong, D. Jang, K. Luinstra, M. Faught, D. Dalby, J. Sellors, and M. Chernesky, “Urine specimens from pregnant and nonpregnant women inhibitory to

- amplification of *Chlamydia trachomatis* nucleic acid by PCR, ligase chain reaction, and transcription-mediated amplification: identification of urinary substances associated with inhibition,” *J. Clin. Microbiol.*, vol. 36, no. 11, pp. 3122–3126, 1998.
- [16] G. T. Walker, M. S. Fraiser, J. L. Schram, M. C. Little, J. G. Nadeau, and D. P. Malinowski, “Strand displacement amplification-an isothermal, in vitro DNA amplification technique,” *Nucleic Acids Res.*, vol. 20, no. 7, pp. 1691–1696, 1992.
- [17] F. B. Dean, J. R. Nelson, T. L. Giesler, and R. S. Lasken, “Rapid amplification of plasmid and phage DNA using Phi 29 DNA polymerase and multiply-primed rolling circle amplification.,” *Genome Res.*, vol. 11, no. 6, pp. 1095–9, 2001.
- [18] M. Vincent, Y. Xu, and H. Kong, “Helicase-dependent isothermal DNA amplification,” *EMBO Rep.*, vol. 5, no. 8, pp. 795–800, 2004.
- [19] T. Notomi, H. Okayama, H. Masubuchi, T. Yonekawa, K. Watanabe, N. Amino, and T. Hase, “Loop-mediated isothermal amplification of DNA,” *Nucleic Acids Res.*, vol. 28, no. 12, p. 63, 2000.
- [20] Y. Zhao, F. Chen, Q. Li, L. Wang, and C. Fan, “Isothermal Amplification of Nucleic Acids,” *Chem. Rev.*, vol. 115, no. 22, pp. 12491–12545, 2015.
- [21] T. Nagamine, T. Hase, and T. Notomi, “Accelerated reaction by loop-mediated isothermal amplification using loop primers,” *Mol. Cell. Probes*, vol. 16, no. 3, pp. 223–229, 2002.
- [22] K. A. Curtis, D. L. Rudolph, and S. M. Owen, “Rapid detection of HIV-1 by reverse-transcription, loop-mediated isothermal amplification (RT-LAMP),” *J. Virol. Methods*, vol. 151, no. 2, pp. 264–270, 2008.
- [23] T. Notomi, Y. Mori, N. Tomita, and H. Kanda, “Loop-mediated isothermal

- amplification (LAMP): principle, features, and future prospects,” *J. Microbiol.*, vol. 53, no. 1, pp. 1–5, 2015.
- [24] D. J. Beebe, G. A. Mensing, and G. M. Walker, “Physics and Applications of Microfluidics in Biology,” *Annu. Rev. Biomed. Eng.*, vol. 4, no. 1, pp. 261–286, 2002.
- [25] D. Figeys and D. Pinto, “Lab-on-a-Chip: A Revolution in Biological and Medical Sciences,” *Anal. Chem.*, vol. 72, no. 9, pp. 330–335, 2000.
- [26] J. Mairhofer, K. Roppert, and P. Ertl, “Microfluidic Systems for Pathogen Sensing: A Review,” *Sensors*, vol. 9, no. 6, pp. 4804–4823, 2009.
- [27] L. M. Pilarski, S. Adamia, P. M. Pilarski, R. Prakash, J. Lauzon, and C. J. Backhouse, “Improved Diagnosis and Monitoring of Cancer Using Portable Microfluidics Platforms,” in *2004 International Conference on MEMS, NANO and Smart Systems (ICMENS’04)*, 2004, pp. 340–343.
- [28] A. Noori, P. R. Selvaganapathy, and J. Wilson, “Microinjection in a microfluidic format using flexible and compliant channels and electroosmotic dosage control,” *Lab Chip*, vol. 9, no. 22, p. 3202, 2009.
- [29] P. Rezai, A. Siddiqui, P. R. Selvaganapathy, and B. P. Gupta, “Electrotaxis of *Caenorhabditis elegans* in a microfluidic environment,” *Lab Chip*, vol. 10, no. 2, pp. 220–226, 2010.
- [30] Y. Zhang and P. Ozdemir, “Microfluidic DNA amplification-A review,” *Anal. Chim. Acta*, vol. 638, no. 2, pp. 115–125, 2009.
- [31] J. J. Sninsky, M. A. Innis, and D. H. Gelfand, *PCR applications : protocols for functional genomics*. Academic Press, 1999.

- [32] Y. K. Cho, J. Kim, Y. Lee, Y. A. Kim, K. Namkoong, H. Lim, K. W. Oh, S. Kim, J. Han, C. Park, Y. E. Pak, C.-S. Ki, J. R. Choi, H. K. Myeong, and C. Ko, "Clinical evaluation of micro-scale chip-based PCR system for rapid detection of hepatitis B virus," *Biosens. Bioelectron.*, vol. 21, no. 11, pp. 2161–2169, 2006.
- [33] A. . Gnanappa, K. Cathy, O. Slattery, and M. Sheehan, "Thermal Performance Analysis of a Silicon Microreactor for Rapid DNA Analysis," in *Thermal and Thermomechanical Proceedings 10th Intersociety Conference on Phenomena in Electronics Systems, 2006. IThERM 2006.*, pp. 1330–1335.
- [34] Y. Hataoka, L. Zhang, T. Yukimasa, and Y. Baba, "Rapid Microvolume PCR of DNA Confirmed by Microchip Electrophoresis," *Anal. Sci.*, vol. 21, no. 1, pp. 53–56, 2005.
- [35] C. Ke, A. M. Kelleher, H. Berney, M. Sheehan, and A. Mathewson, "Single step cell lysis/PCR detection of *Escherichia coli* in an independently controllable silicon microreactor," *Sensors Actuators B Chem.*, vol. 120, no. 2, pp. 538–544, 2007.
- [36] C. R. Poulsen, J. El Ali, I. R. Perch-Nielsen, D. D. Bang, P. Telleman, and A. Wolff, "Detection of a putative virulence *cadF* gene of *campylobacter jejuni* obtained from different sources using a microfabricated PCR chip," *J. Rapid Methods Autom. Microbiol.*, vol. 13, no. 2, pp. 111–126, 2005.
- [37] K. Shen, X. Chen, M. Guo, and J. Cheng, "A microchip-based PCR device using flexible printed circuit technology," *Sensors Actuators B Chem.*, vol. 105, no. 2, pp. 251–258, 2005.
- [38] J. S. Marcus, W. French Anderson, and S. R. Quake, "Parallel Picoliter RT-PCR Assays Using Microfluidics," *Anal. Chem.*, vol. 78, no. 3, pp. 956–958, 2006.

- [39] K. Y. Lien, W. C. Lee, H. Y. Lei, and G. Bin Lee, "Integrated reverse transcription polymerase chain reaction systems for virus detection," *Biosens. Bioelectron.*, vol. 22, no. 8, pp. 1739–1748, 2007.
- [40] G. Hu, Q. Xiang, R. Fu, B. Xu, R. Venditti, and D. Li, "Electrokinetically controlled real-time polymerase chain reaction in microchannel using Joule heating effect," *Anal. Chim. Acta*, vol. 557, pp. 146–151, 2006.
- [41] P. Neuzil, C. Zhang, J. Pipper, S. Oh, and L. Zhuo, "Ultra fast miniaturized real-time PCR: 40 cycles in less than six minutes," *Nucleic Acids Res.*, vol. 34, no. 11, p. 77, 2006.
- [42] H. Nakano, K. Matsuda, M. Yohda, T. Nagamune, I. Endo, and T. Yamane, "High Speed Polymerase Chain Reaction in Constant Flow," *Biosci. Biotechnol. Biochem.*, vol. 58, no. 2, pp. 349–352, 1994.
- [43] M. U. Kopp, A. J. Mello, and A. Manz, "Chemical Amplification: Continuous-Flow PCR on a Chip," *Science.*, vol. 280, no. 5366, pp. 1046–1048, 1998.
- [44] S. Li, D. . Fozdar, M. . Ali, H. Li, D. Shao, D. . Vykoukal, J. Vykoukal, P. . Floriano, M. Olsen, J. . McDevitt, P. R. . Gascoyne, and S. Chen, "A Continuous-Flow Polymerase Chain Reaction Microchip With Regional Velocity Control," *J. Microelectromechanical Syst.*, vol. 15, no. 1, pp. 223–236, 2006.
- [45] I. Schneega, R. Brutigam, and J. M. Khler, "Miniaturized flow-through PCR with different template types in a silicon chip thermocycler," *Lab Chip*, vol. 1, no. 1, pp. 42–49, 2001.
- [46] M. Hashimoto, P. C. Chen, M. W. Mitchell, D. E. Nikitopoulos, S. a Soper, and M. C. Murphy, "Rapid PCR in a continuous flow device.," *Lab Chip*, vol. 4, no. 6, pp.

638–645, 2004.

- [47] K. T. L. Trinh, W. Wu, and N. Y. Lee, “Planar poly(dimethylsiloxane) (PDMS)-glass hybrid microdevice for a flow-through polymerase chain reaction (PCR) employing a single heater assisted by an intermediate metal alloy layer for temperature gradient formation,” *Sensors Actuators, B Chem.*, vol. 190, pp. 177–184, 2014.
- [48] G. Münchow, D. Dadic, F. Doffing, S. Hardt, and K. S. Drese, “Automated chip-based device for simple and fast nucleic acid amplification.,” *Expert Rev. Mol. Diagn.*, vol. 5, no. 4, pp. 613–620, 2005.
- [49] J. A. Kim, J. Y. Lee, S. Seong, S. H. Cha, S. H. Lee, J. J. Kim, and T. H. Park, “Fabrication and characterization of a PDMS-glass hybrid continuous-flow PCR chip,” *Biochem. Eng. J.*, vol. 29, no. 1–2, pp. 91–97, 2006.
- [50] J. West, B. Karamata, B. Lillis, J. P. Gleeson, J. Alderman, J. K. Collins, W. Lane, A. Mathewson, and H. Berney, “Application of magnetohydrodynamic actuation to continuous flow chemistry.,” *Lab Chip*, vol. 2, no. 4, pp. 224–230, 2002.
- [51] J. Y. Cheng, C. J. Hsieh, Y. C. Chuang, and J. R. Hsieh, “Performing microchannel temperature cycling reactions using reciprocating reagent shuttling along a radial temperature gradient,” *Analyst*, vol. 130, no. 6, p. 931, 2005.
- [52] L. G. And and C. L. Ren, “Numeric Simulation of Heat Transfer and Electrokinetic Flow in an Electroosmosis-Based Continuous Flow PCR Chip,” *Anal. Chem.*, vol. 78, no. 17, pp. 6215–6222, 2006.
- [53] J. Chen, M. Wabuye, H. Chen, D. Patterson, M. Hupert, H. Shadpour, D. Nikitopoulos, and S. A. Soper, “Electrokinetically Synchronized Polymerase Chain

- Reaction Microchip Fabricated in Polycarbonate,” *Anal. Chem.*, vol. 77, no. 2, pp. 658–666, 2005.
- [54] J. Liu, “A nanoliter rotary device for polymerase chain reaction,” *Electrophoresis*, vol. 23, no. 10, pp. 1531–1536, 2002.
- [55] M. Bu, T. Melvin, G. Ensell, J. S. Wilkinson, and A. G. R. Evans, “Design and theoretical evaluation of a novel microfluidic device to be used for PCR,” *J. Micromechanics Microengineering*, vol. 13, no. 4, pp. 125–130, 2003.
- [56] C. Zhang and D. Xing, “Parallel DNA amplification by convective polymerase chain reaction with various annealing temperatures on a thermal gradient device,” *Anal. Biochem.*, vol. 387, no. 1, pp. 102–112, 2009.
- [57] V. M. Ugaz and M. Krishnan, “Novel convective flow based approaches for high-throughput PCR thermocycling,” *J. Assoc. Lab. Autom.*, vol. 9, no. 5, pp. 318–323, 2004.
- [58] Y. Hataoka, L. Zhang, Y. Mori, N. Tomita, T. Notomi, and Y. Baba, “Analysis of Specific Gene by Integration of Isothermal Amplification and Electrophoresis on Poly(methyl methacrylate) Microchips,” *Anal. Chem.*, vol. 76, no. 13, pp. 3689–3693, 2004.
- [59] S. Y. Lee, C. N. Lee, H. Mark, D. R. Meldrum, and C. W. Lin, “Efficient, specific, compact hepatitis B diagnostic device: Optical detection of the hepatitis B virus by isothermal amplification,” *Sensors Actuators B Chem.*, vol. 127, no. 2, pp. 598–605, 2007.
- [60] L. Lam, S. Sakakihara, K. Ishizuka, S. Takeuchi, H. F. Arata, H. Fujita, and H. Noji, “Loop-mediated isothermal amplification of a single DNA molecule in

- polyacrylamide gel-based microchamber,” *Biomed. Microdevices*, vol. 10, no. 4, pp. 539–546, 2008.
- [61] C. Liu, M. G. Mauk, and H. H. Bau, “A disposable, integrated loop-mediated isothermal amplification cassette with thermally actuated valves,” *Microfluid. Nanofluidics*, vol. 11, no. 2, pp. 209–220, 2011.
- [62] C. Liu, M. G. Mauk, R. Hart, X. Qiu, and H. H. Bau, “A self-heating cartridge for molecular diagnostics,” *Lab Chip*, vol. 11, no. 16, pp. 2686–2692, 2011.
- [63] C. H. Wang, K. Y. Lien, J. J. Wu, G. Bin Lee, N. C. Quaglia, A. Dambrosio, D. Buonavoglia, M. D’Abramo, C. Buonavoglia, P. Francois, D. Mark, G. Roth, R. Zengerle, and F. von Stetten, “A magnetic bead-based assay for the rapid detection of methicillin-resistant *Staphylococcus aureus* by using a microfluidic system with integrated loop-mediated isothermal amplification,” *Lab Chip*, vol. 11, no. 8, p. 1521, 2011.
- [64] M. Safavieh, M. U. Ahmed, M. Tolba, and M. Zourob, “Microfluidic electrochemical assay for rapid detection and quantification of *Escherichia coli*,” *Biosens. Bioelectron.*, vol. 31, no. 1, pp. 523–528, 2012.
- [65] A. M. Chaudhari, T. M. Woudenberg, M. Allin, and K. E. Goodson, “Transient liquid crystal thermometry of microfabricated PCR vessel arrays,” *J. Microelectromechanical Syst.*, vol. 7, no. 4, pp. 345–354, 1998.
- [66] Q. Xiang, B. Xu, R. Fu, and D. Li, “Real Time PCR on Disposable PDMS Chip with a Miniaturized Thermal Cycler,” *Biomed. Microdevices*, vol. 7, no. 4, pp. 273–279, 2005.
- [67] J. Luo, X. Fang, D. Ye, H. Li, H. Chen, S. Zhang, and J. Kong, “A real-time

microfluidic multiplex electrochemical loop-mediated isothermal amplification chip for differentiating bacteria,” *Biosens. Bioelectron.*, vol. 60, pp. 84–91, 2014.

- [68] K. Hsieh, A. S. Patterson, B. S. Ferguson, K. W. Plaxco, and H. T. Soh, “Rapid, Sensitive, and Quantitative Detection of Pathogenic DNA at the Point of Care through Microfluidic Electrochemical Quantitative Loop-Mediated Isothermal Amplification,” *Angew. Chemie Int. Ed.*, vol. 51, no. 20, pp. 4896–4900, 2012.
- [69] Q. Zou, Y. Miao, Y. Chen, U. Sridhar, C. S. Chong, T. Chai, Y. Tie, C. H. L. Teh, T. M. Lim, and C. Heng, “Micro-assembled multi-chamber thermal cyclers for low-cost reaction chip thermal multiplexing,” *Sensors Actuators A Phys.*, vol. 102, no. 1–2, pp. 114–121, 2002.
- [70] C. S. Liao, G. Bin Lee, J. J. Wu, C. C. Chang, T. M. Hsieh, F. C. Huang, and C. H. Luo, “Micromachined polymerase chain reaction system for multiple DNA amplification of upper respiratory tract infectious diseases,” *Biosens. Bioelectron.*, vol. 20, no. 7, pp. 1341–1348, 2005.
- [71] X. Fang, Y. Liu, J. Kong, and X. Jiang, “Loop-mediated isothermal amplification integrated on microfluidic chips for point-of-care quantitative detection of pathogens,” *Anal. Chem.*, vol. 82, no. 7, pp. 3002–3006, 2010.
- [72] Z. Q. Zou, X. Chen, Q. H. Jin, M. S. Yang, and J. L. Zhao, “A novel miniaturized PCR multi-reactor array fabricated using flip-chip bonding techniques,” *J. Micromechanics Microengineering*, vol. 15, no. 8, pp. 1476–1481, 2005.
- [73] K. W. Oh, C. Park, K. Namkoong, J. Kim, K. S. Ock, S. Kim, Y. A. Kim, Y. K. Cho, C. Ko, J. H. Nevin, A. J. Helmicki, H. T. Henderson, and C. H. Ahn, “World-to-chip microfluidic interface with built-in valves for multichamber chip-based PCR

assays,” *Lab Chip*, vol. 5, no. 8, pp. 845–850, 2005.

- [74] Y. Matsubara, K. Kerman, M. Kobayashi, S. Yamamura, Y. Morita, and E. Tamiya, “Microchamber array based DNA quantification and specific sequence detection from a single copy via PCR in nanoliter volumes,” *Biosens. Bioelectron.*, vol. 20, no. 8, pp. 1482–1490, 2005.
- [75] C. Duarte, E. Salm, B. Dorvel, B. Reddy, and R. Bashir, “On-chip parallel detection of foodborne pathogens using loop-mediated isothermal amplification,” *Biomed. Microdevices*, vol. 15, no. 5, pp. 821–830, 2013.
- [76] T. Morrison, J. Hurley, J. Garcia, K. Yoder, A. Katz, D. Roberts, J. Cho, T. Kanigan, S. E. Ilyin, D. Horowitz, J. M. Dixon, and C. J. . Brenan, “Nanoliter high throughput quantitative PCR,” *Nucleic Acids Res.*, vol. 34, no. 18, p. 123, 2006.
- [77] N. Ramalingam, T. C. San, T. J. Kai, M. Y. M. Mak, and H. Q. Gong, “Microfluidic devices harboring unsealed reactors for real-time isothermal helicase-dependent amplification,” *Microfluid. Nanofluidics*, vol. 7, no. 3, pp. 325–336, 2009.
- [78] X. Fang, H. Chen, S. Yu, X. Jiang, and J. Kong, “Predicting viruses accurately by a multiplex microfluidic loop-mediated isothermal amplification chip,” *Anal. Chem.*, vol. 83, no. 3, pp. 690–695, 2011.
- [79] D. M. Turlousse, F. Ahmad, R. D. Stedtfeld, G. Seyrig, J. M. Tiedje, and S. Hashsham, “A polymer microfluidic chip for quantitative detection of multiple water- and foodborne pathogens using real-time fluorogenic loop-mediated isothermal amplification,” *Biomed. Microdevices*, vol. 14, no. 4, pp. 769–778, 2012.
- [80] R. D. Stedtfeld, D. M. Turlousse, G. Seyrig, T. M. Stedtfeld, M. Kronlein, S. Price,

- F. Ahmad, E. Gulari, J. M. Tiedje, and S. A. Hashsham, "Gene-Z: a device for point of care genetic testing using a smartphone," *Lab Chip*, vol. 12, no. 8, p. 1454, 2012.
- [81] R. D. Stedtfeld, Y. C. Liu, T. M. Stedtfeld, T. Kostic, M. Kronlein, O. Srivannavit, W. T. Khalife, J. M. Tiedje, E. Gulari, M. Hughes, B. Etchebarne, and S. A. Hashsham, "Static self-directed sample dispensing into a series of reaction wells on a microfluidic card for parallel genetic detection of microbial pathogens," *Biomed. Microdevices*, vol. 17, no. 5, pp. 1–12, 2015.
- [82] C. N. Liu, N. M. Toriello, and R. A. Mathies, "Multichannel PCR-CE Microdevice for Genetic Analysis," *Anal. Chem.*, vol. 78, pp. 5474–5479, 2006.
- [83] N. M. Toriello, C. N. Liu, and R. A. Mathies, "Multichannel Reverse Transcription-Polymerase Chain Reaction Microdevice for Rapid Gene Expression and Biomarker Analysis," *Anal. Chem.*, vol. 78, no. 23, pp. 7997–8003, 2006.
- [84] X. Yu, D. Zhang, T. Li, L. Hao, and X. Li, "3-D microarrays biochip for DNA amplification in polydimethylsiloxane (PDMS) elastomer," *Sensors Actuators A Phys.*, vol. 108, no. 1, pp. 103–107, 2003.
- [85] O. Frey, S. Bonneick, A. Hierlemann, and J. Lichtenberg, "Autonomous microfluidic multi-channel chip for real-time PCR with integrated liquid handling," *Biomed. Microdevices*, vol. 9, no. 5, pp. 711–718, 2007.
- [86] Q. Zhu, Y. Gao, B. Yu, H. Ren, L. Qiu, S. Han, W. Jin, Q. Jin, and Y. Mu, "Self-priming compartmentalization digital LAMP for point-of-care.," *Lab Chip*, vol. 12, no. 22, pp. 4755–63, 2012.
- [87] W. Du, L. Li, K. P. Nichols, and R. F. Ismagilov, "SlipChip," *Lab Chip*, vol. 9, no. 16, pp. 2286–2292, 2009.

- [88] F. Shen, W. Du, J. E. Kreutz, A. Fok, and R. F. Ismagilov, "Digital PCR on a SlipChip.," *Lab Chip*, vol. 10, no. 20, pp. 2666–2672, 2010.
- [89] F. Shen, E. K. Davydova, W. Du, J. E. Kreutz, O. Piepenburg, and R. F. Ismagilov, "Digital Isothermal Quantification of Nucleic Acids via Simultaneous Chemical Initiation of Recombinase Polymerase Amplification Reactions on SlipChip," *Anal. Chem.*, vol. 83, no. 9, pp. 3533–3540, 2011.
- [90] M. Focke, F. Stumpf, B. Faltin, P. Reith, D. Bamarni, S. Wadle, C. Müller, H. Reinecke, J. Schrenzel, P. Francois, D. Mark, G. Roth, R. Zengerle, and F. Von Stetten, "Microstructuring of polymer films for sensitive genotyping by real-time PCR on a centrifugal microfluidic platform.," *Lab Chip*, vol. 10, no. 19, pp. 2519–2526, 2010.
- [91] S. Lutz, P. Weber, M. Focke, B. Faltin, J. Hoffmann, C. Müller, D. Mark, G. Roth, P. Munday, N. Armes, O. Piepenburg, R. Zengerle, and F. Von Stetten, "Microfluidic lab-on-a-foil for nucleic acid analysis based on isothermal recombinase polymerase amplification (RPA)," *Lab Chip*, vol. 10, no. 7, pp. 887–893, 2010.
- [92] J. H. Jung, S. J. Choi, B. H. Park, Y. K. Choi, and T. S. Seo, "Ultrafast Rotary PCR system for multiple influenza viral RNA detection," *Lab Chip*, vol. 12, no. 9, pp. 1598–1600, 2012.
- [93] S. J. Oh, B. H. Park, J. H. Jung, G. Choi, D. C. Lee, D. H. Kim, and T. S. Seo, "Centrifugal loop-mediated isothermal amplification microdevice for rapid, multiplex and colorimetric foodborne pathogen detection," *Biosens. Bioelectron.*, vol. 75, pp. 293–300, 2016.

- [94] S. Y. Teh, R. Lin, L. H. Hung, and A. P. Lee, "Droplet microfluidics," *Lab Chip*, vol. 8, no. 2, p. 198, 2008.
- [95] N. R. Beer, B. J. Hindson, E. K. Wheeler, S. B. Hall, K. A. Rose, I. M. Kennedy, and B. W. Colston, "On-Chip, Real-Time, Single-Copy Polymerase Chain Reaction in Picoliter Droplets," *Anal. Chem.*, vol. 79, pp. 8471–8475, 2007.
- [96] X. Leng, W. Zhang, C. Wang, L. Cui, and C. J. Yang, "Agarose droplet microfluidics for highly parallel and efficient single molecule emulsion PCR," *Lab Chip*, vol. 10, no. 21, pp. 2841–2843, 2010.
- [97] Y. Zeng, R. Novak, J. Shuga, M. T. Smith, and R. A. Mathies, "High-Performance Single Cell Genetic Analysis Using Microfluidic Emulsion Generator Arrays," *Anal Chem.*, vol. 82, no. 8, pp. 3183–3190, 2011.
- [98] P. J. Asiello and A. J. Baeumner, "Miniaturized isothermal nucleic acid amplification, a review.," *Lab Chip*, vol. 11, no. 8, pp. 1420–1430, 2011.
- [99] S. Ayyash, W. I. Wu, and P. R. Selvaganapathy, "Fast and inexpensive detection of bacterial viability and drug resistance through metabolic monitoring," 2014 IEEE Healthc. Innov. Conf. HIC 2014, pp. 22–25, 2014.
- [100] H. Liu, H. Gong, and N. Ramalingam, "Micro air bubble formation and its control during polymerase chain reaction (PCR) in polydimethylsiloxane (PDMS) microreactors," *J. Micromechanics Microengineering*, vol. 17, pp. 2055–2064, 2007.
- [101] R. Irawan, S. C. Tjin, P. Yager, and D. Zhang, "Cross-talk problem on a fluorescence multi-channel microfluidic chip system," *Biomed. Microdevices*, vol. 7, no. 3, pp. 205–211, 2005.
- [102] A. Mata, A. J. Fleischman, and S. Roy, "Characterization of Polydimethylsiloxane

- (PDMS) Properties for Biomedical Micro/ Nanosystems Characterization of Polydimethylsiloxane (PDMS) Properties for Biomedical Micro / Nanosystems,” *Biomed. Microdevices*, vol. 7, no. 4, pp. 281–293, 2005.
- [103] J. E. Blanco, M. Blanco, M. P. Alonso, A. Mora, G. Dahbi, M. A. Coira, and J. Blanco, “Serotypes , Virulence Genes , and Intimin Types of Shiga Toxin ( Verotoxin ) -Producing Escherichia coli Isolates from Human Patients : Prevalence in Lugo , Spain , from 1992 through 1999,” *J. Clin. Microbiol.*, vol. 42, no. 1, pp. 311–319, 2004.
- [104] Biotium, “Product Information EvaGreen Dye,” pp. 4–5, 2007.
- [105] Mao et al, “United States Patent Application Publication,” vol. 1, no. 12, 2002.
- [106] Y. Xia and G. M. Whitesides, “Soft Lithography,” *Annu. Rev. Mater. Sci.*, vol. 28, no. 1, pp. 153–184, 1998.
- [107] J.Liu and P. R. Selvaganapathy, “Xurographic microwire integration technique for lab on chip applications,” *McMaster Univ.*, 2017.
- [108] B. Dhananjay and K. M. Chantal, “Hydrophilization and hydrophobic recovery of PDMS by oxygen plasma and chemical treatment—An SEM investigation,” *Sensors Actuators B Chem.*, vol. 123, no. 1, pp. 368–373, 2007.
- [109] Y. S. Zhang, J. Ribas, A. Nadhman, J. Aleman, Š. Selimović, S. C. Lesher-Perez, T. Wang, V. Manoharan, S. R. Shin, A. Damilano, N. Annabi, M. R. Dokmeci, S. Takayama, and A. Khademhosseini, “A cost-effective fluorescence mini-microscope for biomedical applications,” *Lab Chip*, vol. 15, no. 18, pp. 3661–3669, 2015.
- [110] P. Concus and R. Finn, “On the behaviour of a capillary surface in a wedge,” *PNAS*,

vol. 63, no. 2, pp. 292–299, 1969.

- [111] R. J. Jackman, D. C. Duffy, E. Ostuni, N. D. Willmore, and G. M. Whitesides, “Fabricating Large Arrays of Microwells with Arbitrary Dimensions and Filling Them Using Discontinuous Dewetting,” *Anal. Chem.*, vol. 70, no. 11, pp. 2280–2287, 1998.
- [112] F. Ahmad, G. Seyrig, D. M. Turlousse, R. D. Stedtfeld, J. M. Tiedje, and S. A. Hashsham, “A CCD-based fluorescence imaging system for real-time loop-mediated isothermal amplification-based rapid and sensitive detection of waterborne pathogens on microchips,” *Biomed. Microdevices*, vol. 13, no. 5, pp. 929–937, 2011.
- [113] W. Yamazaki, M. Taguchi, M. Ishibashi, M. Kitazato, M. Nukina, N. Misawa, and K. Inoue, “Development and evaluation of a loop-mediated isothermal amplification assay for rapid and simple detection of *Campylobacter jejuni* and *Campylobacter coli*,” *J. Med. Microbiol.*, vol. 57, pp. 444–451, 2008.
- [114] T. J. Anchordoquy and M. C. Molina, “Preservation of DNA,” *Cell Preserv. Technol.*, vol. 5, no. 4, pp. 180–188, 2007.
- [115] M. d. C. Molina, T. K. Armstrong, Y. e. Zhang, M. M. Patel, Y. K. Lentz, and T. J. Anchordoquy, “The Stability of lyophilized lipid/DNA complexes during prolonged storage,” *J. Pharm. Sci.*, vol. 93, no. 9, pp. 2259–2273, 2004.
- [116] C. Zhang and D. Xing, “Single-Molecule DNA Amplification and Analysis Using Microfluidics,” *Chem. Rev.*, vol. 110, no. 8, pp. 4910–4947, 2010.

- [117] C. Duarte, E. Salm, B. Dorvel, B. Reddy, and R. Bashir, “On-chip parallel detection of foodborne pathogens using loop-mediated isothermal amplification,” *Biomed. Microdevices*, vol. 15, no. 5, pp. 821–830, 2013.
- [118] J. S. Kuo, D. T. Chiu, J. T. Koepsel, K. C. Carver, S. J. Zelski, W. L. Murphy, L. A. Schuler, E. T. Alarid, D. J. Beebe, S. Takayama, J. Ducree, U. J. Balis, R. G. Tompkins, D. A. Haber, M. Toner, T. J. Lynch, M. Toner, D. A. Haber, L. V Sequist, M. Toner, D. A. Haber, S. Maheswaran, and M. Toner, “Disposable microfluidic substrates: Transitioning from the research laboratory into the clinic,” *Lab Chip*, vol. 11, no. 16, pp. 2656–2665, 2011.
- [119] C. Liu, M. G. Mauk, R. Hart, X. Qiu, and H. H. Bau, “A self-heating cartridge for molecular diagnostics.,” *Lab Chip*, vol. 11, no. 16, pp. 2686–2692, 2011.